

CANADIAN THESES ON MICROFICHE

I.S.B.N.

THESES CANADIENNES SUR MICROFICHE



National Library of Canada
Collections Development Branch

Canadian Theses on
Microfiche Service

Ottawa, Canada
K1A 0N4

Bibliothèque nationale du Canada
Direction du développement des collections

Service des thèses canadiennes
sur microfiche

NOTICE

The quality of this microfiche is heavily dependent upon the quality of the original thesis submitted for microfilming. Every effort has been made to ensure the highest quality of reproduction possible.

If pages are missing, contact the university which granted the degree.

Some pages may have indistinct print especially if the original pages were typed with a poor typewriter ribbon or if the university sent us a poor photocopy.

Previously copyrighted materials (journal articles, published tests, etc.) are not filmed.

Reproduction in full or in part of this film is governed by the Canadian Copyright Act, R.S.C. 1970, c. C-30. Please read the authorization forms which accompany this thesis.

THIS DISSERTATION
HAS BEEN MICROFILMED
EXACTLY AS RECEIVED

AVIS

La qualité de cette microfiche dépend grandement de la qualité de la thèse soumise au microfilmage. Nous avons tout fait pour assurer une qualité supérieure de reproduction.

S'il manque des pages, veuillez communiquer avec l'université qui a conféré le grade.

La qualité d'impression de certaines pages peut laisser à désirer, surtout si les pages originales ont été dactylographiées à l'aide d'un ruban usé ou si l'université nous a fait parvenir une photocopie de mauvaise qualité.

Les documents qui font déjà l'objet d'un droit d'auteur (articles de revue, examens publiés, etc.) ne sont pas microfilmés.

La reproduction, même partielle, de ce microfilm est soumise à la Loi canadienne sur le droit d'auteur, SRC 1970, c. C-30. Veuillez prendre connaissance des formules d'autorisation qui accompagnent cette thèse.

LA THÈSE A ÉTÉ
MICROFILMÉE TELLE QUE
NOUS L'AVONS REÇUE

National Library
of CanadaBibliothèque nationale
du Canada

Canadian Theses Division

Division des thèses canadiennes

Ottawa, Canada
K1A 0N4

56886

PERMISSION TO MICROFILM — AUTORISATION DE MICROFILMER

• Please print or type — Écrire en lettres moulées ou dactylographier

Full Name of Author — Nom complet de l'auteur

RAJENDER RAZDAN

Date of Birth — Date de naissance

12 MARCH ~~1956~~ 1956

Country of Birth — Lieu de naissance

INDIA

Permanent Address — Résidence fixe

Electrical Engineering Dept.
University of Alberta
T6G-2JH

Title of Thesis — Titre de la thèse

AN INVESTIGATION OF MULTILEVEL PAM AND PWM
FOR FIBER-OPTIC COMMUNICATION SYSTEMS

University — Université

UNIV. OF ALBERTA

Degree for which thesis was presented — Grade pour lequel cette thèse fut présentée

M. Sc.

Year this degree conferred — Année d'obtention de ce grade

1982

Name of Supervisor — Nom du directeur de thèse

DR. P. GOUD AND C.G. ENGLEFIELD

Permission is hereby granted to the NATIONAL LIBRARY OF
CANADA to microfilm this thesis and to lend or sell copies of
the film.The author reserves other publication rights, and neither the
thesis nor extensive extracts from it may be printed or other-
wise reproduced without the author's written permission.L'autorisation est, par la présente, accordée à la BIBLIOTHÈ-
QUE NATIONALE DU CANADA de microfilmer cette thèse et de
prêter ou de vendre des exemplaires du film.L'auteur se réserve les autres droits de publication; ni la thèse
ni de longs extraits de celle-ci ne doivent être imprimés ou
autrement reproduits sans l'autorisation écrite de l'auteur.

Date

April 26, 1982

Signature

Rajender Razdan

THE UNIVERSITY OF ALBERTA

AN INVESTIGATION OF MULTILEVEL PAM AND PWM FOR FIBER-OPTIC
COMMUNICATION SYSTEMS

by

RAJENDER RAZDAN

A THESIS

SUBMITTED TO THE FACULTY OF GRADUATE STUDIES AND RESEARCH
IN PARTIAL FULFILMENT OF THE REQUIREMENTS FOR THE DEGREE
OF MASTER OF SCIENCE

ELECTRICAL ENGINEERING

EDMONTON, ALBERTA

SPRING 1982

THE UNIVERSITY OF ALBERTA

RELEASE FORM

NAME OF AUTHOR RAJENDER RAZDAN
TITLE OF THESIS AN INVESTIGATION OF MULTILEVEL PAM AND PWM FOR
FIBER-OPTIC COMMUNICATION SYSTEMS
DEGREE FOR WHICH THESIS WAS PRESENTED MASTER OF SCIENCE
YEAR THIS DEGREE GRANTED SPRING 1982

Permission is hereby granted to THE UNIVERSITY OF ALBERTA LIBRARY to reproduce single copies of this thesis and to lend or sell such copies for private, scholarly or scientific research purposes only.

The author reserves other publication rights, and neither the thesis nor extensive extracts from it may be printed or otherwise reproduced without the author's written permission

(SIGNED)

Rajender Razdan

PERMANENT ADDRESS

% DR. H. RAZDAN
BARC - NRL, ZAKURA, SONBET
KASHMIR, INDIA - 190006

DATED 31st DEC. 1981

THE UNIVERSITY OF ALBERTA
FACULTY OF GRADUATE STUDIES AND RESEARCH

The undersigned certify that they have read, and recommend to the Faculty of Graduate Studies and Research, for acceptance, a thesis entitled AN INVESTIGATION OF MULTILEVEL PAM AND PWM FOR FIBER-OPTIC COMMUNICATION SYSTEMS submitted by RAJENDER RAZDAN in partial fulfilment of the requirements for the degree of MASTER OF SCIENCE

Paul G. Goud

Supervisor

C. G. Engelfield

Supervisor

J. Mandelk

R. S. S. S.

Date 31st Dec. 1981

ABSTRACT

Multilevel transmission is advantageous when compared with binary transmission, since, for a channel of fixed bandwidth, more information can be transmitted. In this thesis, a theoretical investigation of the noise present in multilevel PAM and PWM fiber-optic systems is carried out and the error probability predictions are experimentally verified for a four-level PAM system. It is shown that, using multilevel transmission, very low error rates can be achieved, provided that a fiber with sufficiently large bandwidth is used. Multilevel PAM is more useful where such wideband fibers are not available.

The mathematical model makes use of the Gram-Charlier series to approximate the probability density function of the receiver output. Introduced into the Gram-Charlier series model is the effect of intersymbol interference, which is an important factor in limiting the performance of a fiber-optic system. Numerical results are provided to assess the performance of 4-level PAM and PWM systems.

The experiment involved the transmission of a four level pseudorandom PAM sequence, operating at 4.023 Mb/s, over a 0.5 km multimode fiber. Error rates of the system were measured as a function of the avalanche gain and the optical power incident on the photodiode. The experimental values were seen to match closely with the theoretical predictions.

ACKNOWLEDGEMENTS

The author wishes to express his appreciation to the following:

- Dr. P.A. Goud and Dr. C.G. Englefield for suggesting this project and for their interest, advice and encouragement during the supervision of this work.
- Mr. Dai Xianda, visiting scholar from the Beijing Institute of Aeronautics, with whom the author has worked closely. The author's frequent discussions with Mr. Xianda have been of invaluable assistance. Mr. Xianda's contribution, especially in the area of PWM systems, is gratefully acknowledged.
- Dr. A. Javed, Bell Northern Research, and Mr. M. Mansuripur, Xerox Research Centre of Canada, for their advice and stimulating discussions.
- Mr. Bert Telder and Mr. Doug Lind for skilful technical assistance in designing and testing some of the circuits used in the experiment.
- Santanu Das and Sudhesh Mysore as well as other members of the Microwave and Optical Communications Group, for their helpful discussions, understanding and encouragement.

Appreciation is also extended to the following organisations:

- The Department of Electrical Engineering for teaching and research assistantships.
- The Natural Sciences and Engineering Research Council of Canada (under Grant NSERC-A3725) for supporting some of the research work reported in this thesis.

The author also expresses his sincere thanks to his parents, teachers and all others who have contributed in one way or another towards the completion of the research work reported in this thesis.

<u>Chapter</u>	<u>Table of Contents</u>	<u>Page</u>
1	INTRODUCTION	1
1.1	FIBER-OPTIC SYSTEMS	1
1.2	OPTICAL-COMMUNICATIONS LINK	5
1.2.1	Signal Shaper/Encoder	5
1.2.2	Source Driver and Optical Source	7
1.2.3	Source-Fiber Coupler	10
1.2.4	Optical Cable	10
1.2.5	Repeater	11
1.2.6	Fiber-Detector Coupler	11
1.2.7	Detector	11
1.2.8	Amplifier and Signal Shaper-Decoder	12
1.3	THESIS OBJECTIVES	12
1.4	ORGANISATION OF THE THESIS	13
2	ERROR PROBABILITY CALCULATIONS FOR FIBER-OPTIC RECEIVERS	14
2.1	NOISE SOURCES IN A FIBER-OPTIC SYSTEM	15
2.2	THE ANALYTICAL APPROACH TO DETERMINE ERROR PROBABILITY	19
2.2.1	Shot Noise	24
2.2.2	Thermal Noise	25
2.2.3	Receiver Sensitivity	28
2.2.4	Optimum Avalanche Gain	30
2.2.5	Remarks on Analytical Methods	30
2.3	OTHER APPROACHES TO ERROR PROBABILITY CALCULATIONS	31
2.3.1	Numerical Methods	33
2.3.2	Statistical Methods	37
2.4	DETAILED ANALYSIS OF THE GRAM-CHARLIER SERIES METHOD	38
2.4.1	Derivation of Cumulants	41
2.4.2	Comments on the Gram-Charlier Series	48
2.4.3	Error Probability Calculations	49
3	MULTILEVEL PULSE AMPLITUDE MODULATION	51
3.0.1	Intersymbol Interference	57

3.0.2	Numerical Example	59
3.1	EXPERIMENTAL SETUP FOR THE 4-LEVEL PAM SYSTEM	65
3.1.1	Overall Experimental Setup	65
3.1.2	The Data Error Analyser	68
3.1.3	Four-level Modulator and LED Driver	69
3.1.4	The Choice of the Fiber	72
3.1.5	Receiver Section	72
3.1.6	Integrate-and-Dump Filter	75
3.1.7	Demodulator	77
3.1.8	Error Rate Measurements	77
3.2	DISCUSSION OF RESULTS	77
4.	MULTILEVEL PULSE WIDTH MODULATION	86
4.1	MATHEMATICAL MODEL OF THE MULTILEVEL PWM SYSTEM	87
4.2	NOISE IN A 4-LEVEL PWM SYSTEM	92
4.2.1	LPF system	92
4.2.2	IDF system	95
4.3	ERROR PROBABILITY FORMULATION FOR A 4-LEVEL PWM SYSTEM	98
4.4	NUMERICAL EXAMPLES	99
4.5	DISCUSSION OF RESULTS	103
5.	SUMMARY AND CONCLUSIONS	106
	APPENDIX I	110
	APPENDIX II	116
	APPENDIX III	120
	REFERENCES	136

List of Figures

<u>Figure</u>		<u>Page</u>
1.1	Comparison of binary and four-level modulation schemes at (a) 140 Mb/sec and (b) 70 Mb/sec, using a LED-PIN configuration. The curves show minimum peak power required to achieve BER of 10^{-9} , versus fiber length. The solid line, ———, is for a fiber with modal dispersion of 4 ns/km. The broken line, - - - -, is for an ideal fiber without modal dispersion.	4
1.2	Block diagram of a typical optical fiber communication system.	6
1.3	Various coding schemes employed in optical fiber communication systems.	8
1.4	Power emitted from an LED and from an ILD as a function of direct current. The knee in the ILD curve is at the threshold current which depends on the device and its construction. The nonlinearity in the curves at high currents is due to junction heating.	9
2.1	A simple model of a photodetector along with its associated biasing resistor.	16
2.2	The Photon-counting process in a photodetector diode.	18
2.3	Noise mechanisms in a fiber-optic communication system.	20
2.4	Equivalent circuit for the fiber-optic receiver.	21
2.5	Probability density curves for an OFF and an ON pulse, assuming a Gaussian distribution. The mean value of the OFF and ON pulse are m_0 and m_1 , respectively. The corresponding variances of the OFF and ON pulses are σ_{off} and σ_{on} . The threshold, V_{th} , is chosen using the equal area criterion (i.e. the shaded areas A and B are set equal).	29
2.6	Simplified fiber-optic receiver block diagram.	32
2.7	Graphical description of the shot noise analysed by Rice.	42
2.8	Probability density curves for binary transmission (a) using the non-normalised variable X' and (b) using the normalised variable X	50
3.1	Block diagram of a multilevel PAM fiber optic communication system.	53
3.2	The probability density function of the output voltage for a 4-level PAM system.	55
3.3	The effect of the worst-case intersymbol interference on the pulse shape and the probability density function due to the highest level signal flanking the lowest level signal on both sides.	63
3.4	Plot of error probability as a function of the mean avalanche gain for a 4-level PAM system.	64
3.5	Plot of error probability as a function of the mean optical power reaching the detector.	66

Figure	Page
3.6 The experimental four-level PAM fiber optic system	67
3.7 Algorithm for troubleshooting of the optical fiber system	70
3.8 Circuit diagram of the 4-level modulator and LED driver	71
3.9 Circuit diagram of the FET preamplifier	74
3.10 Circuit diagram of the integrate-and-dump filter used for the 4-level PAM system. Also shown are the input and output waveforms and the control signal	76
3.11 The 4-level demodulator circuit diagram	79
3.12 Timing diagram of the 4-level PAM demodulator	80
3.13 Error probability as a function of the mean avalanche gain of the APD for an experimental 4 level PAM system	81
3.14 Error probability as a function of the average optical power at the input to the receiver for a 4 level PAM system	82
3.15 Mean avalanche gain of an APD as a function of the reverse bias voltage	84
4.1 Block diagram of a multilevel PWM optical-fiber communication system	88
4.2 Assumed pulse-shape of the optical output power of the fiber	89
4.3 Impulse response of (a) an ideal IDF and (b) an ideal LPF	91
4.4 Relationship between the noise amplitude and the timing error at the output of the LPF	93
4.5 Probability density function of the random timing error at the output of a four-level PWM system using an LPF	96
4.6 Probability density function of the random timing error at the output of a four-level PWM system using an IDF	97
4.7 Error probability versus P_m for both the LPF and IDF schemes	101
4.8 Error probability versus $\langle G \rangle$ for both LPF and IDF schemes: $t_{\sigma} = 1$ ns	102
4.9 Error probability versus t_{σ} for the LPF scheme	104
A1.1 Schematic of the avalanche region in an APD	111

LIST OF TABLES

<u>Table</u>	<u>Page</u>
3.1 Parameters used in numerical calculations (Multilevel PAM).....	60
3.2 Required pulse amplitude levels and thresholds for a range of error probabilities.....	61
3.3 Measured values of signal levels and thresholds for the experimental four-level PAM system.....	82
4.1 Parameters used in numerical calculations (Multilevel PWM).....	100
4.2 Required pulse width levels and thresholds, using an ideal LPF and IDF for a range of error probabilities.....	100

CHAPTER I

INTRODUCTION

1.1 FIBER-OPTIC SYSTEMS

The potential of optical fiber as a versatile transmission medium for communication applications is well recognized [1],[2]. Attractive features of optical fiber compared to conventional systems are

1. larger bandwidth and lower loss.
2. reduced size and weight.
3. higher system channel capacity.
4. lower basic material (glass) cost.
5. freedom from electromagnetic interference and pickup.
6. higher temperature capability and
7. greater security since it is difficult to tap.

The attractive features of fiber-optics as a means of communication have been recognized for a long time but could only be realized after the development of low-loss fibers in 1970 [3]. Improvements made in the design of low-loss fibers spurred the growth of related components for optical-data links such as, light sources, modulators, multiplexers, couplers, connectors, detectors, demodulators, demultiplexers and receivers. A number of field trials, eg. those cited in references [4],[5], were conducted using fiber optical data links, and these performed sufficiently well that many of these links are still in regular service.

The purpose of a fiber optical communication link is the transmission of information from one point to another without introducing unacceptable degradation of the signal. This degradation normally is measured in terms of the bit error rate (BER) or signal-to-noise ratio (SNR) and signal distortion. Either analog or digital modulation can be used in fiber transmission. In a digital communication link, the signal consists of a series of discrete pulses which must be distinguished from each other upon reception. In an analog communication link, the information is contained in the detailed shape of the transmitted waveform.

The choice between analog and digital transmission depends on which type will provide the required quality at the overall lowest cost. Analog intensity modulation is suitable for low bandwidth signals and has the appeal of system simplicity. On the other hand, digital modulation is highly immune to noise, provided that the system has a large bandwidth. Digital modulation is therefore ideally suited for fiber transmission, a medium of large bandwidth. For digital transmission, a SNR of only about 20 db yields a BER of 10^{-9} , a figure accepted by industry for high quality systems. Also the frequency division multiplexing equipment used for analog transmission is more expensive than the time division multiplexing used for digital transmission. The disadvantages of digital transmission are that a wide-band transmission medium and complex encoding/decoding circuits are required. Fiber-optics, with its inherent wide-band capacity, is ideally suited for digital transmission.

Digital transmission tends to concentrate on the bit-rates used for telephony and derivatives of those bit-rates. This has been done to provide standardised modulator/demodulator equipment. Thus preferred rates are 1.5, 6.3, 44.7, 274 Mb/sec and 1.1 Gb/sec. There is a trend towards using higher modulation rates, however, the present characteristics of light emitting diodes (LEDs) limit the achievable bit-rate to about 140 Mb/sec for a line length of about 500 m, when using binary modulation. The modulation capability using lasers reaches 560 Mb/sec and operation at 1.1 Gb/sec is also reported [6].

A method used to improve the transmission capacity of the LED or the injection laser diode (ILD) employs multilevel signalling. The relation between the information rate and the number of levels is given by [7]:

$$R = \log_2(M/T) \quad (1.1)$$

where

R = information rate in bauds/sec.

M = number of levels, assumed to be equally likely

T = digit interval in seconds

Thus, increasing M from 2 to 4 increases the information rate by a factor of two. One could also decrease T in order to increase the information rate; this would, however,

necessitate a higher bandwidth system. This has been discussed in greater detail in Chapter III. A comparison between the binary and 4-level modulation schemes, with respect to the required optical power, for a system using a commercially available LED and a PIN-JFET trans-impedance receiver is given in Fig 1.1 [8]. Intersymbol interference, i.e. the effect of pulses from adjacent time slots on the pulse under consideration, has been neglected. A real-life link would be subject to intersymbol interference and this would impose a penalty of a few extra decibels of peak power. The penalty for using a larger number of levels is increased intersymbol interference, and thereby greater power penalty. Thus, though 8-level modulation would seem to increase the information rate by three times, in actual practice the increase is much less due to increased intersymbol interference. Another disadvantage of using a larger number of levels is that the electronics becomes more complex. Four-level modulation seems to be a good compromise between binary and 8-level (or higher) modulation for obtaining increased information capability without creating too much intersymbol interference and circuit complexity.

The transmission capacity for an ILD might be doubled, as for the LED, by using four-level modulation. This would, however, require a very high or a very well defined extinction ratio (on-to-off ratio of light levels). Both these requirements are beyond the capability of currently available ILDs. Also, bit rates of 560 Mb/sec and 1.1 Gb/sec will not be readily usable until gigabit logic becomes available.

Another possible modulation scheme, suitable for multilevel transmission, is the Pulse-Width-Modulation (PWM) scheme. PWM is suitable for high bandwidth systems requiring extremely low bit error rates. The SNR of PWM can be improved by decreasing the rise and fall times of the optical pulses; i.e., by using a higher bandwidth system. This is not possible with PAM systems. The requirement of short rise and fall times makes the electronics necessary for PWM schemes rather complex. The finite rise times of commercially available LEDs, lasers, fibers, detectors and the associated circuitry limit the achievable error probability for a PWM system. Multilevel PWM systems provide increased transmission capability compared to binary PWM systems, in the same manner as for PAM systems.

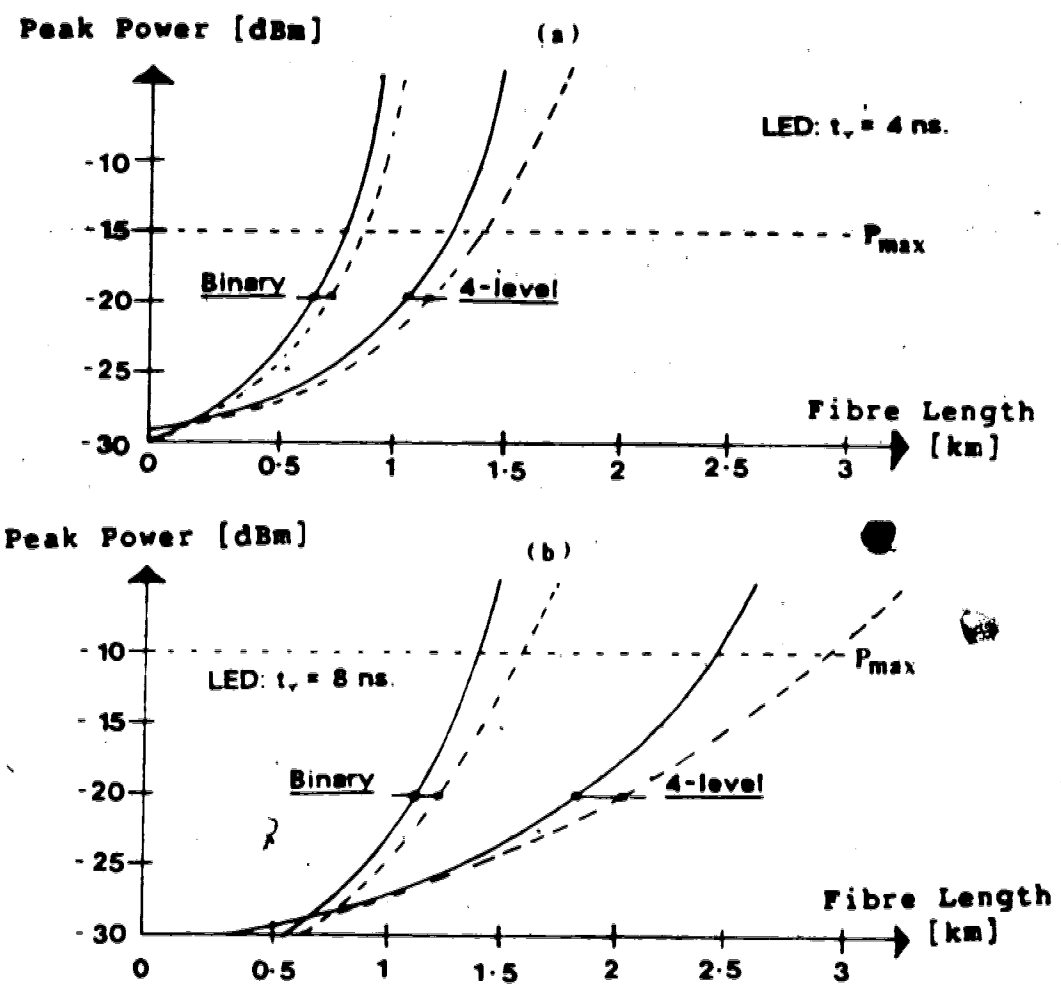


Figure 1.1 Comparison of binary and four-level modulation schemes at (a)140 Mb/sec and (b)70 Mb/sec, using a LED-PIN configuration. The curves show minimum peak power required to achieve BER of 10^{-9} , versus fiber length. The solid line, ———, is for a fiber with modal dispersion of 4 ns/km. The broken line, - - - -, is for an ideal fiber without modal dispersion.

1.2 OPTICAL-COMMUNICATIONS LINK

A generalized diagram of a digital fiber-optic communication link is shown in Fig. 1.2. This diagram applies both to the binary and multilevel modulation schemes. The following sections describe each of the stages shown in Fig. 1.2.

1.2.1 Signal:Shaper/Encoder

The electrical signal is first fed into an encoder/signal shaper. In a digital system the encoder stage detects the incoming data and regenerates and retimes the symbols appropriately for the optical driver. Normally, fiber-optic systems employ intensity modulation using various schemes such as pulse code modulation (PCM), pulse-position modulation (PPM) and pulse amplitude modulation (PAM). PPM has the disadvantage of requiring a large spectrum bandwidth and a jitter free clock. PAM is attractive for band-limited systems, whereas PWM is attractive for systems with wide bandwidth.

There are also a large number of codes possible such as bi-phase (Manchester), delay modulation (Miller), binary return to zero (RZ), binary non return to zero (NRZ) and 2-level alternate mark inversion (AMI) [9]. Choosing a code involves consideration of the following:

1. Power constraint on ILD. The code should have a small duty cycle so as to avoid overdriving the ILD.
2. Error Monitoring. The code should have provision to detect and correct errors occurring during transmission.
3. Dispersion in the fiber (pulse broadening). The code should be such that pulse broadening will not result in too much intersymbol interference.
4. The circuitry required to generate the code should be easy to design.

Other important considerations are clock regeneration and baseline wander.

The signal source normally provides an inherent clock along with the message sequence. The clock can be synthesized from the message signal at the receiver end. To achieve proper clock regeneration and to facilitate the power output control for laser transmitters, it is necessary that the data stream be sufficiently random. Scrambling circuits to achieve randomization of the data scheme and descrambling circuits to recover the original data are readily available.

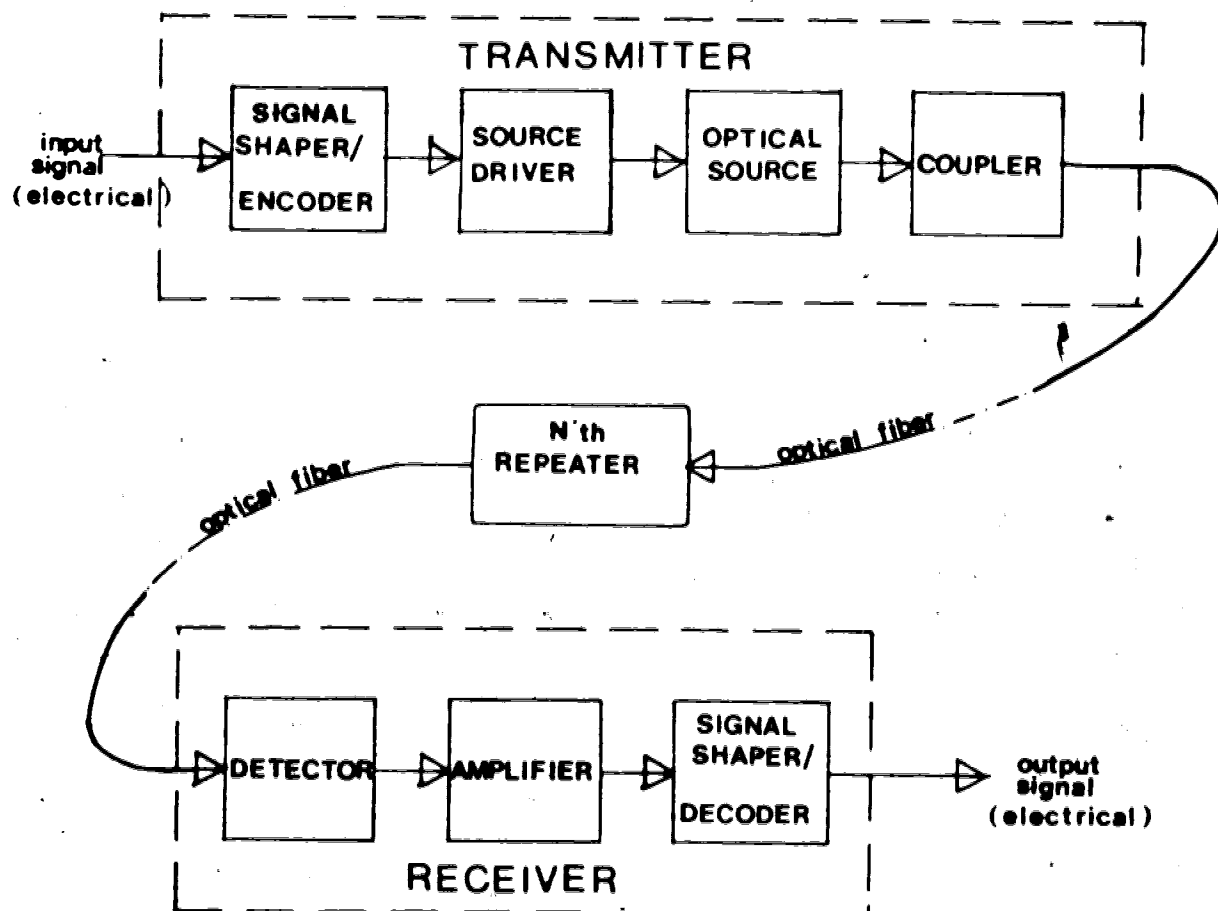


Figure 1.2 Block diagram of a typical optical fiber communication system.

Baseline wander (i.e., the shift in the dc level of a long pulse sequence), arises in digital systems for ac-coupled transmission links using RZ and NRZ codes. When a single positive pulse passes through an ac-coupled system the output pulse has a long tail of opposite polarity. For a sequence of pulses passing through an ac-coupled system, the effect of the tails of individual pulses can accumulate to cause the baseline wander effect. Baseline wander can be reduced by using bipolar coding. The price one has to pay for this is the transmission of a ternary signal (containing the same information as a regular binary signal). A better method to reduce baseline wander is to use a scrambler. Fig. 1.3 shows a number of coding schemes commonly used.

1.2.2 Source Driver and Optical Source

The encoded signal is applied to the source driver. The driver modulates the current flowing through the optical source to produce the desired optical signal. The principal requirements of the source are:

- a. good linearity of the output optical power vs input current characteristics for faithful reproduction of the electrical signal,
- b. narrow spectral bandwidth,
- c. high optical output at low current density,
- d. small emitting area to couple the radiated power efficiently into the fiber,
- e. high frequency response and
- f. long lifetime even with high current density.

Along with these requirements is the additional constraint that these sources should emit radiation in the spectral region where the fiber attenuation is low - 0.8 to 0.9 μm and 1.0 to 1.6 μm . Diodes that emit stimulated radiation are called laser diodes, and those that emit incoherent radiation are denoted as light emitting diodes (LEDs). These diodes are made of single-crystal semiconductor materials (GaAlAs and GaAs for the 0.8 to 0.9 μm spectral region and InGaAs or InGaAsP for the 1.0 to 1.6 μm region) and usually employ a heterojunction structure, where the p- and n- type layers of different energy bandgaps are combined to produce mode confinement.

LEDs are characterised by a threshold current, I_{th} , for stimulated emission as shown in Fig. 1.4 [10]. Above I_{th} the carrier lifetime is very short (thus allowing high

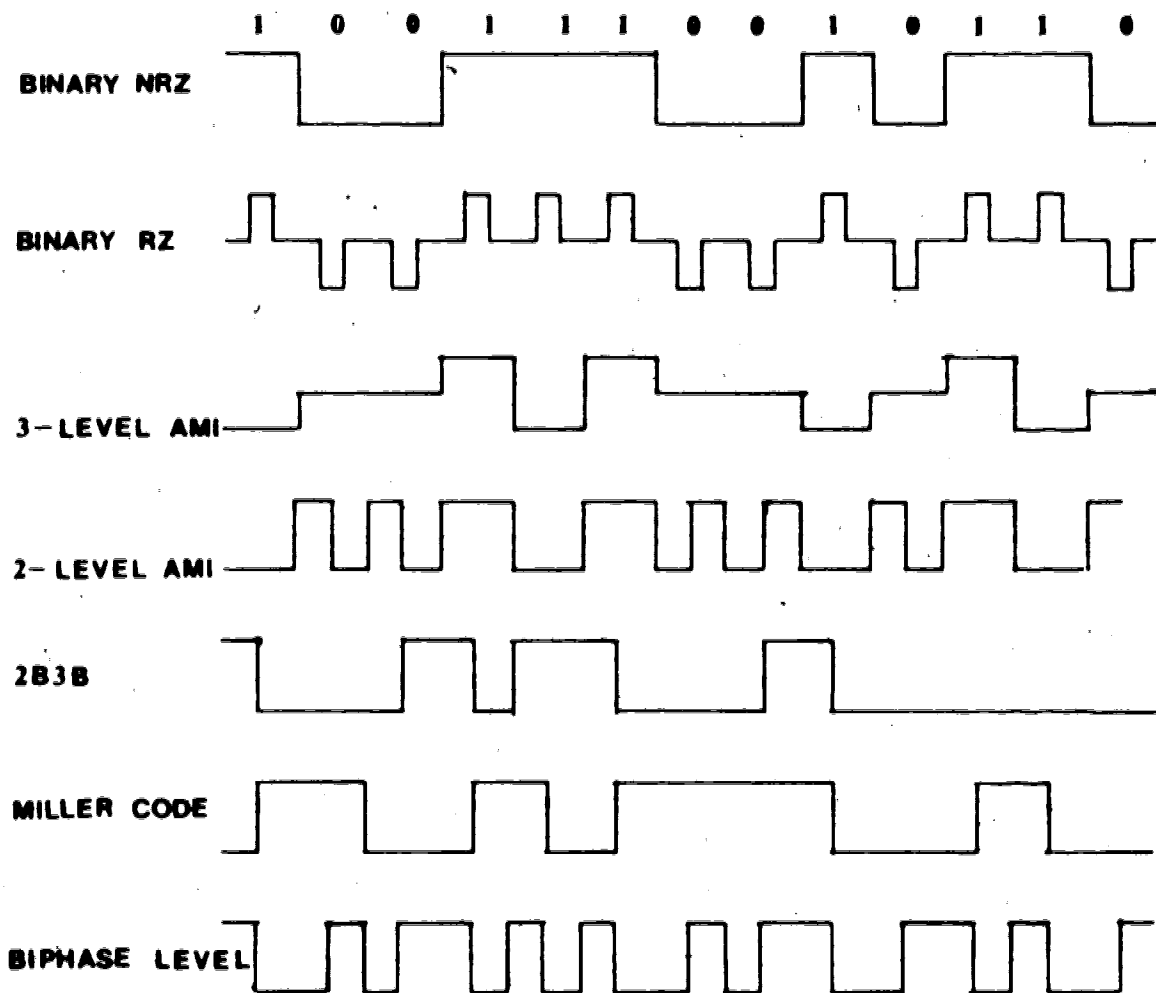


Figure 1.3 Various coding schemes employed in fiber-optic communication systems.

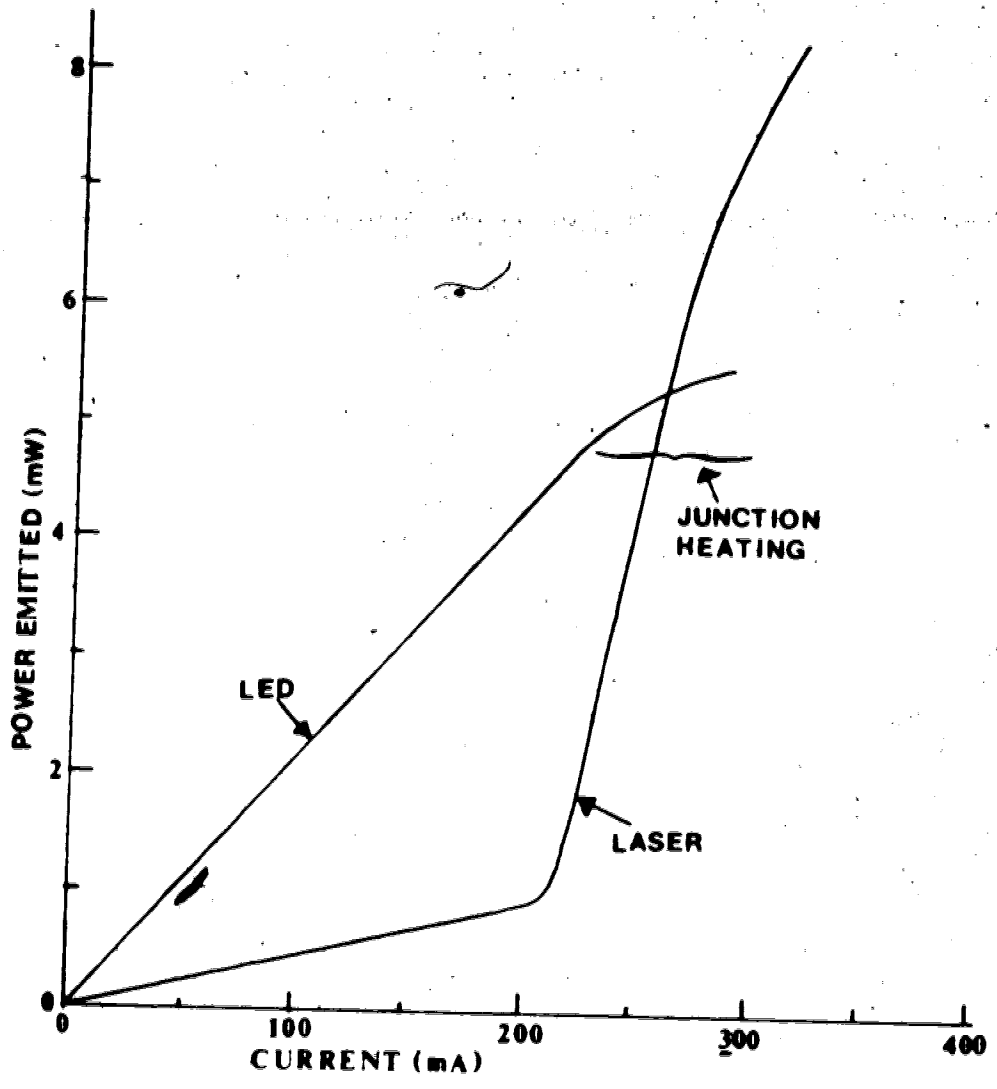


Figure 1.4 Power emitted from an LED and from an ILD as a function of direct current. The knee in the ILD curve is at the threshold current which depends on the device and its construction. The nonlinearity in the curves at high currents is due to junction heating.

modulation rates), the spectral emission narrows down to a few angstrom units of wavelength, the beam becomes highly directional and the quantum efficiency is very high. The LED, on the other hand, has a broad emission spectrum (typically about 100 Å units), a broad-angle beam and a modulation capability limited by the carrier lifetime of approximately 1 ns under optimum conditions.

Although both CW laser diodes and LEDs can emit several milliwatts of optical power, their applications differ. The LED is useful for systems requiring limited bandwidth capability and short-to-moderate transmission distances. The CW laser diode is useful for high data rate and long-distance applications. Being a device with a temperature-dependent threshold, the laser diode is somewhat more difficult to use than the LED. Its reliability and lifetime are also not as high as that of the LED. Keeping all the above considerations in mind, one can then select the optical source best suited for a particular application.

1.2.3 Source-Fiber Coupler

The purpose of the source-fiber coupler is to efficiently launch the optical power into the waveguide. Source-to-fiber coupling techniques include direct butt coupling, the use of microlenses and of tapered or bulb-ended fiber pigtailed. Despite the many different coupling techniques available [11], the butt-joint connector is the one most commonly used. A butt-joint tolerates lateral and axial displacements in the fiber of about 10% of the core diameter and angular misalignments of a few degrees, without a drastic increase in coupling loss.

1.2.4 Optical Cable

The optical cable transmits the optical signal from the transmitter to the receiver either over a single fiber or over a fiber bundle. The principal requirements are low loss and low dispersion but other criteria, such as the dimensional characteristics, modal interaction, bending radius and economic considerations, may be equally important. The fiber types that can be employed in wide-band networks are the graded-index (GI) and single-mode fibers. The advantage of the single-mode fiber is its extremely large bandwidth of many GHz km. This is obtained by using a very small core diameter, which

imposes extremely tight tolerances on splicing and connector techniques. GI fibers have a much larger core diameter than single-mode fibers but still have fairly large bandwidths (in excess of 1 GHz km). GI fibers, because of their ease in splicing and making connections, are much more commonly used than are single-mode fibers.

Depending on the fiber, source and detector characteristics and the total system length, it may be necessary to regenerate the optical signal by the use of repeaters.

1.2.5 Repeater

The repeater acts as a regenerative system element and is designed to enhance the amplitude and the shape of the signal degraded during transmission over the optical fiber. It consists of a photodetector, amplifying and reshaping circuitry, optical source and coupler. Conceptually, the repeater can be described as a back-to-back receiver-transmitter combination.

1.2.6 Fiber-Detector Coupler

The purpose of the fiber-detector coupler is to efficiently couple the optical signals radiating from the fiber into the photodetector. It is designed to minimize the reflective losses at the fiber-detector interface and to match the respective cross-sectional areas.

1.2.7 Detector

The detector converts the received optical power into an electrical current. It must be able to follow the signal emerging from the fiber both in amplitude and phase. These devices should be able to operate in the range of optical frequencies between 0.8 to 0.9 μm and between 1.0 and 1.6 μm . In most optical fiber systems the photodetector used is a p-i-n or an avalanche photodiode, though in principle a phototransistor or photomultiplier could be used. In the 0.8 - 0.9 μm band these photodiodes are made from silicon which provides an excellent spectral match to the emission from sources made from the AlGaAs system. In the 1.0 - 1.6 μm band, detectors using germanium have been made but they have higher leakage current and higher excess noise than their silicon counterparts. Devices using quaternary compounds such as GaAlSb, GaAlAsSb and

InGaAsP are also being developed at these longer wavelengths and they promise characteristics similar to those of silicon detectors at shorter wavelengths.

1.2.8 Amplifier and Signal Shaper-Decoder

The amplifier enhances the electrical signal generated by the detector and increases it to a level at which it can be reshaped for proper further use. The amplifier must have low distortion and its bandwidth should be larger than that of the signal. The signal shaper and decoder finally converts the electrical signal into a form suitable for use. Its design is a function of the intended application.

1.3 THESIS OBJECTIVES

The major objective of this thesis is to correlate the experimental results obtained for a 4-level PAM system with the values theoretically predicted using the Gram-Charlier series model. In keeping with this major objective, the following points are considered:

1. To describe and compare various models used for evaluating error probability in fiber-optic systems.
2. To show the suitability of the Gram-Charlier series model for error probability analysis of fiber-optic systems. Also to develop this model so that it can be applied to multilevel PAM and PWM systems.
3. To incorporate intersymbol interference into the Gram-Charlier series.
4. To design and test a 4-level PAM system using an optical fiber as the transmission medium. The error probability is evaluated as a function of the average optical power reaching the receiver and as a function of the average avalanche gain of the APD.

1.4 ORGANISATION OF THE THESIS

The remaining chapters of this thesis have been organised as follows:

Chapter II discusses the different techniques available for estimating the error probability for fiber-optic systems. Considered in this chapter are the various noise sources existing in a fiber-optic link and their effect on the receiver sensitivity. Special emphasis is given to the Gram-Charlier series method because of the computational ease with which error probability analysis can be carried out using this method. Incorporated into the Gram-Charlier series is the intersymbol interference noise term.

Chapter III describes multilevel PAM systems. The Gram-Charlier series approach is used to compute the optimum power levels and thresholds needed for minimum error probability. The effect of intersymbol interference on the error rate of a 4-level PAM system is analysed. Graphs of BER vs the average optical power and BER vs the mean avalanche gain of the detector are also plotted and the results are analysed. A 4-level PAM system employing a fiber-optic link has been designed, fabricated and tested for a transmission rate of 4.0 Mb/sec. A detailed analysis of this experiment is described in Chapter III. The error probability for different power levels and avalanche gains are obtained experimentally and these are compared to the theoretical values.

Chapter IV deals with the analysis of multilevel PWM systems. The comparison of PWM and PAM systems is also given in this chapter. Multilevel PWM is shown to be an attractive alternative to multilevel PAM, especially for fiber-optic systems.

Chapter V presents the overall conclusions of this thesis and gives some recommendations for further research.

CHAPTER II

ERROR PROBABILITY CALCULATIONS FOR FIBER-OPTIC RECEIVERS

A key element in any optical fiber communication system is the receiver. The basic purpose of the receiver is to convert the modulated light incident upon it into an electrical signal, from which the information impressed on the light at the transmitter is recovered. A digital receiver essentially consists of a photodetector and preamplifier, an amplifier, a filter and a threshold detector.

The incident light is converted into an electrical current by the photodetector. The preamplifier enhances the low-level electrical signal without introducing excessive noise. The filter is used to limit the bandwidth (and thereby eliminate the out-of-band noise). The threshold detector checks if the output signal is below or above a certain threshold and thereby decides whether a 'ONE' or a 'ZERO' was transmitted. Depending upon the overall noise of the system, the threshold detector will make a certain number of errors in decision. The characterisation of the noise sources and their effect on the bit error rate forms the basis of this chapter.

Several methods exist for the analysis of error probability in optical-fiber receivers. The analytical approach of Personick [12],[13] provides the most comprehensive explanation of the various noise sources involved. A slightly simplified approach, suggested by Smith and Garret [14], is described here in detail. Some of the other methods, more suitable for computational purposes, are the Chernoff Bound method [15], the Characteristic Function method [16],[17], the Monte Carlo simulation method [18] and the Gram-Charlier Series method [19]. The relative merits and demerits of these methods are discussed here. A detailed analysis of the Gram-Charlier Series method is given because it will be used for the subsequent analysis of multilevel PAM and PWM systems. Introduced into the Gram-Charlier Series are the intersymbol interference and the thermal noise terms.

¹A binary PCM transmission is assumed here. The two signal levels are denoted by 'ONE' and 'ZERO' which correspond to the higher and lower levels, respectively.

2.1 NOISE SOURCES IN A FIBER-OPTIC SYSTEM

Traditional communication systems involve transmission of electrical signals through wires and cables or via microwave links. The system in all these cases is subject to noise whose mathematical distribution is Gaussian. Such a noise arises from a large number of independent small fluctuations in the transmission medium. The Central Limit Theorem asserts that a system consisting of a large number of independent noise sources has a Gaussian distribution. Because of its simplicity, most of the mathematical analysis in traditional communication systems has centered around Gaussian noise. The Gaussian model is often used to describe an optical fiber system, but such an approach is inaccurate. Light detection is based upon photon counting, which is subject to statistical fluctuations of a Poisson nature. This Poisson noise causes the probability density function (PDF) to depart from the symmetry of a Gaussian density function and introduces a certain skewness in the PDF.

The basic photodetector can be modelled as a current source in parallel with a capacitor and a resistor. This is shown in Fig. 2.1, where C_D represents the overall capacitance (including the photodiode, packaging and lead capacitances) and R_b represents the biasing resistor connecting the detector to the biasing voltage. Consider a light pulse of period T seconds incident on the photodetector. The action of the photodetector is to absorb the incident light power $p(t)$, and to generate hole-electron pairs at times $\{t_n\}$. These hole-electron pairs separate under the influence of the internal electric field, thus resulting in a displacement current $i_s(t)$. The average value of this current is given by:

$$\langle i_s(t) \rangle = Rp(t) \quad (2.1)$$

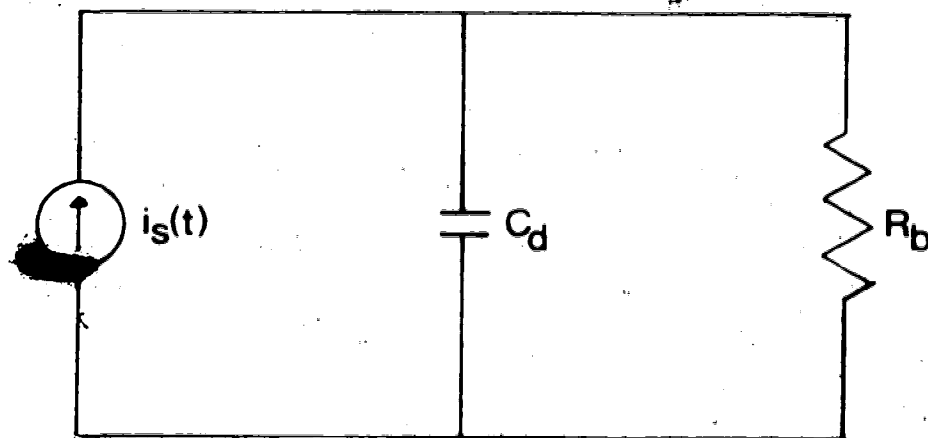
where R = responsivity of the detector

= emitted current / incident power

The average number of hole-electron pairs, λ , that are produced during an interval T is given by [12]:

$$\lambda = (\eta/h\nu) \int_0^T p(t) dt = (\eta/h\nu) E \quad (2.2)$$

where



R_b → biasing resistor

C_d → photodiode capacitance

+ packaging and lead capacitance

+ stray capacitance

$i_s(t)$ → photodiode current

Figure 2.1 A simple model of a photodetector along with its associated biasing resistor.

η = quantum efficiency of the detector (ie. the fraction of incident photons which release hole-electron pairs.)

E = energy of pulse, $p(t)$, over interval T .

Equations (2.1) and (2.2) provide a simplified expression for the current output and the number of hole-electron pairs produced by the photodetector. A complete description of these is only possible by considering the noise arising due to the randomness of the actual number of hole-electron pairs, N , generated by the detector. In addition, the time of occurrence of these events, $\{t_n\}$, is also random. Such a system can be modelled as a Poisson process.

The probability of a photon arriving in a given time interval is proportional to the intensity of the incident light. Thus, a strong signal corresponds to a large number of similarly sized, but randomly timed events.

Fig. 2.2 graphically depicts the photon-counting process. The waveform of $p(t)$ is assumed, for illustrative purposes, to be triangular. Assume that the electron-hole pairs are generated at random times $\{t_n\}$. For a perfect optical detector, the voltage response across the load resistor, for a single electron-hole pair, should be an impulse. Fig. 2.2(c) gives the output of such an optical detector when a single photon has been detected. Fig. 2.2(d) shows the same output considering the finite response of the detector, $h(t)$. The overall pulse output, $v(t)$, resulting from the responses to all the electron-hole pairs (as shown in fig. 2.2(e)) has a smooth mean envelope pulse, which follows the mean arrival rate for photons, but has superimposed upon it a large, signal-dependent noise. The pulse output, $v(t)$, can be described as:

$$v(t) = \sum_{n=1}^N a_n h(t-t_n) \quad (2.3)$$

where a_n are the received levels and $h(t)$ is the response of the detector. The value of a_n depends on the number of counts, N , made during a pulse interval. The probability of n electron-hole pairs being produced is given by the Poisson distribution:

$$P(N=n) = (\lambda^n e^{-\lambda}) / n! \quad (2.4)$$

From Poisson statistics, a mean number, λ , of photons is expected and there is a random fluctuation of N about that mean from pulse to pulse. This signal dependent

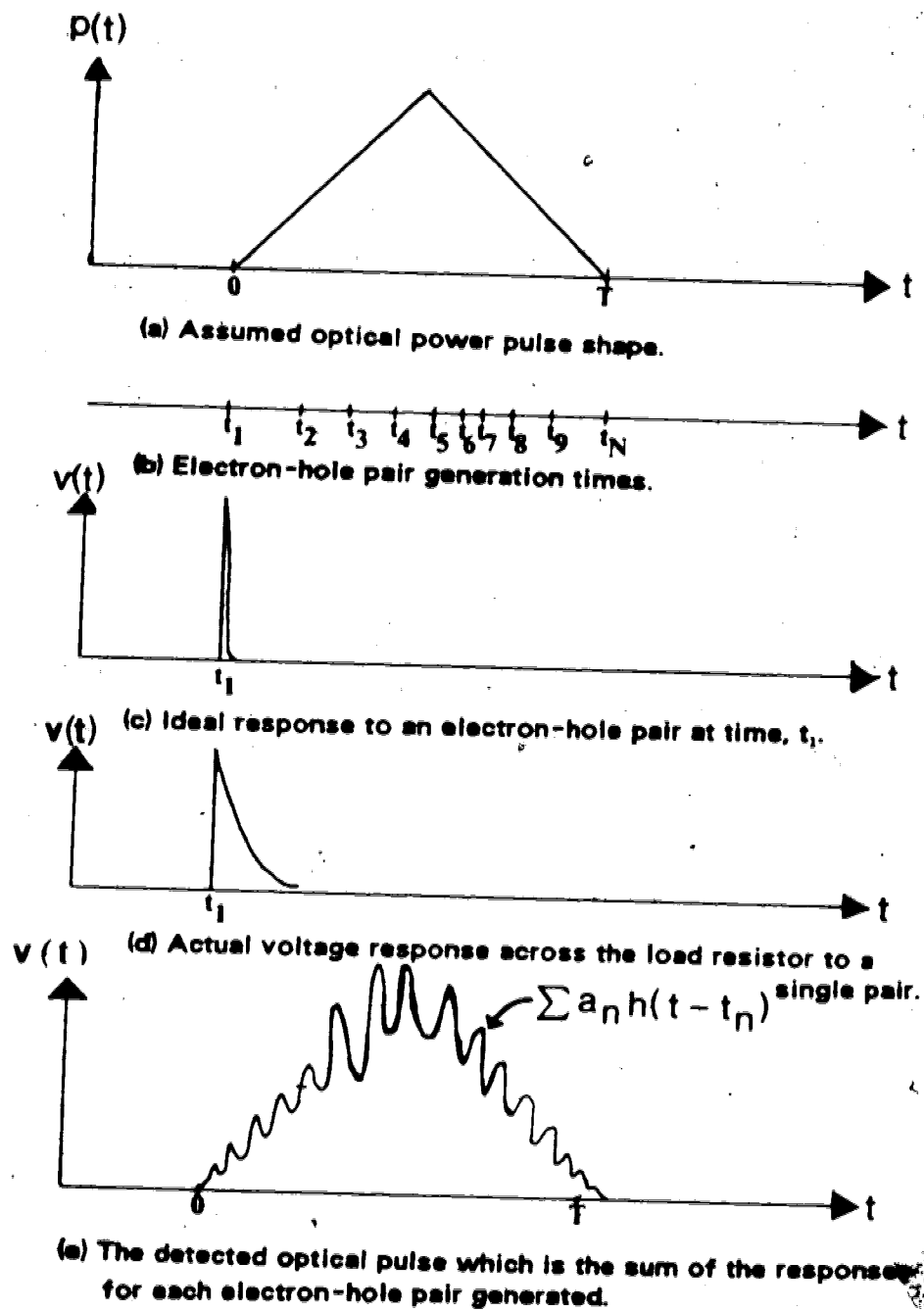


Figure 2.2 The Photon-counting process in a photodetector diode

noise, called *quantum noise*, is shown in Fig. 2.2a.

In addition to the quantum noise, there is also the noise due to random gain mechanisms of the avalanche photodiode. Such a noise is often termed *excess noise*. Despite the excess noise, avalanche multiplication of the electron-hole pairs can increase the sensitivity of receivers. Other noise sources existing in fiber optic detectors are the dark current and the thermal noise. There are actually two types of dark current noise. The first, called simply *dark current*, consists of hole-electron pairs which are thermally liberated in the p-n junction and which are multiplied by the avalanche gain. The other dark current noise, referred to as *leakage current*, bypasses the drift region and experiences no avalanche gain. Fig. 2.3 shows all these noise sources and, in addition, other noise sources in a fiber-optic system, such as *beat noise* for an LED, *device noise* of the active element, *surface leakage current* and the *thermal noise* of the amplifier. Beat noise occurs for an incoherent source (such as an LED) due to beats between spectral components. Beat noise is typically very small and is normally neglected in error probability and sensitivity analysis. The dark current and the surface leakage current can be reduced by a proper choice of the detector material and careful design of the detector as well as the preamplifier. The quantum noise, the dark-current noise, the surface-leakage-current noise and the excess noise are grouped together as shot noise, which is characterised by Poisson statistics. The signal-dependent shot noise results in a departure of the PDF from symmetry (i.e., causes skewness).

2.2 THE ANALYTICAL APPROACH TO DETERMINE ERROR PROBABILITY

The analytical approach of Personick [12],[13], as modified by Smith and Garrret [14] is considered here. Fig. 2.4 is an equivalent circuit for the receiver. The receiver consists of a photo-detector with biasing circuit, an amplifier, an equaliser and a threshold detector. The photo-detector is modelled as a current source, $i_b(t)$, in parallel with the capacitance, C_D . The biasing resistor is represented by R_b . The amplifier is modelled as an ideal high gain, infinite input impedance amplifier with a shunt capacitance and resistance (C_A and R_A) across the input. The Johnson current noise (thermal noise) source due to R_b is modelled as $i_b(t)$. The amplifier current and voltage noise sources are $i_a(t)$ and $e_a(t)$ respectively. All these noise sources are assumed to be white, Gaussian

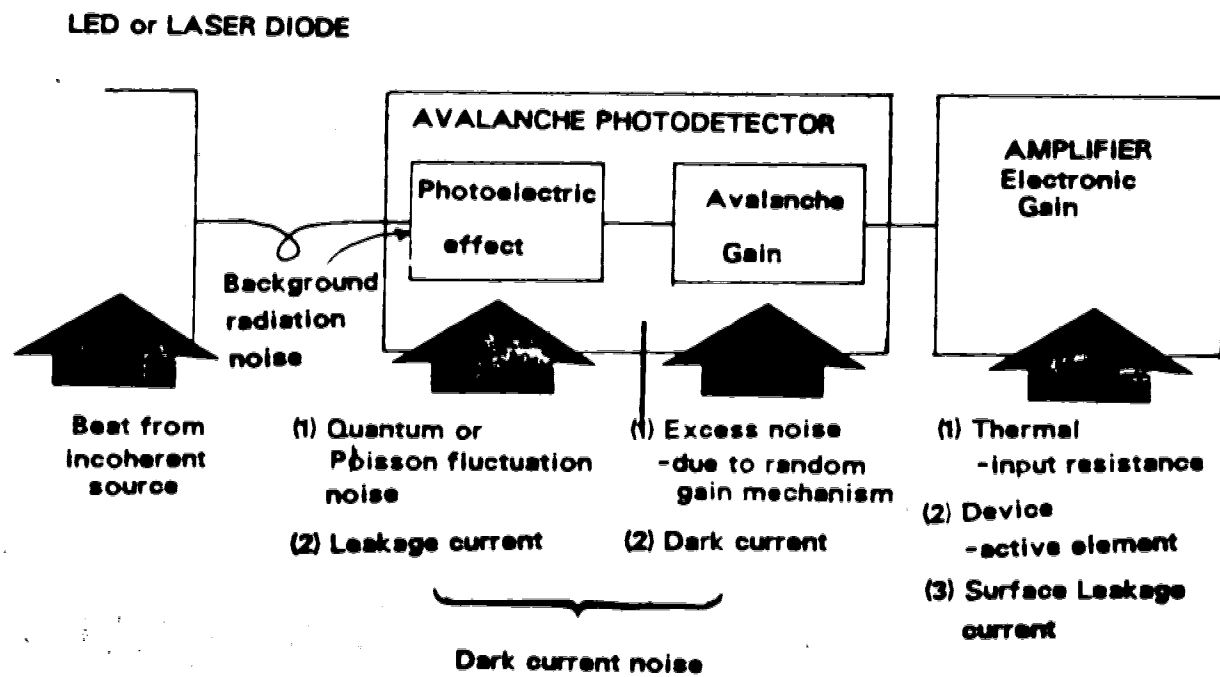


Figure 2.3 Noise mechanisms in a fiber-optic communication system.

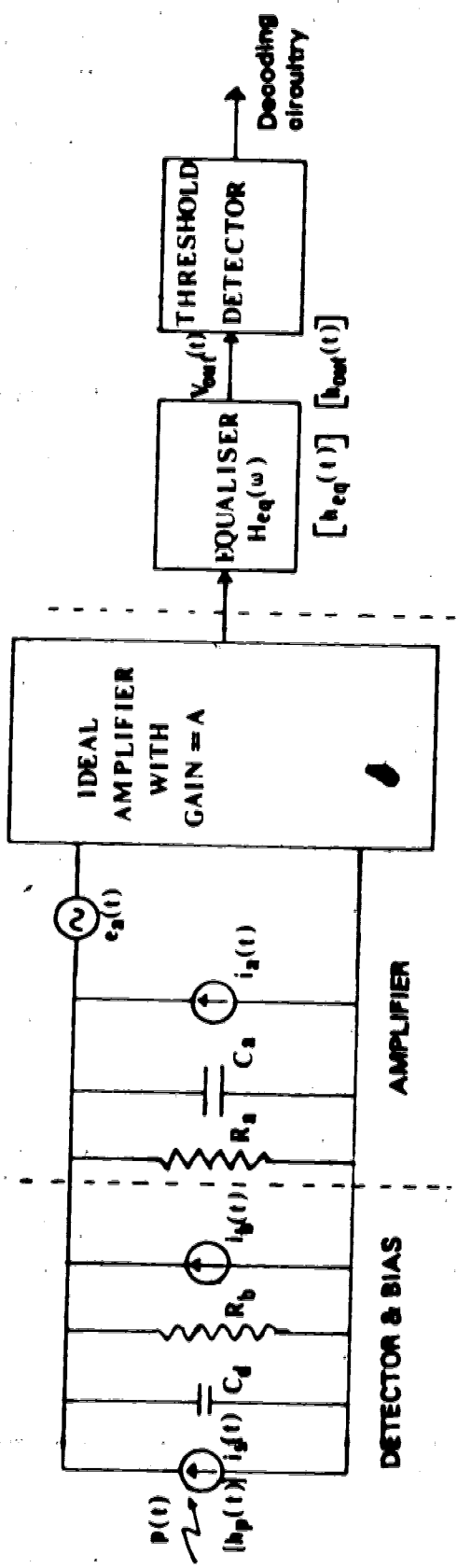


Figure 2.4 Equivalent circuit for the fiber-optic receiver.

and uncorrelated

Assume that the optical signal, $p(t)$, incident on the detector is a digital pulse stream², represented by:

$$p(t) = \sum_{n=-\infty}^{\infty} b_n h_p(t-nT) \quad (2.5)$$

where:

T = bit time slot

$h_p(t)$ = pulse shape:

b_n = energy in the n th pulse, which can take two values, depending on whether a 'ZERO' or a 'ONE' was transmitted.

The probability of producing exactly N counts during time interval (t_0, t_0+T) is given by (2.4).

$$P[N, (t_0, t_0+T)] = (\Lambda^N e^{-\Lambda}) / N! \quad (2.6)$$

where:

$$\Lambda = \int_{t_0}^{t_0+T} \lambda(t) dt$$

and where $\lambda(t)$ is the average rate of electron-hole pair production.

$$\lambda(t) = (\eta/h\nu) p(t) + \lambda_0 \quad (2.7)$$

λ_0 denotes the dark current counts per second

The average detector current output, $\langle i_s(t) \rangle$, is given by:

$$\langle i_s(t) \rangle = (\eta q / (h\nu)) \langle g \rangle p(t) + \langle g \rangle q \lambda_0 \quad (2.8)$$

where:

$\langle g \rangle$ = average avalanche gain of the APD

q = electron charge

Neglecting the dark current noise term in (2.8), the average voltage at the equaliser output is:

²Multilevel systems are considered in the next chapter.

$$\langle v_{out}(t) \rangle = (\eta q / (h\nu)) \langle g \rangle A_p(t) * h_b(t) * h_{eq}(t) \quad (2.9)$$

where $h_b(t)$ is the amplifier input circuit current impulse response given by:

$$h_b(t) = \mathcal{F} \left[\left(\frac{1}{R_T} + j\omega C_T \right) \right] \quad (2.10)$$

and where:

$h_{eq}(t)$ = impulse response of the equaliser

$$R_T = R_a // R_b$$

$$C_T = C_a + C_d$$

The average output voltage can also be described in series form as:

$$\langle v_{out}(t) \rangle = \sum_{-\infty}^{\infty} b_n h_{out}(t - nT) \quad (2.11)$$

where $h_{out}(t)$ represents the output pulse shape.

Superimposed on this average voltage are the various noise sources described earlier

$$\begin{aligned} v_{out}(t) &= \langle v_{out}(t) \rangle + n(t) \\ &= \sum_{-\infty}^{\infty} b_n h_{out}(t - nT) \end{aligned} \quad (2.12)$$

where $n(t)$ is the noise voltage at the equaliser output.

The variance of $n(t)$, N , is defined as:

$$N = \langle n^2(t) \rangle = \langle v_{out}^2(t) \rangle - \langle v_{out}(t) \rangle^2 \quad (2.13)$$

Assuming all the noise sources are mutually independent

$$\begin{aligned} N &= \langle n_s^2(t) \rangle + \langle n_r^2(t) \rangle \\ &\quad + \langle n_d^2(t) \rangle + \langle n_{T_1}^2(t) \rangle \end{aligned} \quad (2.14)$$

where

$n_s(t)$ = The output noise voltage due to the shot noise current, $i(t)$, produced by the detector.

$n_r(t)$ = The output Johnson noise voltage due to the resistor R_T .

$n_i(t)$ = The output noise due to the amplifier input current noise source, $i_g(t)$, and

$n_e(t)$ = Output noise voltage due to the amplifier input voltage noise source, $e_g(t)$.

2.2.1 Shot Noise

Personick [12] has evaluated the shot noise term, $n_i(t)$, at the equaliser output as a function of time within the bit time slot, T . This results in a comprehensive but rather complicated analysis. Smith and Garret [14] make the assumption that the shot noise is constant within the bit time slot. The resulting analysis is much simpler and is still quite accurate. The shot noise expression is given by [14]:

$$\langle n_i^2(t) \rangle = 2q \langle i_0 \rangle_T \langle g^2 \rangle B_N R_T^2 A^2 \quad (2.15)$$

where:

$\langle i_0 \rangle_T$ is the mean unity-gain photocurrent over the bit time T . Contributions from neighbouring pulses may affect $\langle i_0 \rangle_T$, if they spread out into the bit time under decision.

B_N is the noise equivalent bandwidth, defined as

$$\begin{aligned} 2B_N &= (1/R_T^2) \left[\int_{-\infty}^{\infty} |H_{eq}(f) H_p(f)|^2 df \right] \\ &= (1/R_T^2) |h\nu / (A\eta q \langle g \rangle)|^2 \int_{-\infty}^{\infty} |H_{eq}(f) / H_p(f)|^2 df \end{aligned} \quad (2.16)$$

where $H(f)$ is the Fourier transform of $h(t)$.

The shot noise expression of (2.15) will now be evaluated for the worst intersymbol interference case, i.e., when all neighbouring pulses are ON. The two possible cases, i.e. an ON pulse or an OFF pulse at the decision time, will be considered separately.

When there is an ON pulse at the decision time, the average power, $P_{avg}(t)$, during time slot $\{-(T/2), (T/2)\}$ due to a pulse centered at $t = nT$ is:

$$P_{avg}(t) = (b_1/t) \int_{-T/2}^{T/2} h_p(t-nT) dt \quad (2.17)$$

Therefore the mean unity gain photocurrent,

$$\begin{aligned}
\langle I_o \rangle_{T, ON} &= \sum_{n=0}^{\infty} (\eta q / h\nu) (b_1 / T) \int_{-T/2}^{T/2} h_p(t - nT) dt \\
&\quad - (\eta q / h\nu) (b_1 / T) \sum_{n=0}^{\infty} \int_{-T/2}^{T/2} h_p(t - nT) dt \\
&\quad - (\eta q / h\nu) (b_1 / T) \int_{-T/2}^{T/2} h_p(t) dt = (\eta q / h\nu) (b_1 / T)
\end{aligned} \tag{2.18}$$

When there is an OFF pulse at the decision point

$$\begin{aligned}
\langle I_o \rangle_{T, OFF} &= \sum_{n=0}^{\infty} (\eta q / h\nu) (b_1 / T) \int_{-T/2}^{T/2} h_p(t - nT) dt \\
&= (\eta q / h\nu) (b_1 / T) (1 - \gamma)
\end{aligned} \tag{2.19}$$

where

$$\gamma = \int_{-T/2}^{T/2} h_p(t) dt$$

Equations (2.18) or (2.19), when substituted into the shot noise expression (2.15), give the worst case shot-noise, $\langle n_s^2(t) \rangle_{ON}$ or $\langle n_s^2(t) \rangle_{OFF}$ respectively

2.2.2 Thermal Noise

The thermal noise contribution to the output noise voltage arises from the bias resistor, $\langle V_R^2 \rangle$, the amplifier noise current, $\langle V_I^2 \rangle$ and the amplifier noise voltage, $\langle V_E^2 \rangle$. These are expressed as

$$\begin{aligned}
\langle V_R^2 \rangle &= (4k\theta / R_p) B_N R_p^2 A^2 \\
\langle V_I^2 \rangle &= 2S_p B_N R_p^2 A^2 \\
\langle V_E^2 \rangle &= 2S_p B_N A^2
\end{aligned} \tag{2.20}$$

where

$$\begin{aligned}
2B_N &= \int_{-\infty}^{\infty} |H_{out}(f)|^2 df \\
&= |(h\nu) / (A\eta q \langle g \rangle)|^2 \int_{-\infty}^{\infty} |H_{out}(f) / (H_p(f) H_b(f))|^2 df
\end{aligned} \tag{2.21}$$

and B_N is as defined in (2.16).

These results are derived from the well known formula

$$S_{out}(f) = S_{in}(f) |H(f)|^2 \quad (2.22)$$

where:

$S_{out}(f)$ = Output power spectral density.

$S_{in}(f)$ = Input power spectral density.

$H(f)$ = filter response.

The overall thermal noise term is, therefore

$$\begin{aligned} \langle V_{th}^2 \rangle &= \langle V_R^2 \rangle + \langle V_I^2 \rangle + \langle V_N^2 \rangle \\ &= ((2k\theta/R_b) + S_I) 2B_N R_T^2 A^2 + 2S_N B_N^2 A^2 \end{aligned} \quad (2.23)$$

The overall noise term, including the shot noise and thermal noise is:

$$\begin{aligned} \langle V_N^2 \rangle &= [((2k\theta/R_b) + S_I) A^2 + q \langle I_0 \rangle_T \langle g^2 \rangle A^2] \cdot \\ &\quad 2B_N R_T^2 + 2S_N B_N^2 A^2 \\ &= [(2k\theta/R_b) + S_I + q \langle I_0 \rangle_T g^{2+\alpha}] \cdot \\ &\quad \Lambda^2 |h\nu| / (\Lambda \eta q \langle g \rangle) \int_{-\infty}^{\infty} |H_{out}(f)/H_p(f)|^2 df \\ &\quad + S_N \Lambda^2 |h\nu| / (\Lambda \eta q \langle g \rangle) \int_{-\infty}^{\infty} |H_{out}(f)/(H_p(f)H_b(f))|^2 df \end{aligned} \quad (2.24)$$

Here, the approximation $\langle g^2 \rangle = \langle g \rangle^2$ has been used [20]. A more accurate expression is given later, but to simplify the calculations, it is not used here.

In order to make the bandwidth integrals of (2.24) independent of bit time, T , and a function of only the pulse shape, the following dimensionless time and frequency variables are introduced:

$$\xi = t/T \text{ and } \varphi = fT.$$

Therefore,

$$H_p'(\varphi) = H_p(f) \text{ and } H_{out}'(\varphi) = H_{out}(f)/T \quad (2.25)$$

$H_p'(\varphi)$ and $H_{out}'(\varphi)$ depend only on the shape of $H_p(\omega)$ and $H_{out}(\omega)$ and not upon the time slot width, T .

Let us define the following integrals:

$$I_2 = \int_{-\infty}^{\infty} |H_{out}(\varphi)/H_p(\varphi)|^2 d\varphi \quad (2.26)$$

$$I_3 = \int_{-\infty}^{\infty} \varphi^2 |H_{out}(\varphi)/H_p(\varphi)|^2 d\varphi \quad (2.27)$$

Then:

$$\int_{-\infty}^{\infty} |H_{out}(f)/H_p(f)|^2 df = TI_2 \quad (2.28)$$

and

$$\begin{aligned} \int_{-\infty}^{\infty} |H_{out}(f)/(H_p(f)H_b(f))|^2 df \\ = \int_{-\infty}^{\infty} |H_{out}(f)/H_p(f)|^2 |R_T + j\omega C_T|^2 df \\ = R_T^2 TI_2 + (2\pi C_T)^2 I_3/T \end{aligned} \quad (2.29)$$

Substituting (2.28) and (2.29) into (2.24) gives

$$\begin{aligned} \langle V_n^2 \rangle &= [(2k\theta/R_b) + S_T q \langle I_0 \rangle_T \langle g \rangle^{2+n}] |h\nu / (\eta q \langle g \rangle)|^2 TI_2 \\ &\quad + S_E |h\nu / (\eta q \langle g \rangle)|^2 [R_T^2 TI_2 + (2\pi C_T)^2 I_3/T] \\ &= (h\nu\eta)^2 \{ \langle g \rangle^2 \langle I_0 \rangle_T TI_2/q + Z/\langle g \rangle^2 \} \end{aligned} \quad (2.30)$$

where Z is the thermal noise term given by

$$\begin{aligned} Z &= [S_T + (2k\theta/R_b) + (S_E/R_T)] TI_2 / \langle g \rangle^2 \\ &\quad + (2\pi C_T)^2 S_E I_3 / (T \langle g \rangle^2) \end{aligned} \quad (2.31)$$

From the above equation one can clearly see that increasing R_T and decreasing C_T lowers the thermal noise term, Z. This is made use of in the high input impedance amplifier approach. Other amplifier designs are discussed in Chapter 3.

Using the above equations one can proceed to calculate the receiver sensitivity and the optimum avalanche gain.

2.2.3 Receiver Sensitivity

Although the shot noise, $\langle n_s(t) \rangle$, has a Poisson distribution, the inaccuracy resulting from using the Gaussian approximation is not large [12]. The other noise term, i.e. the thermal noise, is already Gaussian. Therefore the overall noise term, $\langle v_N(t) \rangle$, is also Gaussian. The signal amplitude dependence of the shot noise is taken into account by the variance of the Gaussian distribution. σ_{ON} and σ_{OFF} are defined as the worst case values of $\langle v_N(t) \rangle$ for ON and OFF pulses respectively. These are obtained by substituting $\langle n_s(t) \rangle_{ON}$ and $\langle n_s(t) \rangle_{OFF}$ into (2.14), i.e.

$$\begin{aligned}\sigma_{ON} &= \langle v_N^2 \rangle^{1/2} | \langle n_s(t) \rangle_{ON} - \langle n_s(t) \rangle_{OFF} | \\ \sigma_{OFF} &= \langle v_N^2 \rangle^{1/2} | \langle n_s(t) \rangle_{OFF} - \langle n_s(t) \rangle_{OFF} |\end{aligned}\quad (2.32)$$

Let m_0 and m_1 be the mean signal values for an OFF pulse and an ON pulse respectively, as illustrated in Fig 2.5. Assuming that the threshold, V_{th} , is set to give equal area probability, P_E , for ON and OFF pulses (i.e. the equal area criteria), then

$$[(m_1 - V_{th}) / \sigma_{ON}] = [(V_{th} - m_0) / \sigma_{OFF}] = Q \quad (2.33)$$

where

$$P_E = (2\pi)^{-1/2} \int_Q^\infty \exp(-x^2/2) dx = 0.5 \operatorname{erfc}(Q/\sqrt{2}) \quad (2.34)$$

If m_0 is zero, then from (2.33)

$$[(m_1 - V_{th}) / \sigma_{ON}] = (V_{th} / \sigma_{OFF}) = Q \quad (2.35)$$

$$\text{or } m_1 = Q(\sigma_{ON} + \sigma_{OFF})$$

$$\begin{aligned} &= (Q/\langle g \rangle) (h\nu/\eta) \{ [\langle g \rangle^{2\alpha} (\eta/h\nu) b_{on} I_0 + Z]^{1/2} \\ &\quad + [\langle g \rangle^{2\alpha} (\eta/h\nu) b_{off} (1-\gamma) I_0 + Z]^{1/2} \} \end{aligned}\quad (2.36)$$

Equation (2.36) is the required sensitivity of the receiver for a given P_E (and therefore for a given Q value). For a PIN diode detector (with $\langle g \rangle = 1$) this equation reduces to the simple form:

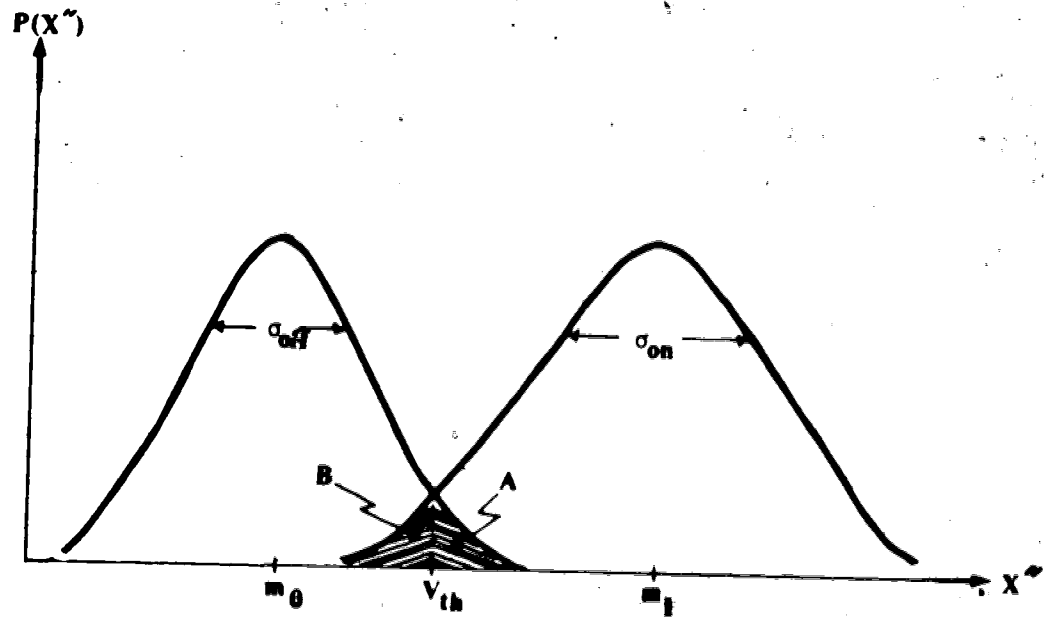


Figure 2.5 Probability density curves for an OFF and an ON pulse assuming Gaussian distribution. The mean value of the OFF and ON pulse are m_0 and m_1 respectively. The corresponding variances of the OFF and ON pulses are σ_{OFF} and σ_{ON} . The threshold, V_{th} , is chosen using the equal area criterion (i.e. the shaded areas A and B are set equal).

$$m_1 = 2Q(h\nu/\eta) \sqrt{L} \quad (2.37)$$

2.2.4 Optimum Avalanche Gain

The optimum avalanche gain is found by differentiating (2.36): i.e., $\partial b_{on} / \partial \langle g \rangle = 0$. This results in the following equation from which the optimum gain, g_{opt} , is calculated:

$$g_{opt}^{(2+\pi)} m_1 = (h\nu/\eta) (Z/2I_2) ((2-\gamma)/(1-\gamma)) K \quad (2.38)$$

where:

$$k = -1 + \left[1 + 16 \left(\frac{1+x}{x^2} \right) \left(\frac{1-\gamma}{(2-\gamma)^2} \right) \right]^{1/2}$$

Corresponding to this the minimum value of m_1 is:

$$m_{1,min} = Q \left(\frac{2+x}{1+x} \right) (h\nu/\eta) Z \frac{x}{2+2x} I_2 \frac{1}{1+x} L \quad (2.39)$$

where:

$$L^{1+\pi} = \left[2(1-\gamma)/k(2-\gamma) \right] \cdot \left\{ \left[0.5 \left(\frac{2-\gamma}{1-\gamma} \right) k + 1 \right]^{1/2} + \left[0.5(2-\gamma)k + 1 \right]^{1/2} \right\}^{2+\pi}$$

2.2.5 Remarks on Analytical Methods

The analytical approach basically makes use of the theory developed by Personick [12]. The probability density function, $p(x)$, can be derived from equations (2.30) and (2.31). However, an exact analytical solution to these equations is not possible without making a few simplifying assumptions. One of the most commonly used approximations is the Gaussian approximation. The major advantage of the Gaussian approximation is that one requires only the mean and variance of the output voltage. These are normally easy to obtain. The Gaussian approximation, however, does not take into account the extreme skewness of the avalanche gain distribution. As a result it tends to overestimate the optimal avalanche gain and underestimate the optimal threshold level. An alternative to the

Gaussian approximation is the Chernoff bound method [15]. The Chernoff Bound replaces the exact solution by a simpler solvable formulation that gives the upper bound solution. The Chernoff Bound method is very effective because it gives us the upper bound of the error probability. Nevertheless, to estimate how close these bounds are to the real solution requires the use of numerical and statistical methods.

2.3 OTHER APPROACHES TO ERROR PROBABILITY CALCULATIONS

Consider the fiber-optic communication system depicted in Fig. 2.6. The current output of the photodetector is denoted as $x(t)$ and the filter output as $y(t)$. To compute the error rate, one needs to know the statistics of the voltage at the decision making point, i.e. at the output of the filter in Fig. 2.6. The output of the filter is given by:

$$y(t) = \int_{-\infty}^{\infty} x(\tau) h(t-\tau) d\tau \quad (2.40)$$

The error probability can then be computed as:

$$P_E = a_0 P_0(y) + a_1 P_1(y) \quad (2.41)$$

where:

a_0 and a_1 are the probabilities of sending ZERO and ONE signals, respectively and

Y is the threshold.

$P(y) = P(y|ZERO)$ dy is the cumulative distribution for a ZERO signal transmitted.

$$= \int_Y^{\infty} p(y_{t_0}|ZERO) dy \quad (2.42)$$

$P(Y) = P(y|ONE)$ dy is the cumulative distribution when a ONE signal is transmitted.

$$= \int_{-\infty}^Y p(y_{t_0}|ONE) dy \quad (2.43)$$

There are three different approaches to solving (2.40) and (2.41). These are

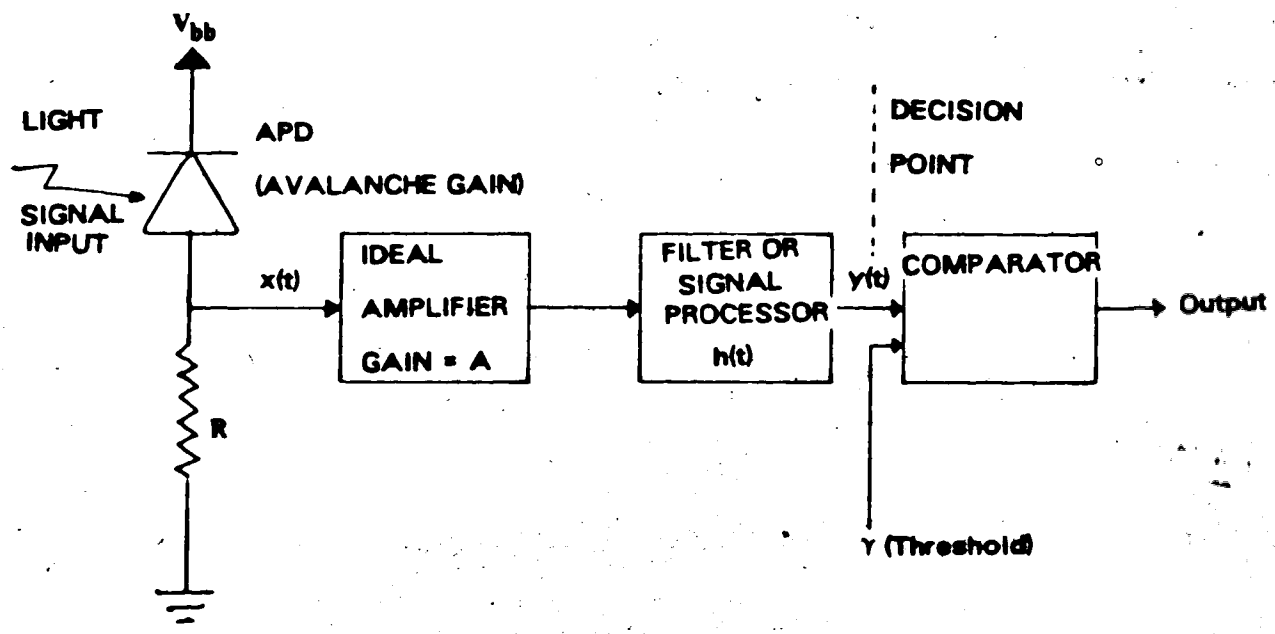


Figure 2.6 Simplified fiber-optic receiver block diagram.

1. Analytical methods
2. Numerical methods
3. Statistical methods

The Analytical approach has already been discussed in great detail. The Numerical and Statistical methods are discussed in the subsequent sections.

2.3.1 Numerical Methods

Many numerical methods exist for solving (2.40) and (2.41). Normally, $x(t)$ is broken up into two components, $x_s(t)$ and $x_{th}(t)$, i.e. the signal output of the avalanche diode and the Gaussian thermal noise generated by the amplifier. If t_0 is the sampling time, chosen so as to maximise $y(t_0)$, then

$$y(t_0) = \int_{-\infty}^{\infty} x(\tau) h(t_0 - \tau) d\tau \quad (2.44)$$

Since

$$x(t) = x_s(t) + x_{th}(t) \quad (2.45)$$

Therefore

$$\begin{aligned} y(t_0) &= \int_{-\infty}^{\infty} x_s(\tau) h(t_0 - \tau) d\tau \\ &\quad + \int_{-\infty}^{\infty} x_{th}(\tau) h(t_0 - \tau) d\tau \\ &= y_s(t_0) + y_{th}(t_0) \end{aligned} \quad (2.46)$$

The output voltage, $y(t)$, is consequently composed of two parts, the signal dependent voltage, $y_s(t_0)$ and the Gaussian term, $y_{th}(t_0)$. The standard deviation of y_{th} is

$$\sigma_{th} = (4kTB_w/R_{th})^{1/2} \quad (2.47)$$

where B_w is the effective noise bandwidth of $h(t)$ and R_{th} is the thermal resistance

The effective noise bandwidth is defined as

$$B_w = (1/|H_0|^2) \int_0^{\infty} |H(f)|^2 df \quad (2.48)$$

where $H(f)$ is the Fourier transform of $h(t)$ and $|H_0|$ is the maximum absolute value of $H(f)$

Assuming a rectangular shape for $x_s(t)$ and a raised cosine shape for $h(t)$, the discrete

The probability distribution of $y_{th}(t_0)$ is Gaussian since x_{th} is a thermally generated noise

approximation of the signal $y_s(t)$ is:

$$y_s = (T/N) \sum_{n=1}^N x_n h_{n-s} \quad (2.49)$$

where T is the duration of the signal and N is the number of samples used in the approximation. The samples x_n are independent and have a distribution dictated by equations (2.30) and (2.31) for a time interval $\Delta T = T/N$. An approximation for the probability density function (PDF), $p(x)$, suitable for computing purposes, was obtained by Webb, McIntyre and Conradi [21]. This approximate PDF for the current at the output of the APD is:

$$p(x) = \left\{ \frac{1}{[(2\pi)^{0.5} \sigma [1 + ((x-M)/\sigma\lambda)]^{0.5}]} \right\} \cdot \exp\left\{ -\frac{(x-M)^2}{2\sigma^2 [1 + ((x-M)/\sigma\lambda)]} \right\} \quad (2.50)$$

where

$M = (\eta_e \cdot q/T)G =$ mean output current

$q =$ charge of an electron

$T =$ time interval between pulses

$G =$ average avalanche gain

$\eta_e = (\eta T/h\nu) P_{opt} =$ number of primary electrons

$\eta =$ optical conversion efficiency

$P_{opt} =$ average optical power in time T

$h\nu =$ energy of a photon

$\lambda = \sqrt{\eta_e \cdot F_e} (F_e - 1)$

$\sigma^2 = G^2 \eta_e F_e \cdot (q/t)^2 =$ variance of the diode current

$F = k_{eff} G + [2 - (1/G)](1 - k_{eff}) =$ excess noise factor

$k_{eff} =$ effective ionisation ratio

Since the random variables x_n are independent, the density of their sum equals the convolution of their respective densities.

$$p(y_s) = \left[\frac{1}{(\Delta T)^N \prod_{n=0}^{N-1} h_n} \right] \left\{ P\left[\frac{x_1}{(\Delta T \cdot h_{N-1})} \right] \cdot P\left[\frac{x_2}{(\Delta T \cdot h_{N-2})} \right] \cdot \dots \cdot P\left[\frac{x_N}{(\Delta T \cdot h_0)} \right] \right\} \quad (2.51)$$

The thermal noise is also additive and independent, therefore the overall probability density function, $p(y)$, of the output voltage, $y(t)$, is:

$$p(y) = p(y_0) * p(y_{1N}) \quad (2.52)$$

The fastest and simplest way to compute $p(y)$ is to transform all partial densities using the *Fast Fourier Transform (FFT)*, multiply them and take an inverse FFT.

$$p(y) = [1/(\Delta T)^n \prod_{i=1}^n |K(h_{iN})|] \cdot \mathcal{F}^{-1} \left(\prod_{i=1}^n \mathcal{F} [P(x_{iN}/\Delta T, h_{iN-1})] \right) \mathcal{F} [p(y_{1N})] \quad (2.53)$$

The Fourier Transform method suffers from numerical errors since it is computed as a sum of positive and negative numbers⁴

Direct convolution produces less truncation error in $p(y)$, because the probability densities are positive functions. This method, however, requires an excessive number of arithmetic operations. For example, if we have n distributions each having M points, the number of operations (multiplication and addition) will be

$$N = n! M^2 / 2^n \quad (2.54)$$

For $M = 100$ and $n = 2$, $N = 10^4$ which is a manageable number. But for $M = 100$ and $n = 10$, $N = 3.5 \times 10^7$, which is excessive. Thus the convolution method is of use for only limited cases.

The *Gauss Quadrature rule method* is a numerical technique used to evaluate the integrals for the conditional probability densities in (2.41). Most numerical integration techniques consist of approximating the integrand by a polynomial in a region and then integrating the polynomial exactly. If the integrand is a complicated function, approximating it by a polynomial may be difficult. Often a complicated integrand can be factored into a weight function and another function better approximated by a polynomial. As an example, if $g(t)$ is a complicated function which has to be integrated for t between the limits c and b , it can be factored as $w(t)f(t)$ where $w(t)$ is the weight function and $f(t)$ is a simple function (i.e. one which can easily be approximated by a

⁴Since the regions of interest are the tails of the distribution (error rate of 10^{-6}), where the various terms consist of small positive and negative numbers, the numerical errors as a result of addition will be large.

polynomial). Thus,

$$\int_a^b g(t) dt = \int_a^b w(t) f(t) dt = \sum_{j=1}^N w_j f(t_j) \quad (2.55)$$

The quadrature rule $\{w_j, t_j\}$, corresponding to the weight function $w(t)$, is available sometimes in tabulated form¹. Often, however, these rules are not available in tabulated form. Golub and Welsch [23] have presented algorithms for generating the Gaussian Quadrature Rule, provided the moments of the weight function are known or can be calculated. This is precisely the situation existing for the fiber-optic system. The Gauss Quadrature rules can be used to evaluate the conditional probabilities in equation (2.41).

$$\begin{aligned} P_0(y) &= \int_{-\infty}^{\infty} P(y, t_0 | \text{ZERO}) dy = \int_{-\infty}^{\infty} f^{(0)}(y) p(y, t_0 | \text{ZERO}) dy \\ &= \sum_{j=1}^N f^{(0)}(y_j^0) w_j^0 \end{aligned} \quad (2.56)$$

Similarly,

$$P_1(y) = \sum_{j=1}^N f^{(1)}(y_j^1) w_j^1 \quad (2.57)$$

where

$$f^{(0)}(y) = \begin{cases} 1 & \text{for } y \geq \gamma \\ 0 & \text{otherwise} \end{cases} \quad (2.58)$$

and

$$f^{(1)}(y) = 1 - f^{(0)}(y) \quad (2.59)$$

The abscissas y_j and the weights w_j may be calculated by methods of functional analysis from the conditional moments $E\{(y(t_0)|b_0)\}$. Hauk *et. al.* [24] have evaluated these integrals and thereby derived the error probability.

Other numerical techniques include the Gram-Charlier Series method [19] and the Characteristic Function method [16],[17]. The *Gram-Charlier Series* method involves the calculation of the cumulants of individual noise sources which can then be added up to

¹The book "Handbook of Mathematical Functions" by Abramowitz and Stegun provides an excellent tabulation of some useful weight functions [22].

compute the overall cumulant, and thereby the probability density function. The major advantage of the Gram-Charlier Series method is that it requires very little computing time as compared to other methods. A detailed analysis of the Gram-Charlier Series is provided in the next section.

The *Characteristic Function* method is essentially similar to the Gram-Charlier Series method: instead of adding the cumulants of the individual noise sources, the characteristic functions of the individual noise sources are multiplied to obtain the overall PDF. The PDF of all the noise sources is described by a trigonometric series. The total characteristic function is related to the Fourier coefficients of the periodic probability density function. This results in an expression which can then be used to determine the error probability for a given bit rate as a function of the transmitted power.

2.3.2 Statistical Methods

The only statistical method that will be considered here is the *Monte Carlo simulation* method. The Monte Carlo simulation method is normally employed for systems whose parameters have known statistical distributions. The Monte-Carlo method starts with the use of the statistical distribution of the system together with random number generators to produce a large number of sample systems. These systems are then analysed on the computer and empirical results about system performance are obtained. There are, however, limitations on the straight-forward application of the Monte-Carlo method for fiber-optic systems. Since error rates are typically of the order 10^{-4} to 10^{-9} , at least 10 to 100 samples are needed in this region of low probability. This entails the need for as many as 10^{11} samples, which is impracticable. A modification known as the importance sampling, solves this difficulty by modifying the distribution so that more samples can be taken from the important region. This reduces the number of simulation runs by 5 or 6 orders of magnitude.

A detailed analysis of Monte Carlo simulation using Importance Sampling is given in (18).

2.4 DETAILED ANALYSIS OF THE GRAM-CHARLIER SERIES METHOD

A Gram-Charlier Series expansion for the probability distribution of noise in a fiber-optic receiver is considered here. This representation is more general than the previously published work of Rice [25] and Personick [12].

1. It takes into account the randomness of the avalanche gain as well as the amplifier's thermal noise and permits the consideration of any generalised processing filters. Previously reported calculation methods [15][16][18] permit thermal noise to be included only at the expense of additional approximations and require complicated numerical techniques to solve for error probabilities.
2. Each of the noise sources can be considered separately and, provided they are independent, the cumulants of the noise sources can be added to obtain the overall cumulant. Thus the effect of intersymbol interference, dark current noise and modal noise can be easily incorporated.
3. The probability distribution of physical noise sources can often be obtained by finding the characteristic function and then taking the Fourier transform. There are, however, situations where the characteristic function cannot be obtained in closed form. In such cases, it is often easier to describe the PDF as a Gram-Charlier series expansion.
4. This method is suitable for application to multilevel PAM & PWM systems.

The Gram-Charlier Series involves the expansion of an 'unknown' probability function in terms of the derivatives of a 'known' density function. For a system with a large number of independent noise sources, the output is nearly Gaussian by virtue of the Central Limit Theorem. The Gram-Charlier Series derives an expression for the PDF which exhibits the limiting Gaussian characteristics. For the Gaussian function, only the first few terms would exist. As the function becomes more non-Gaussian in shape, the number of terms increases.

If we expand the logarithm of the characteristic function $\Psi(s)$, in a Taylor series, the coefficients of this series are, by definition, the cumulants of the stochastic process [26].

$$\ln \Psi(s) = \sum_{n=0}^{\infty} \lambda_n s^n / n! \quad (2.60)$$

Central to the Gram-Charlier Series approach is the use of the cumulants, λ_n , to calculate the PDF due to a combination of noise sources. Thermal noise processes, which have a Gaussian distribution, have cumulants only up to an order of two. There are, however, processes such as shot noise and impulse noise which have cumulants of higher order. These higher order cumulants can be used to describe the non-Gaussian character of the process.

The description of probability density by means of cumulants arises in a natural manner if we approximate the functions by means of a series of Hermite Polynomials. The Hermite polynomial is generated as the Gaussian function is successively differentiated. These functions are orthogonal over the extended real line with respect to the Gaussian weighting function. Such a series, known as Gram-Charlier Series, is given by [19].

$$p(x) = \sum_{n=0}^{\infty} a_n \varphi_n(x) \quad (2.61)$$

where

$$\varphi_n(x) = d^n/dx^n [(1/(2\pi)^{0.5}) \exp(-x^2/2)] \quad (2.62)$$

and

$$a_n = (-1)^n \mu_n / n! \quad (2.63)$$

where $\mu_n(x)$ is the n th central moment of x .

Another common practice, convenient for computational purposes, is the normalisation of the random variable such that it has a zero mean and unit variance. If m is the mean of the random variable x and σ^2 is its variance, and if we denote \tilde{x} as the normalised variable, the relation between x and \tilde{x} is given by,

$$\tilde{x} = (x-m)/\sigma \quad (2.64)$$

The corresponding normalised cumulants are denoted by

$$\tilde{\lambda}_1 = 0, \quad \tilde{\lambda}_n = \lambda_n / \lambda_2^{n/2} \quad n \geq 2 \quad (2.65)$$

The normalised characteristic function $\tilde{\psi}(s)$ is similar to (2.60) with λ_n replaced by

$\tilde{\lambda}_n$, i.e.

$$\tilde{\Psi}(s) = \exp\left\{\sum_{n=1}^{\infty} \tilde{\lambda}_n s^n/n!\right\} \quad (2.66)$$

The normalised characteristic function, $\tilde{\Psi}(s)$ is also directly given by

$$\tilde{\Psi}(s) = \int_{-\infty}^{\infty} \exp(Sx) p(x) dx \quad (2.67)$$

Substituting the expression for $p(x)$ from (2.61) into (2.67) gives:

$$\begin{aligned} \tilde{\Psi}(s) &= \sum_{n=0}^{\infty} a_n \int_{-\infty}^{\infty} \exp(Sx) \frac{d^n}{dx^n} \left[(1/(2\pi)^{0.5}) \exp(-x^2/2) \right] dx \\ &= \sum_{n=0}^{\infty} (-1)^n a_n S^n \exp(S^2/2) \end{aligned} \quad (2.68)$$

Substituting relation (2.63) into (2.68)

$$\tilde{\Psi}(s) = \left[\sum_{n=0}^{\infty} \mu_n S^n/n! \right] \exp(S^2/2) \quad (2.69)$$

Using (2.66) and (2.68) and noting that $\tilde{\lambda}_1 = 0$ and $\tilde{\lambda}_2 = 1$ it follows that

$$\begin{aligned} \left[\sum_{n=0}^{\infty} \mu_n S^n/n! \right] \exp(S^2/2) &= \exp\left\{\sum_{n=1}^{\infty} \tilde{\lambda}_n S^n/n!\right\} \\ &= \exp\left\{\sum_{n=2}^{\infty} \tilde{\lambda}_n S^n/n!\right\} \exp(S^2/2) \end{aligned} \quad (2.70)$$

Equation (2.70) can be simplified by dividing both sides by $\exp(S^2/2)$ and expanding the right hand side in a Taylor series. This results in:

$$\begin{aligned} \sum_{n=0}^{\infty} \mu_n S^n/n! &= \exp\left\{\sum_{n=2}^{\infty} \tilde{\lambda}_n S^n/n!\right\} \\ &= 1 + \left(\sum_{n=2}^{\infty} \tilde{\lambda}_n S^n/n!\right) + 0.5 \left[\sum_{n=2}^{\infty} \tilde{\lambda}_n S^n/n!\right]^2 + \dots \end{aligned} \quad (2.71)$$

From (2.71) the recursive relation between the central moments and cumulants, $\tilde{\lambda}_n$ can be derived and is seen to be:

$$\begin{aligned} \mu_0 &= 1 \\ \mu_1 &= \mu_2 = 0 \\ \mu_3 &= \tilde{\lambda}_3 \\ \mu_{n+1} &= \tilde{\lambda}_{n+1} + \sum_{m=2}^n C_m \tilde{\lambda}_{n+1} \mu_{n-m} \quad n \geq 3 \end{aligned} \quad (2.72)$$

Using equation (2.72) and (2.63), one can calculate the Gram-Charlier coefficients a_n .

There still, however, remains the task of calculating the various cumulants.

2.4.1 Derivation of Cumulants

The method used in the derivation of the cumulants is based on the work of Rice [26]. Rice obtained the characteristic function of the noise generated in an electronic vacuum diode. In order to obtain the probability distribution he required the inverse Fourier transform, which was impossible to obtain in closed form. He effected a power series expansion in which he could obtain the inverse Fourier transform of the individual terms. The resultant series is recognisable as a Gram-Charlier series. The Poisson noise or the shot noise is well-suited for a cumulant description of the sort used by Rice.

The distinguishing characteristics of this type of noise are

1. It is the result of the superposition of events occurring at random times. For example, let us consider a vacuum tube. Assume that the arrival of an electron at time $t = 0$, produces an effect $F(t)$ at some point in the output circuit. If the output circuit is such that the effects of the various electrons add linearly, the total effect at time t , due to all the electrons, is

$$I(t) = \sum_k a_k F(t - t_k) \quad (2.73)$$

where the k 'th electron arrives at the time t_k & causes effect $F(t - t_k)$ at time t (Refer to Fig. 2.7)

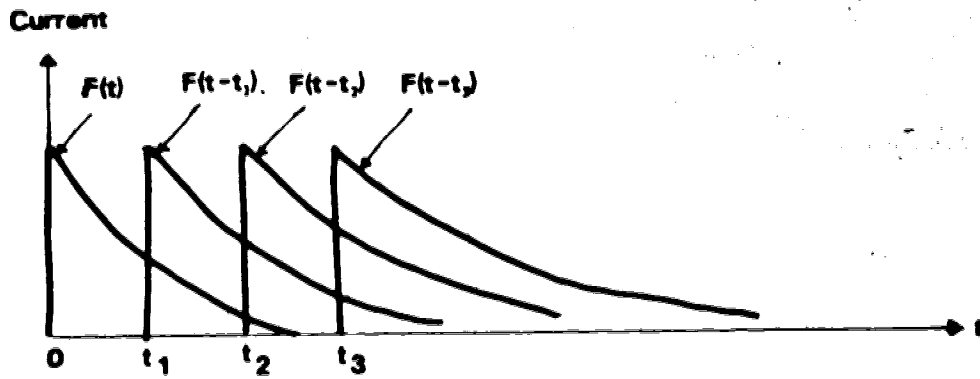
Consider the case of electron multiplication. Instead of only one electron arriving at t , a_k electrons arrive at each instant. The same idea could be used in a fiber-optic receiver model. For a PIN diode $a_k = 1$ and for an APD, $a_k = g_k$, where g_k is the number of electron-hole pairs produced by a photon arriving at time $t = t_k$.

2. The occurrence times t_k are assumed to form a Poisson sequence with an average rate λ per second. This condition holds true for the fiber-optic receiver

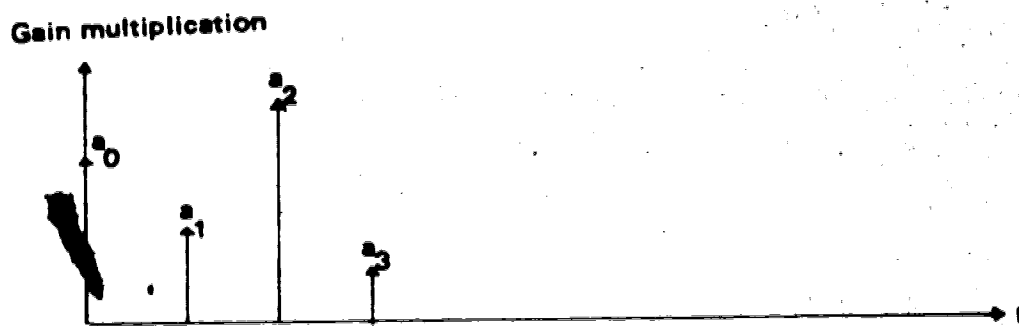
Rice has shown that, for a system having a noise process which satisfies the above condition, the n 'th cumulant can be given by:

$$\lambda_n = n! \int_0^\infty [F(t)]^n dt \quad (2.74)$$

A formula similar to (2.74) will be derived for the fiber-optic receiver shown in Fig. 2.6



(a) Response to an electron arriving at times t_0 , t_1 , t_2 and t_3 , each considered separately. The arrival of an electron at time $t = t_k$ produces effect $F(t-t_k)$.



(b) Random gain multiplications.

The total effect, at time t , due to all the electrons is:

$$\sum_{k=0}^{\infty} a_k F(t-t_k)$$

Figure 2.7 Graphical description of the shot noise analysed by Rice

The receiver in Fig. 2.6 consists of an APD, a voltage amplifier and a linear, time-invariant filter. The APD and the amplifier are assumed to have an infinite bandwidth and $h(t)$ represents the total impulse response. Each electron generated optically at the input of the APD gives an impulsive current of height (qG) at its output, where q is the electron charge and G is the instantaneous random gain of the diode. After amplification, an impulsive voltage of height $(qGRA)$ is produced at the input of the signal processor which in turn gives an output of $[qGRAh(t-\tau)]$ at time t , where τ is the instant of the release of the initial electron. Assuming both $P(t)$ and $h(t)$ are zero for $t < 0$, we can write

$$V(T) = \sum_{i=1}^k (qRA G) h(T-\tau_i) \quad (2.75)$$

where k is the random number of electrons released in the interval $[0, T]$ and τ_i is the time instant at which the i 'th electron was released. Since the electrons are released independently, the characteristic function of each of these electrons can be multiplied to obtain the overall characteristic function of $V(t)$ [26]. The characteristic function of the i 'th term of $V(t)$ is

$$\begin{aligned} \psi(s) &= E\{e^{(qRA G) h(T-\tau_i) s}\} \\ &= \sum_{G=1}^{\infty} \int_{\tau=0}^T e^{(qRA G) h(T-\tau) s} P_G(G) \cdot P_{\tau}(\tau) d\tau \end{aligned} \quad (2.76)$$

where $P_G(G)$ and $P_{\tau}(\tau)$ are the probability distributions of G and τ respectively*. Also the probability distribution of $P_{\tau}(\tau)$ is given by

$$P_{\tau}(\tau) = P(\tau) / \int_0^T P(\tau) d\tau \quad (2.77)$$

where $P(\tau)$ is the input power.

$$\begin{aligned} \psi(s) &= \int_0^T \sum_{G=1}^{\infty} e^{(qRA G) h(T-\tau) s} \\ &\quad P_G(G) [P(\tau) / \int_0^T P(\tau) d\tau] d\tau \\ &= \left[\int_0^T P(\tau) d\tau \right]^{-1} \int_0^T M[qRA h(T-\tau) S] \cdot \\ &\quad P_0(\tau) d\tau \end{aligned} \quad (2.78)$$

where $M[\cdot]$ is the moment generating function of G as defined in [27].

*Note that G is a discrete random variable

The overall characteristic function of k electrons is the characteristic function of each electron multiplied k times, i.e.

$$\Psi_k(S) = (\Psi(S))^k \quad (2.79)$$

The probability of obtaining k electrons in a time period, T , is

$$\sum_{k=0}^{\infty} \frac{e^{-\bar{k}} (\bar{k})^k}{k!} \quad (2.80)$$

where \bar{k} is the mean number of electrons transmitted in the time interval $[0, T]$

$$\bar{k} = (\eta/h\nu) \int_0^T P(\tau) d\tau \quad (2.81)$$

and where η is the quantum efficiency, h is Planck's constant and ν is the frequency of light. The characteristic function of the output voltage $V(T)$ is therefore given by

$$\begin{aligned} \Psi_{V(T)}(S) &= \sum_{k=0}^{\infty} [e^{-\bar{k}} (\bar{k})^k / k!] (\Psi(S))^k \\ &= e^{-\bar{k}} \sum_{k=0}^{\infty} (\bar{k} \Psi(S))^k / k! \\ &= e^{-\bar{k}} e^{\bar{k} \Psi(S)} \\ &= e^{(\eta/h\nu) \int_0^T P(\tau) [M(qRAh(T-\tau)) - 1] d\tau} \end{aligned} \quad (2.82)$$

Since:

$$\begin{aligned} M(S) &= \sum_{n=0}^{\infty} M^{(n)}(0) S^n / n! \\ &= 1 + \sum_{n=1}^{\infty} \langle G^n \rangle S^n / n! \end{aligned} \quad (2.83)$$

Therefore:

$$\begin{aligned} \Psi_{V(T)}(S) &= \exp\left\{ (\eta/h\nu) \sum_{n=1}^{\infty} \langle G^n \rangle \int_0^T P(\tau) \cdot \right. \\ &\quad \left. [qRAh(T-\tau)]^n (S^n / n!) d\tau \right\} \end{aligned} \quad (2.84)$$

or

$$\begin{aligned} \log_e \Psi_{V(T)}(S) &= \sum_{n=1}^{\infty} \left\{ (\eta/h\nu) (qRA)^n \langle G^n \rangle \right. \\ &\quad \left. \int_0^T P(\tau) h^n (T-\tau) d\tau \right\} S^n / n! \end{aligned} \quad (2.85)$$

The cumulants of the random variable $V(T)$ are:

$$\lambda_n = (\eta/h\nu) (qRA)^2 \langle G^2 \rangle \int_0^T P(\tau) h^2(T-\tau) d\tau \quad (2.86)$$

Knowing the cumulants, it is a straight forward task to calculate the error probability using equations (2.61), (2.63), (2.72), and (2.86). Though thermal noise, dark noise, modal noise and intersymbol interference are not directly considered, they are taken into account by the term $P(t)$ in (2.86): $P(t)$ can be broken up into signal power, dark current power, intersymbol interference and modal noise power, i.e.

$$P(t) = X_d(t) + X_s(t) + X_i(t) + X_N(t) \quad (2.87)$$

where

$X_d(t)$ = dark current

$X_s(t)$ = shot noise term = $d_s g(t)$

$X_i(t)$ = intersymbol interference term

$$= \sum_{j=-p}^q d_j g(t-jT) \quad j \in \{0, 1\}$$

$X_N(t)$ = modal noise term

$g(t)$ = signal waveshape at the filter output

Equations (2.74) and (2.75) can be put together to get the overall cumulant

$$\begin{aligned} \lambda_n &= (\eta/h\nu) (qRA)^2 \langle G^2 \rangle \\ &\int_0^T (X_d + X_s + X_i + X_N) h^2(T-\tau) d\tau \\ &= \lambda_{nd} + \lambda_{ns} + \lambda_{ni} + \lambda_{nN} \end{aligned} \quad (2.88)$$

where

λ_{nd} = dark noise cumulant

$$\lambda_{nd} = (\eta/h\nu) (qRA)^2 \langle G^2 \rangle \int_0^T X_d h^2(T-\tau) d\tau \quad (2.89)$$

λ_{ns} = shot noise cumulant

$$\lambda_{ns} = (\eta/h\nu) (qRA)^2 \langle G^2 \rangle \int_0^T X_s h^2(T-\tau) d\tau \quad (2.90)$$

λ_{ni} = intersymbol interference cumulant

$$\lambda_{th} = (\eta/h\nu) (qRA)^2 \langle G^2 \rangle \int_0^T X_p h^2 (T-\tau) d\tau \quad (2.91)$$

λ_{nN} = modal noise cumulant

$$\lambda_{nN} = (\eta/h\nu) (qRA)^2 \langle G^2 \rangle \int_0^T X_p h^2 (T-\tau) d\tau \quad (2.92)$$

The overall cumulant due to a number of independent noise sources is the sum of individual cumulants. Correspondingly, the characteristic functions of individual noise sources can be multiplied to obtain the overall characteristic function [26]. If we denote Ψ_x to be the overall characteristic function due to the shot noise, dark current, intersymbol interference, and modal noise terms, then:

$$\Psi_x(S) = \Psi_{sd}(S) \Psi_{nN}(S) \Psi_{SI}(S) \Psi_{DN}(S) \quad (2.93)$$

We make use of this in incorporating the thermal noise and intersymbol interference terms into the cumulants.

Thermal Noise

Let $\Psi_{th}(s)$ be the characteristic function for the thermal noise term. Since thermal noise is a Gaussian process, one can expand $\Psi_{th}(s)$ as

$$\Psi_{th}(S) = \exp(\sigma_{th}^2 S^2 / 2) \quad (2.94)$$

Where σ_{th}^2 is the variance of the thermal noise. Since the thermal noise is independent of the other noise processes, its characteristic function can be multiplied by $\Psi_x(s)$ to obtain the complete characteristic function $\Psi_{x-th}(s)$.

$$\begin{aligned} \Psi_{x-th}(S) &= \Psi_x(S) \Psi_{th}(S) \\ &= \exp\left[\sum_{n=1}^{\infty} \lambda_n S^n / n!\right] \exp(\sigma_{th}^2 S^2 / 2) \\ &= \exp\left[\lambda_1 S + (\lambda_2 S^2 / 2) + (\lambda_3 S^3 / 3!) + \dots + (\sigma_{th}^2 S^2 / 2)\right] \\ &= \exp\left[\lambda_1 S + (\lambda_2 + \sigma_{th}^2) S^2 / 2 + (\lambda_3 S^3 / 3!) + \dots\right] \end{aligned} \quad (2.95)$$

The thermal noise term is seen to affect only the second cumulant. Thus, by changing λ_2 to $\lambda_2 + \sigma_{th}^2$, the thermal noise effect can be included, without needing to alter the error probability calculations.

Intersymbol Interference

The cumulant for the intersymbol interference can be derived from the characteristic function of the output voltage. If we denote $x(t)$ as the current output of the diode and $y(t)$ the voltage at the decision point (refer to Fig. 2.5) then:

$$x(t) = x_s(t) + x_{eh}(t)$$

$$X_s(t) = \sum_{k=1}^N g_k \delta(t - t_k) \quad (2.96)$$

= signal term which is a doubly stochastic Poisson process.

here t_k is the time of release of the k 'th electron and N is the random number of electrons emitted during the time slot.

The output of the filter, $y(t)$, has a signal component

$$Y_s(t) = \int_{-\infty}^{\infty} X_s(\tau) h(t - \tau) d\tau \quad (2.97)$$

This has a characteristic function given by

$$\Theta_{Y_s}(j\nu) = \exp\left\{ \int_{-\infty}^{\infty} \xi(\tau) [\Theta_z(j\nu h(t - \tau)) - 1] d\tau \right\} \quad (2.98)$$

where

$$\xi(\tau) = [\mu_s(t)/d_{t=0}] + \mu_d(t) + \left[\sum_{t=0}^{\infty} \mu_t(t)/d_{t=0} \right] \quad (2.99)$$

and where $\mu_s(t)$ is the number of electrons at time t and $\Theta_z(j\nu)$ is the characteristic function of the random avalanche gain mechanism.

$$\Theta_z(j\nu) = (1 - j\nu \langle G \rangle)^{-1} \quad \text{for } \langle G \rangle > 10 \quad (2.100)$$

The proofs of equations (2.98) and (2.100) are given in appendix 2. One can directly derive the cumulants from the characteristic function by noting that:

$$\begin{aligned} \lambda_n &= j^{-n} d^n/d\nu^n [\log_e(\Theta_{Y_s}(j\nu))] |_{\nu=0} \\ &= j^{-n} d^n/d\nu^n \left[\int_{-\infty}^{\infty} \xi(\tau) \{ \Theta_z[j\nu h(t - \tau)] - 1 \} d\tau \right] \end{aligned} \quad (2.101)$$

Using eqs. (2.100) and (2.101) one can readily derive the cumulant to be:

$$\lambda_n = n! \langle G \rangle^n \int_{-\infty}^{\infty} \xi(\tau) h^n(t-\tau) d\tau \quad (2.102)$$

This result appears to be quite similar to the cumulants derived using the Gram-Charlier Series in (2.86). If one takes note of the fact that $\xi(t) = P(t)/n/h\nu$ and $\langle G^n \rangle$ is closely approximated by $n! \langle G \rangle^n$ for $G > 10$, then the two results become identical.

The intersymbol interference term is just a part of this term

$$\lambda_n = \langle G^n \rangle \int_{-\infty}^{\infty} \xi(\tau) h^n(t-\tau) d\tau \quad (2.103)$$

where

$$\xi(\tau) = \left[\sum_{m=0}^{\infty} \mu_m(\tau) / d_{m0} \right] \quad (2.104)$$

The equations given above may not only be used to evaluate the intersymbol interference separately, but also to show the similarity between the Characteristic Function approach and the cumulant approach.

2.4.2 Comments on the Gram-Charlier Series

For computational efficiency it is necessary that the series in (2.60) be truncated to a few terms. The number of terms in the series approximation necessary for a particular desired accuracy depends on X , which is defined as the number of standard deviations from the average, i.e. $X = (V - \bar{V}) / \sigma_s$. Error rate computations require calculations at large values of X (i.e. at the tail of the PDF curves). To maintain accuracy at large values of X , the truncated series must contain more terms. As an example, the truncated series $\sum_{n=0}^3 a_n \varphi^{(n)}(V)$ has less than 1% error up to $X = 8$, for an average laser power of 10 μW and assuming an integrate-and-dump filter which passes a pulse of width 10^{-1} sec.

The convergence of the Gram-Charlier Series is not immediately obvious but has been proved [27]. The convergence of the series is not monotonic, but is in groups of three terms. Furthermore, the terms $a_n \varphi^{(n)}(V)$ do not decrease in importance until

$n > n_0$, where n_0 is an integer which depends on several factors⁷. The addition of thermal noise causes the standard deviation to change from σ_s to $(\sigma_s^2 + \sigma_{th}^2)^{1/2}$ (where σ_s is the shot noise portion and σ_{th} is the thermal noise portion). As a result, the value of X changes from $(V - \bar{V})/\sigma_s$ to $(V - \bar{V})/(\sigma_s^2 + \sigma_{th}^2)^{1/2}$. Thus the n 'th term in the Gram-Charlier Series decreases by a factor of $1/(1 + \sigma_{th}^2/\sigma_s^2)^{1/2}$ due to the thermal noise. This means that the contribution of the higher-order terms (of the Gram-Charlier Series) decreases as the thermal noise increases.

2.4.3 Error Probability Calculations

To evaluate the error probability for a fiber optic system it is necessary to compute the conditional error probabilities (i.e. receiving a zero when a one was transmitted and vice versa). Fig. 2.8 shows the probability density function for the normalised variable X as well as the non-normalised variable X' . These two variables are related by:

$$X = (X' - m) / \sigma \quad (2.105)$$

where m is the mean and σ is the variance. The conditional probabilities are given by

$$\begin{aligned} P[E|0] &= \int_{V_{th}}^{\infty} P_0(x') dx' = \sigma_{x_0} \int_{(V_{th}-m_0)/\sigma_0}^{\infty} P_0(x) dx \\ &= \sigma_{x_0} \int_{(V_{th}-m_0)/\sigma_0}^{\infty} \left[\sum_{n=0}^{\infty} a_{n0} \phi^{(n)}(x) \right] dx \\ &= 0.5 [1 - \text{erf}((V_{th} - m_0) / \sqrt{2} \sigma_0)] \\ &\quad - \sum_{n=0}^{\infty} a_{n0} \phi_{n-1}((V_{th} - m_0) / \sqrt{2} \sigma_0) \end{aligned} \quad (2.106)$$

Similarly

$$\begin{aligned} P[E|1] &= 0.5 [1 + \text{erf}((V_{th} - m_1) / \sqrt{2} \sigma_1)] \\ &\quad + \sum_{n=0}^{\infty} a_{n1} \phi_{n-1}((V_{th} - m_1) / \sqrt{2} \sigma_1) \end{aligned} \quad (2.107)$$

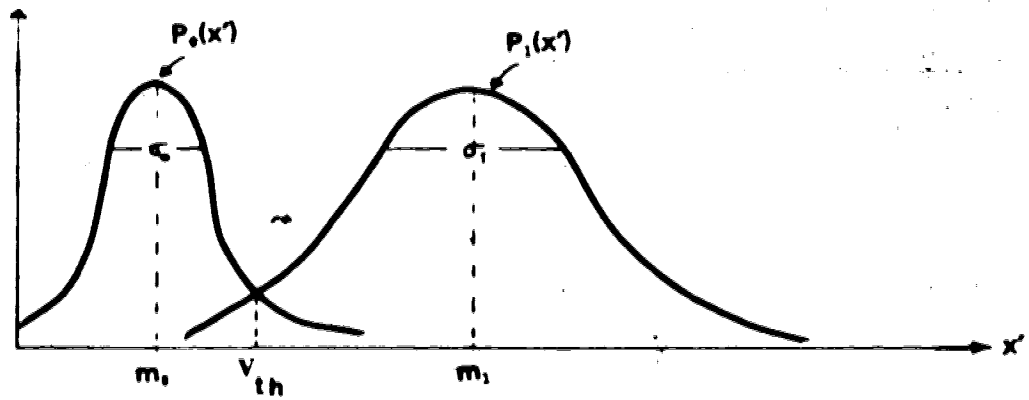
where

$$\text{Erf}(V_{th}) = (1/(2\pi)^{1/2}) \int_0^{V_{th}} e^{-x^2} dx \quad (2.108)$$

These two areas must be equated to obtain the near minimum error probability and then solved for V_{th} . Appendix 3 gives a program which calculates the error probabilities and the near-optimum thresholds.

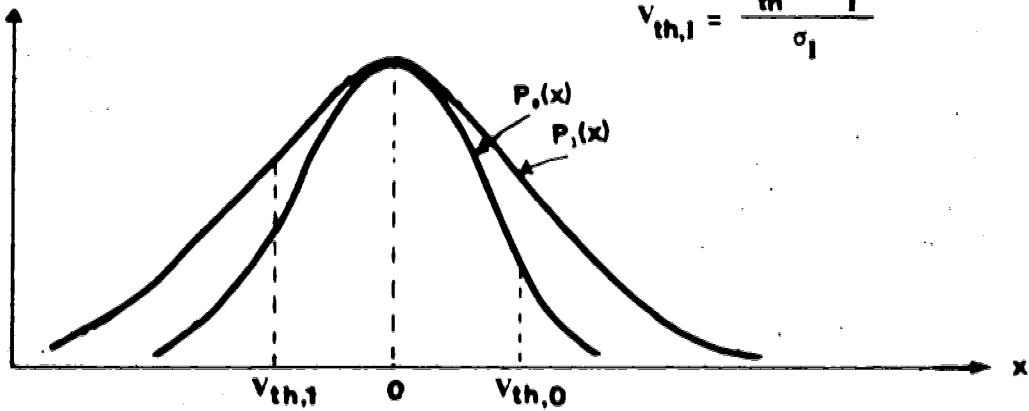
⁷For a fiber-optic system, n_0 depends upon the optical power input, the bit-rate, the mean avalanche gain and the thermal noise.

PDF curves



$$v_{th,0} = \frac{V_{th} - m_0}{\sigma_0}$$

PDF curves



$$v_{th,1} = \frac{V_{th} - m_1}{\sigma_1}$$

Figure 2.8 Probability density curves for binary transmission (a) using the non-normalised variable X' and (b) using the normalised variable X .

CHAPTER III

MULTILEVEL PULSE AMPLITUDE MODULATION

The main advantage of using multilevel signals instead of binary signals is that, for a transmission channel of a given bandwidth, more information can be transmitted. The relation between the information rate and the number of signal levels is given by [28]:

$$f_b = f_s \log_2 (M) \quad (3.1)$$

where:

f_b = equivalent bit rate in Mbits/sec.

M = Number of levels (assumed to be equally likely)

f_s = modulation rate of the fiber in Mbaud.

Equation (3.1) can be interpreted in two ways:

1. If f_b is kept constant, f_s decreases as M increases. This means that a multilevel system does not require as high a bandwidth system as is required by a binary system.
2. If f_s is kept constant, then f_b increases by a factor $\log_2(M)$. Thus one can increase the information rate of the system without increasing the frequency response of the system.

At high bit rates, pulse broadening, which arises due to the finite bandwidth of the system, results in intersymbol interference. One can conceivably reduce the intersymbol interference by the use of equalisers at the receiver [29]. There exists, however, a certain bound on the transmission rate which cannot be exceeded despite the use of equalisers [30]. To exceed such bounds on the information rate, one is forced to use multilevel signals.

Equation (3.1) seems to suggest that one can increase the information rate to any desired value by increasing M . One must realise, however, that (3.1) does not take into account the effect of intersymbol interference. Thus, increasing M from 2 to 4 increases the information rate by a factor of less than two, for a given error rate, due to the effect of intersymbol interference. As the number of levels increases beyond four, intersymbol interference becomes even more pronounced. Another important factor is that the circuit complexity increases as the number of levels increases. Keeping these

considerations in mind, 4-level PAM is a reasonable compromise between increased information rate and increased intersymbol interference and circuit complexity.

In this chapter, the Gram Charlier series will be used to approximate the probability density function of the output voltage and to calculate the optimal pulse amplitude levels and thresholds for a 4-level PAM system. The analysis used can be extended to any general multilevel scheme. Also presented in this chapter are the results obtained from an experimental 4-level PAM system that was designed to operate at $f_b = 8 \text{ Mb/sec}$ using 600m of graded index fiber, an LED as the light source and an APD as the light detector. The experimental results are compared to the values obtained by theoretical calculations.

The 4-level PAM scheme is shown schematically in Fig. 3.1. The message source generates a sequence of statistically independent random variables a_j with values a_1, a_2, a_3 and a_4 .

$$x_o(t) = \sum a_j \delta(t-jT) \quad (3.2)$$

where T is the time slot available for each pulse.

The encoder converts the source signal into a sequence of pulses suitable for transmission.

$$x_e(t) = \sum a_j r(t-jT) \quad (3.3)$$

where $r(t)$ is an ideal rectangular pulse

The encoded pulses, $x_e(t)$, suitably amplified, drive the optical source (LED or LD). The optical pulses generated by the source will depend on the bias current, the modulating signal current and on the source response. The output of the optical source is denoted as:

$$x_L(t) = \sum a_j r_1(t-jT) \quad (3.4)$$

where $r_1(t)$ represents the pulse shape at the output of the optical source.

The optical signal, while passing through the fiber channel, suffers attenuation and distortion. The optical signal incident on the photodetector is assumed to be a 4-level sequence, given by:

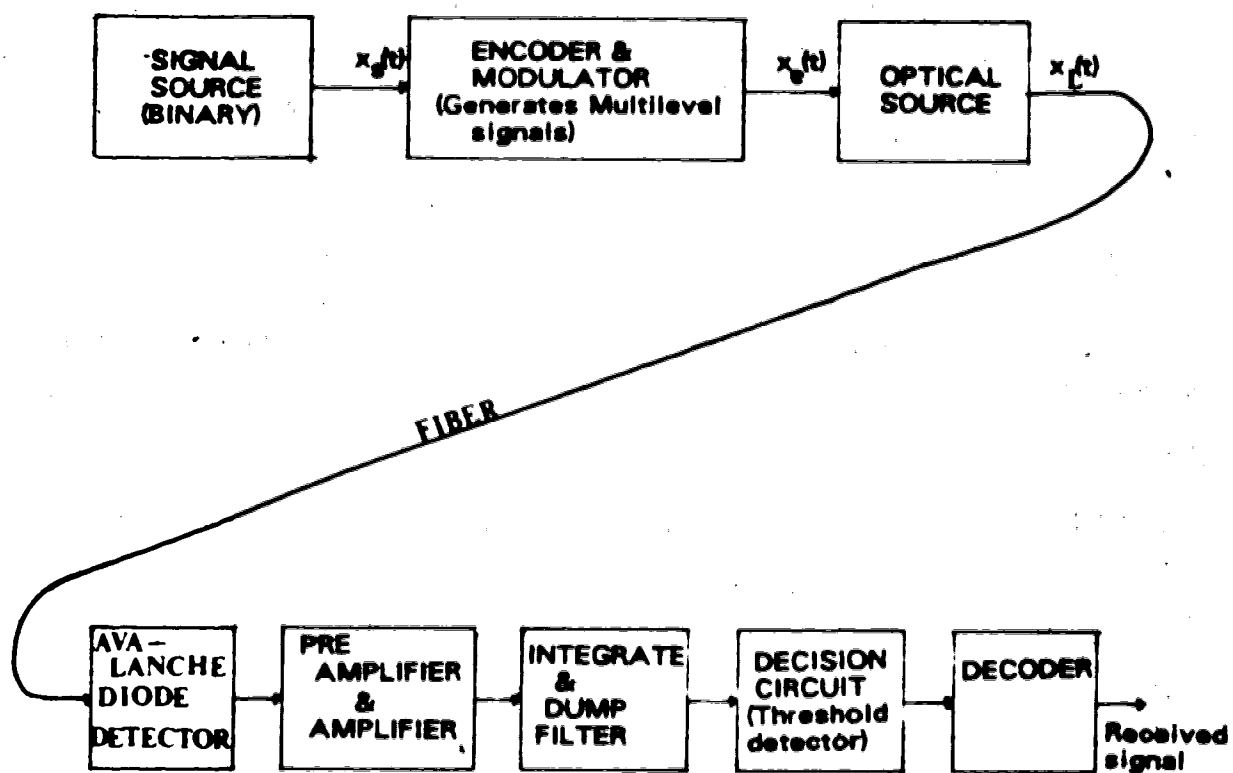


Figure 3.1 Block diagram of a multilevel PAM fiber optic communication system.

$$p(t) = \sum_{i=1}^M P_{mi} g(t-iT) \quad (3.5)$$

where

$p(t)$ is the received optical power

$g(t)$ is the normalised pulse shape and

P_{mi} is the maximum amplitude of the i 'th pulse which can take on 4 values; P_1, P_2, P_3 , and P_4 .

The receiver section consists of an APD, an amplifier, a filter and a decision circuit as shown in Fig. 3.1. The average output voltage at the filter output, at time T , is [19]:

$$v_o(t) = (\eta/h\nu) \cdot (qRA) \cdot \langle G \rangle \cdot \int_0^T P(\tau) h(t-\tau) d\tau \quad (3.6)$$

The n 'th cumulant, λ_n , of the output voltage, is given by (2.86):

$$\lambda_n = (\eta/h\nu) \cdot (qRA)^n \cdot \langle G^n \rangle \cdot \int_0^T P(\tau) h^n(t-\tau) d\tau \quad (3.7)$$

Equations (3.6) and (3.7) give a complete description of the statistics of the output voltage. The output voltage, can then be represented by the Gram-Charlier series as

$$p(x) = \sum_{n=0}^{\infty} a_n \phi_n(x) \quad (3.8)$$

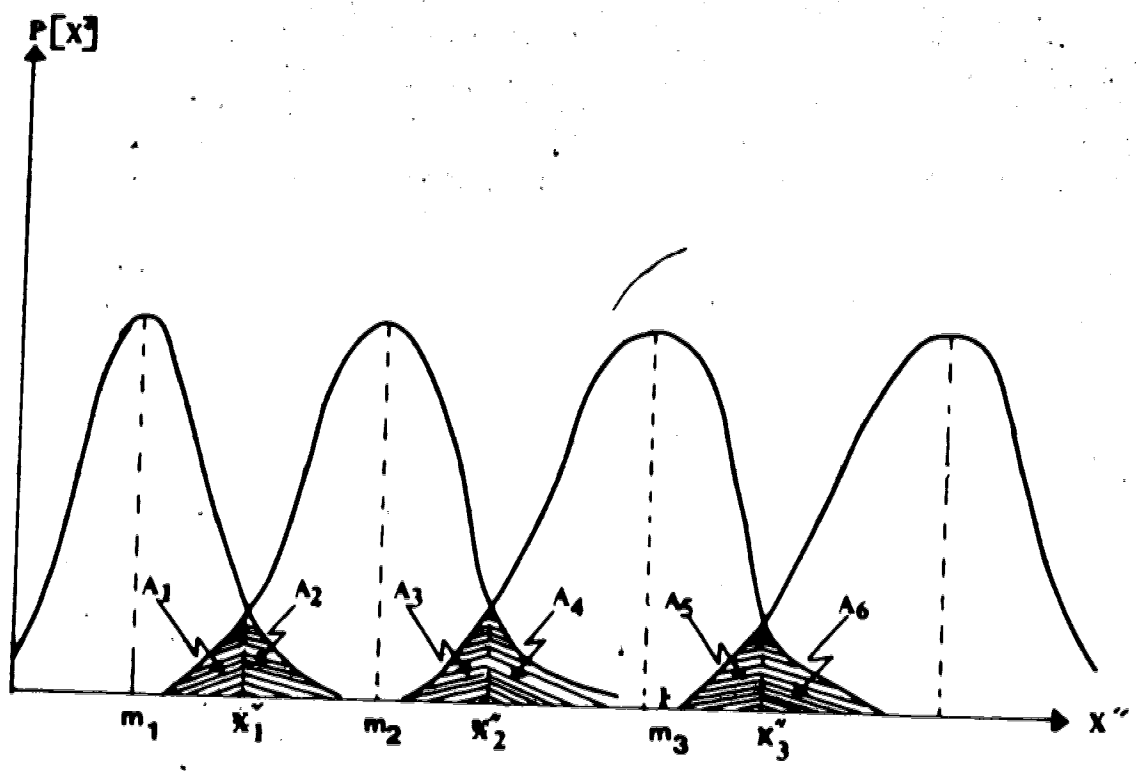
where a_n and ϕ_n are as defined in (2.62) and (2.63). Fig. 3.2 shows the probability density function of the output voltage for a 4-level PAM system. Here m_1, m_2, m_3 , and m_4 are the mean values of the PDFs, corresponding to the four levels transmitted X_1, X_2 , and X_3 , are the thresholds chosen to distinguish between the various levels. The areas A_1, A_2, A_3, A_4, A_5 , and A_6 are the tails of these curves. The error probability is therefore given by:

$$P[\epsilon] = p(1) \{p[2|1]\} + p(2) \{p[1|2] + p[3|2]\} \\ + p(3) \{p[2|3] + p[4|3]\} + p(4) \{p[3|4]\} \quad (3.9)$$

where:

$p(i)$ = probability of the i 'th level being transmitted; $i=1,2,3,4$

$p[i|j]$ = conditional probability that the received signal is interpreted as the i 'th level, when actually the j 'th level was sent $i, j \in \{1,2,3,4\}$



$m_1, m_2, m_3,$ and m_4 are the mean signal levels.
 $x_1'', x_2'',$ and x_3'' are the decision thresholds.

Figure 3.2 The probability density function of the output voltage for a 4-level PAM system.

Equation (3.9) can be simplified by assuming that all the signals are equally probable; i.e., $p(1) = p(2) = p(3) = p(4) = p = 1/4$. The equal area criterion is also used (i.e. $A_1 = A_2 = A_3 = A_4 = A_5 = A_6 = A$) since it simplifies the calculations and results in error probabilities close to the minimum [31]. With these assumptions, the error probability reduces to:

$$P[\varepsilon] = p(A_2) + p(A_1+A_4) + p(A_3+A_6) + p(A_5) = (3/2)A \quad (3.10)$$

Area A_1 is given by the integral,

$$A_1 = \int_{-\infty}^{x_1''} P_1(x'') dx'' \quad (3.11)$$

The other areas can be represented by similar equations. Equation (3.11) can be converted to the normalised case (i.e. zero mean and unit variance) by using the normalised variable

$$\begin{aligned} x &= (x'' - m_1) / \sigma_1 \quad \text{for } P_1(x) \\ x &= (x'' - m_2) / \sigma_2 \quad \text{for } P_2(x) \end{aligned} \quad (3.12)$$

Using (3.8) and (3.12), equation (3.11) reduces to the following form:

$$A_1 = 0.5 [1 - \text{Erf}((x_1'' - m_1) / \sqrt{2}\sigma_1)] - \sum_{n=2}^{\infty} a_n \varphi_{n-1}((x_1'' - m_1) / \sigma_1) \quad (3.13)$$

The other areas are derived in a similar manner.

The derivation of error probability for a 4-level system is a direct extension of the derivation used for a 2-level system. Using (3.9) each of the areas can be equated to two-thirds of the overall error probability. The optimum signal levels and thresholds required to achieve a particular error probability can then be determined by solving (3.13) iteratively. However, one can simplify calculations by assuming the PDF's to have a Gaussian distribution. For such a case, the Gram-Charlier coefficients, a_n , for $n > 2$ are zero. The resulting equations are given below:

$$\text{Erf}((x_1'' - m_1) / \sqrt{2}\sigma_1) = 1 - (4/3)P[\varepsilon] \quad (3.14)$$

$$\text{Erf}((m_2 - x_1'') / \sqrt{2}\sigma_2) = 1 - (4/3)P[\varepsilon] \quad (3.15)$$

$$\text{Erf}\left(\frac{x_2'' - m_2}{\sqrt{2}\sigma_2}\right) = 1 - (4/3)P[\epsilon] \quad (3.16)$$

$$\text{Erf}\left(\frac{m_2 - x_2''}{\sqrt{2}\sigma_2}\right) = 1 - (4/3)P[\epsilon] \quad (3.17)$$

$$\text{Erf}\left(\frac{x_3'' - m_3}{\sqrt{2}\sigma_3}\right) = 1 - (4/3)P[\epsilon] \quad (3.18)$$

$$\text{Erf}\left(\frac{m_3 - x_3''}{\sqrt{2}\sigma_3}\right) = 1 - (4/3)P[\epsilon] \quad (3.19)$$

The σ 's in equations (3.14) to (3.19) represent the variance of the Gaussian PDF's. From Chapter 2, this is seen to be

$$\sigma_i = \sigma_{th}^2 + \lambda_{2i} \quad (3.20)$$

where

(σ_{th} = thermal noise voltage of the system.

λ_{2i} = second cumulant for the i th signal level, having units of volt².

3.0.1 Intersymbol Interference

The intersymbol interference can be incorporated into the Gram-Charlier coefficient for the 4-level case, in the same manner as it was for the 2-level case in the previous chapter. To do this, one needs to change the expression for the power input, $p(t)$, in (3.6) and (3.7), to include the intersymbol interference terms. Making the assumption that only the pulses in the adjacent time slots create intersymbol interference,⁹ $p(t)$ is seen to be:

⁹The intersymbol interference due to pulses in time slots not immediately adjacent are very small and can generally be neglected.

$$p(t) = P_{-1}g(t-T) + P_0g(t) + P_1g(t+T) \quad (3.21)$$

where $P_0g(t)$ is the signal term and $P_{-1}g(t-T)$ and $P_1g(t+T)$ are the intersymbol interference terms from the adjacent time periods. The function, $g(t)$, represents the pulse shape. P_{-1} represents the maximum power level of the pulse just before the time period in consideration and P_1 represents the maximum power level of the pulse just after the time period in consideration. P_0 represents the maximum power of the pulse during the time period under consideration i.e. $(-T/2, T/2)$. It is assumed here that the maximum power for each pulse occurs at the same position in the time slot.

Expression (3.21) can be substituted in (3.6) and (3.7) to get the overall noise, including the intersymbol interference term. There are actually 64 (4^3) possible combinations of levels for intersymbol interference for the 4-level case. One normally considers the worst case intersymbol interference i.e. lowest signal level flanked on both sides by the highest signal level and vice versa. The four power levels will be denoted by P_1, P_2, P_3 and P_4 .

Thus, when the lowest signal level occurs between the two highest levels, the expression for the n 'th cumulant, λ_n , is:

$$\lambda_n = (\eta/h\nu)(qRA)^n \langle G^n \rangle \int_{-T/2}^{T/2} \{P_4g(\tau-T) + P_1g(\tau) + P_4g(\tau+T)\} \cdot h^n(T-\tau) d\tau \quad (3.22)$$

Assuming that $g(t)$ is a Gaussian pulse of unit height and standard deviation, σ , equation (3.22) can be rewritten as:

$$\lambda_n = (\eta/h\nu)(qRA)^n \langle G^n \rangle \int_{-T/2}^{T/2} [P_4 \{e^{-(\tau-T)^2/2\sigma^2} + e^{-(\tau+T)^2/2\sigma^2}\} + P_1 e^{-\tau^2/2\sigma^2}] \cdot h^n(T-\tau) d\tau \quad (3.23)$$

If the use of an integrate and dump filter is assumed, i.e. $h(t)=1$ for $t \in (-T/2, T/2)$, then (3.23) reduces to

$$\lambda_n = (\eta/h\nu)(qRA)^n \langle G^n \rangle \int_{-T/2}^{T/2} [P_4 \{e^{-(\tau-T)^2/2\sigma^2} + e^{-(\tau+T)^2/2\sigma^2}\} + P_1 e^{-\tau^2/2\sigma^2}] d\tau \quad (3.24)$$

Also noting that

$$\text{Erf}(u) = (2\sqrt{\pi}) \int_0^u \exp(-x^2) dx \quad (3.25)$$

Equation (3-24) reduces to:

$$\lambda_n = (\eta/h\nu) (qRA)^n \langle G^n \rangle (2\pi)^{1/2} \sigma \cdot [P_1 \text{erf}(T/(2\sqrt{e}\sigma)) + P_2 \{ \text{erf}(3T/(2\sqrt{e}\sigma)) - \text{erf}(T/(2\sqrt{e}\sigma)) \}] \quad (3.26)$$

In a similar manner one can derive the n 'th cumulant for the case of intersymbol interference, when the highest level signal occurs between time slots occupied by the lowest level:

$$\lambda_n = (\eta/h\nu) (qRA)^n \langle G^n \rangle (2\pi)^{1/2} \sigma \cdot [P_4 \text{erf}(T/(2\sqrt{e}\sigma)) + P_1 \{ \text{erf}(3T/(2\sqrt{e}\sigma)) - \text{erf}(T/(2\sqrt{e}\sigma)) \}] \quad (3.27)$$

Equations (3.14)–(3.20), (3.26) and (3.27) can be solved to find the optimal thresholds and signal levels for a fixed error probability. Conversely, given the signal levels and thresholds, one can calculate the error probability.

3.0.2 Numerical Example

We proceed here, with the calculations of signal levels and thresholds needed to achieve an error probability lying in the range of 10^{-4} to 10^{-10} . The system parameters used in this example are given in Table 3.1. The output optical power waveshape, $g(t)$, is assumed to be Gaussian with variance, t_σ .

Equations (3.14)–(3.20) and (2.86) can be used to calculate the optimum signal levels and thresholds for different error probabilities. The results obtained from solving these equations are given in Table 3.2. These were calculated assuming no intersymbol interference (i.e. the effect of $g(t)$ outside the time slot under consideration is ignored). From Table 3.2 one can see that the optimum signal levels and thresholds are not equally spaced. This results from the fact that the shot noise term increases with increased signal level, thereby making it necessary to keep the thresholds closer to the lower levels (so as to maintain areas A_1, A_2, \dots, A_n , shown in Fig 3.2, equal).

TABLE 3.1

PARAMETERS USED IN NUMERICAL CALCULATIONS

PARAMETER	DEFINITION	VALUE
η	Quantum efficiency of the APD	0.85
R	Amplifier input resistance	700 ohms.
A	Amplifier gain	1500
$\langle G \rangle$	Average avalanche gain	10
ν	Optical carrier frequency	3.614×10^{14} Hz.
K	APD Ionisation ratio	0.02
t_G	Variance of Gaussian optical pulse edge	250 ns.
T	Time slot available per pulse	500 ns.
σ_{th}	Thermal noise	35 μ v.

TABLE 3.2

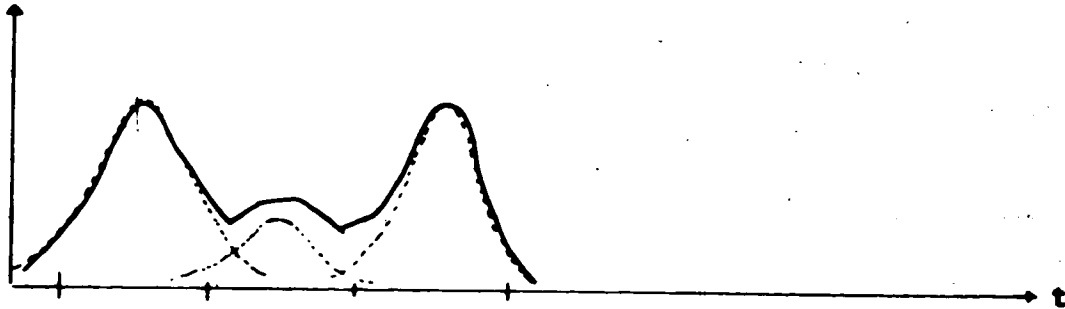
REQUIRED PULSE AMPLITUDE LEVELS AND THRESHOLDS
FOR A RANGE OF ERROR PROBABILITIES
(AMPLITUDES ARE IN MILLIVOLTS)

V_{out}	10^{-4}	10^{-5}	10^{-6}	10^{-7}	10^{-8}	10^{-9}	10^{-10}
m_1	0	0	0	0	0	0	0
x_1''	13.37	15.24	16.92	18.46	19.89	21.22	22.48
m_2	31.92	37.21	42.13	46.78	51.22	55.48	59.59
x_2''	50.46	59.17	67.34	75.11	82.55	89.74	96.71
m_3	74.18	87.86	100.8	113.3	125.3	137.0	148.5
x_3''	97.90	116.6	134.3	151.5	168.1	184.3	200.2
m_4	126.8	151.9	176.1	199.5	222.3	244.7	266.6

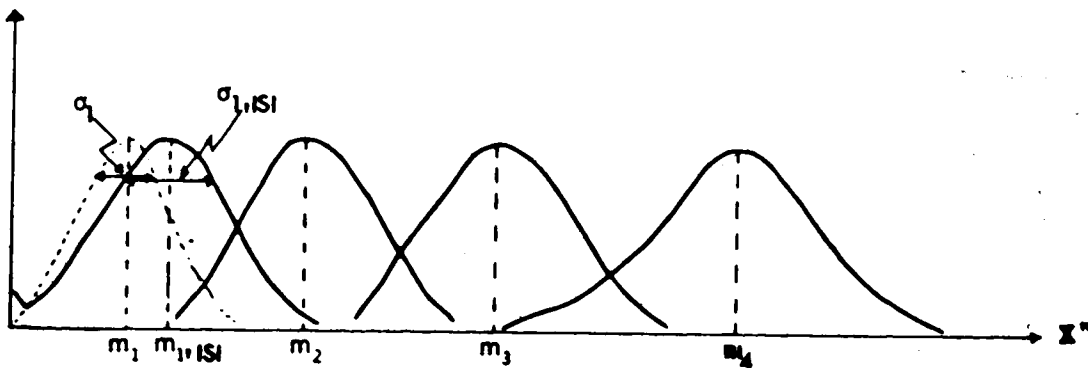
The results obtained above change drastically when one takes into account the effect of intersymbol interference. Fig 3.3 shows graphically the worst case intersymbol interference for a 4-level system, assuming Gaussian shaped optical pulses at the input of the detector. The worst case intersymbol interference occurs when the lowest level signal is flanked on adjacent time slots by the highest level signals. Fig.3.3 clearly shows that the effect of the worst case intersymbol interference is to increase the amplitude of the lowest level signal. There are therefore greater chances of the level-1 signal being detected as the level-2 signal. As a consequence of this, the overall error probability increases. The increase in error probability due to intersymbol interference can also be shown analytically. Equations (3.26) and (3.27) give the cumulants of the output voltage assuming intersymbol interference. Intersymbol interference is seen to increase the cumulants of the output voltage. As a result of the increase in the mean value and variance of the output voltage, the areas A_1 and A_2 , representing the conditional error probabilities $P[1/2]$ and $P[2/1]$, increase. The overall error probability increases due to the increase in the conditional error probabilities.

Using (3.27) along with (3.14) to (3.20) and assuming the same system parameters as before, one can recalculate the error probability taking into account the intersymbol interference. It is seen that, for an optical pulse with a variance, t_{σ} , equal to one-fifth of the time slot, the error probability increases from 10^{-4} to 8.75×10^{-4} . The error rate increases rapidly for larger values of t_{σ} . For an optical pulse with t_{σ} equal to two-fifths of the time-slot the error probability deteriorates to a value of 0.25. Such a condition is, however, an extreme case of intersymbol interference. Appendix 3 gives programs to calculate error probability for various values of t_{σ} .

A plot of error probability as a function of the mean avalanche gain, $\langle G \rangle$, of the APD is given in Fig. 3.4. The value of $\langle G \rangle$ is varied from 10 to 200. It is seen that the error probability decreases as $\langle G \rangle$ increases up to a value near 100. Above $\langle G \rangle = 100$, the error probability starts to increase again. This behaviour is due to the fact that for lower values of $\langle G \rangle$, the system is thermal noise limited. However, for $\langle G \rangle$ greater than 100 the system starts to become shot noise limited. The optimum gain for the above system is therefore near 100. This sort of behaviour has also been observed for two-level systems [4].



(a) The effect of the worst-case intersymbol interference (ISI) on the pulse shape. The dotted line represents the pulse shape without ISI and the thick line represents the pulse shape after ISI. Note the increase in the mean amplitude of the lowest level.



(b) The effect of the worst-case ISI on the PDF of the output voltage. The mean level and variance of 'signal-1' is larger than that without ISI.

Figure 3.3 The effect of the worst-case intersymbol interference on the pulse shape and the probability density function due to the highest level signal flanking the lowest level signal on both sides.

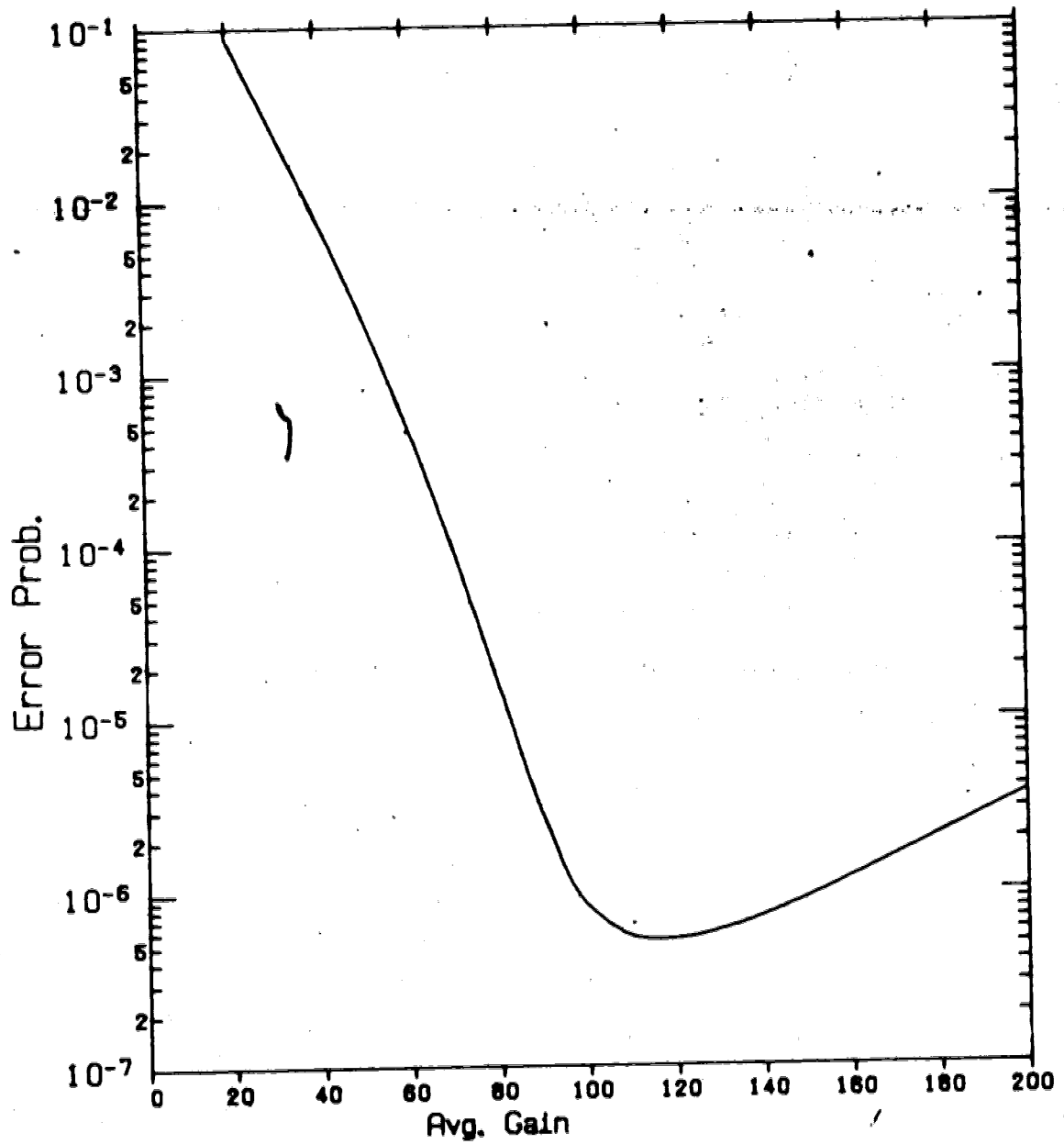


Figure 3.4 Plot of error probability as a function of the mean avalanche gain for a 4-level PAM system.

Fig. 3.5 shows the variation of the error probability as a function of the average optical signal, P_{avg} at the input to the detector. The error probability is seen to decrease with increased optical power reaching the detector. These results were observed for the 2-level case by Mansuripur *et. al.* [19]. Fig. 3.5 also shows the variation of error probability as a function of the average optical power reaching the detector, taking into account intersymbol interference. The variance of the pulse, t_p , is assumed to be one-fifth of the time slot. The programs used to generate these plots are given in Appendix 3.

3.1 EXPERIMENTAL SETUP FOR THE 4-LEVEL PAM SYSTEM

A complete four-level PAM system was designed, built and tested in the laboratory. A major objective for the experimental part of the project was to evaluate the actual performance of the 4-level system and to determine what practical advantages this approach has over other systems. A further objective of this experiment was to verify the validity of the Gram-Charlier series for the characterisation of the PDF of multilevel systems.

With the above objectives in mind, the following measurements were made using the experimental 4-level PAM system.

1. Error probability as a function of the average optical power at the receiver input
2. Error probability as a function of the average avalanche gain of the APD.

The remainder of this chapter describes in detail the circuits used for the experiment, as well as the experimental results.

3.1.1 Overall Experimental Setup

In Fig. 3.6 the 4-level PAM system and test equipment that were used for the experiments are shown. The 1645A Data Error Analyser (manufactured by Hewlett Packard) was used to generate a pseudo-random binary sequence (PRBS) at a rate determined by an external clock. For this experiment, the external clock was set at 4 Mb/sec, which is close to the maximum usable bit rate of the 1645A Data Error Analyser. The fiber-optic system is, however, capable of operating at much higher rates.

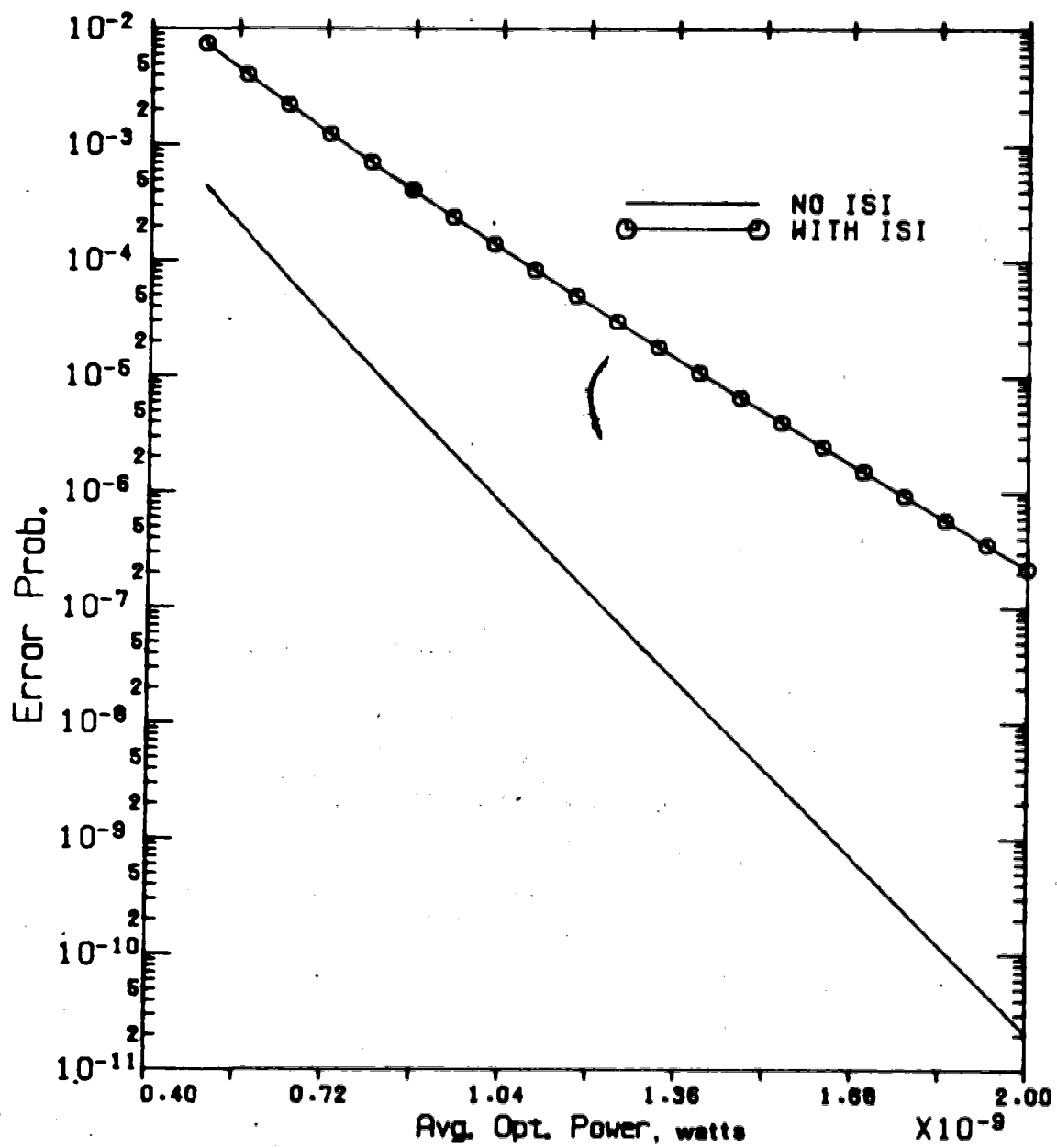


Figure 3.5 Plot of error probability as a function of the mean optical power reaching the detector.

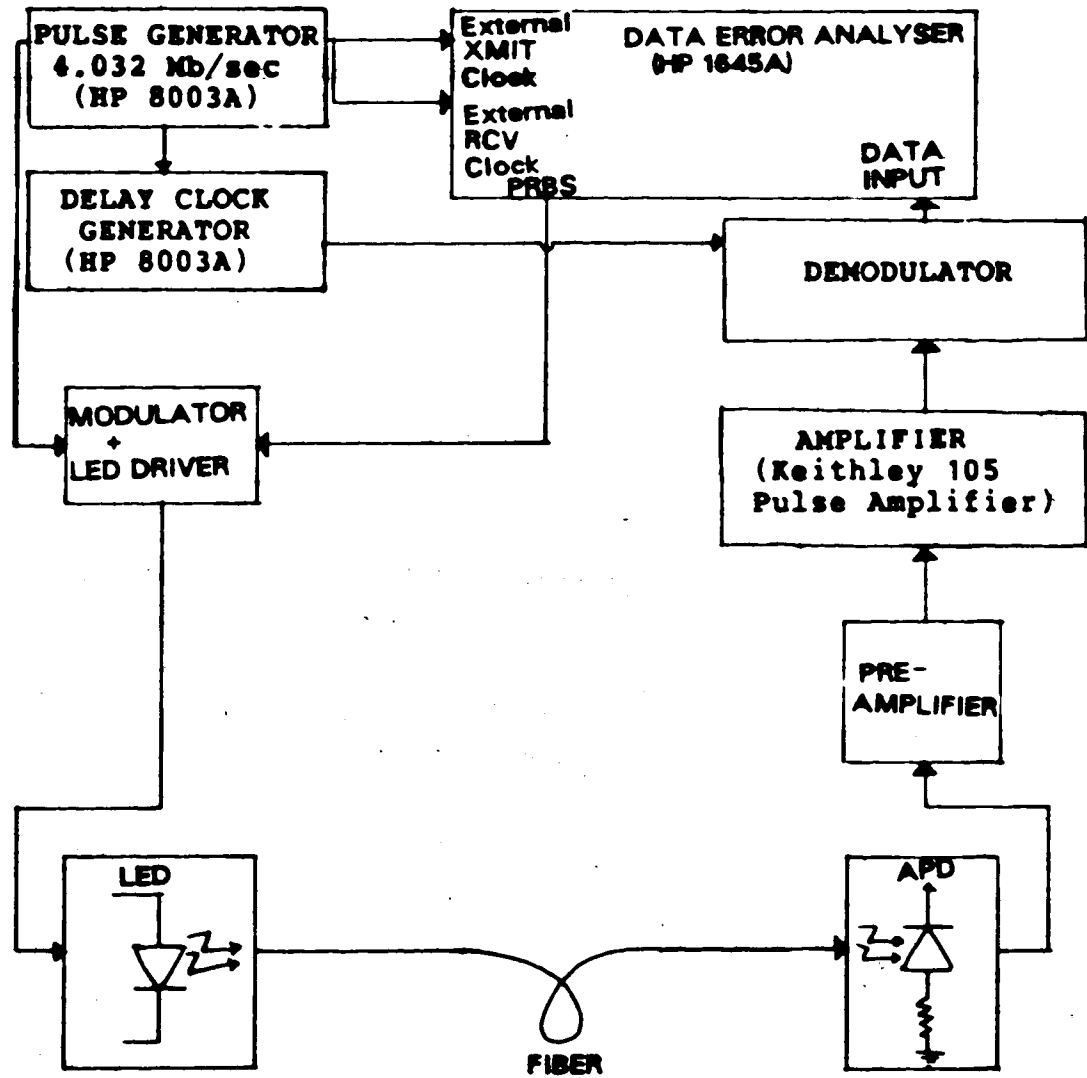


Figure 3.6 The experimental four-level PAM fiber optic system.

The PRBS is applied to a 4-level modulator which in turn intensity modulates the LED output by means of a driver circuit. The optical signal is coupled to a fiber of 600m length. The output of the fiber is coupled to an APD which converts the optical signal back into an electrical signal. The received signal is then routed through a pre-amplifier and main amplifier. The amplified signals are fed to an integrate-and-dump filter to eliminate some of the noise. Finally the signal is demodulated and fed back to the Data Error Analyser as the data input. The Data Error Analyser compares the system input sequence with the system output sequence and displays the BER. Each of these stages are described in detail in the following pages.

3.1.2 The Data Error Analyser

The HP 1645A Data Error Analyser is well suited for data communication systems and has the capability of simultaneously measuring the following parameters: bit error rate (BER), block error rate (BKER), clock slip rate, carrier loss rate, skew, jitter and total peak distortion. These parameters are measured during a test sequence, digitally stored, and read out later.

For the purposes of this project, the BER and BKER measurements were of greatest interest, although the other measurements did provide added insight into the operation of the system.

The 1645A computes the error rate by correlating the received bit pattern with a local replica of the transmitted data sequence. A pseudo-random binary test sequence (PRBS) can be generated of length $2^n - 1$, $2^{n-1} - 1$, $2^k - 1$ or $2^k - 1$ bits. Also sequences of type 7:1 (7 zeroes followed by a one), 3:1 and 1:1 can be generated. The 1645A divides the test data sequence into 1000-bit blocks for test analysis. The BER is the number of times a bit error occurs during the full test sequence. The BKER is an indication of the number of received blocks containing one or more errors. The BER test is used to measure the overall link quality. BKER when compared to BER on the same data base, provides an indication of the burst characteristics of the errors.

If errors occur in a distributed fashion (high BKER) then other tests such as skew, jitter or total peak distortion should be reviewed. Also high BER with low BKER indicates that phase hits (i.e. clock slips) and dropouts should be checked. The SKEW measurement

indicate the percentage of ones changed to zeros. Ideal skew characteristics of erroneous data is 50% i.e. errors should be equally distributed between ones being mistaken for zeros and vice-versa. If errors are skewed, there are two possible causes; errors are being repeated (patterned) or a decision threshold is set at an incorrect level, so that errors are weighted in one direction or the other.

The 1645A also has a digitally matched filter which can be switched in or out ahead of the error detection circuit. The filter removes the high-frequency noise and prevents data sampling on spurious pulses.

The flowchart of Fig. 3.7 summarises the measurement troubleshooting procedure [32].

3.1.3 Four-level Modulator and LED Driver

The 2-level PRBS signal coming out of the 1645A Data Error Analyser is converted to a 4-level signal using the circuit shown in Fig. 3.8. The basic function of this circuit is to combine two binary pulses and generate one out of 4 possible signal levels based on this sequence. The possible sequences are: 00, 01, 10 and 11. A sequence of 00 produces the lowest of the four signal levels and a sequence of 11 produces the largest.

U_{1A} and U_{1B} form a 2-bit shift register. After 2 clock pulses the inputs to U_{1A} and U_{1B} contain the first and second bits respectively. The outputs of U_{1A} and U_{1B} are coupled to transistors Q_1 and Q_2 on the application of a clock pulse from U_1 via U_4 . Since Q_1 and Q_2 are emitter coupled, the current flowing through the LED is the sum of the individual emitter currents which depend on the individual base voltages which in turn depends on the signal sequence. The choice of the optical source was based on considerations of reliability, linearity, dynamic range and cost. The Northern Telecom NT-40-3-30-3 LED was found to best fit these requirements and was consequently selected as the optical source.

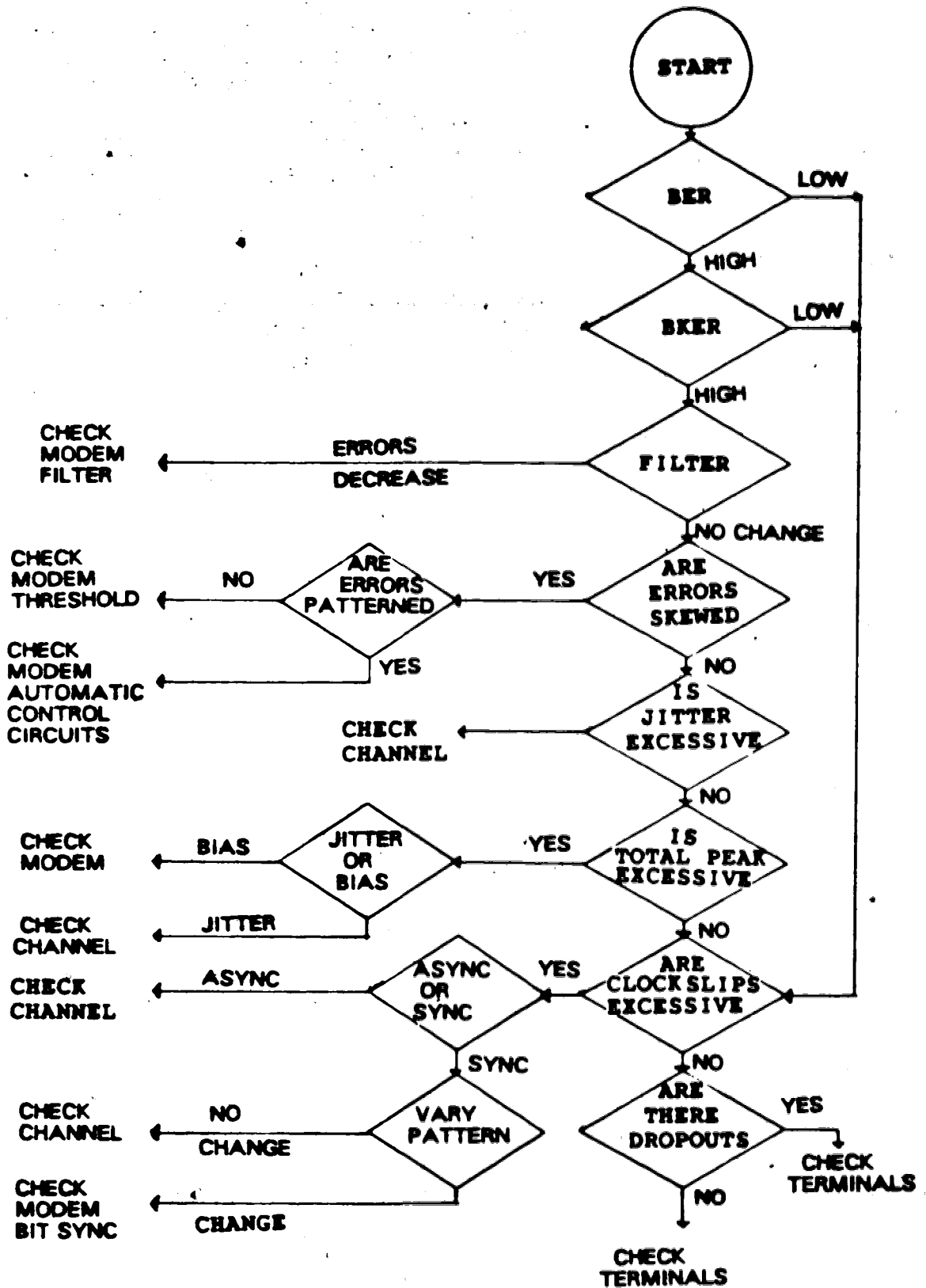


Figure 3.7 Algorithm for the troubleshooting of the optical fiber system.

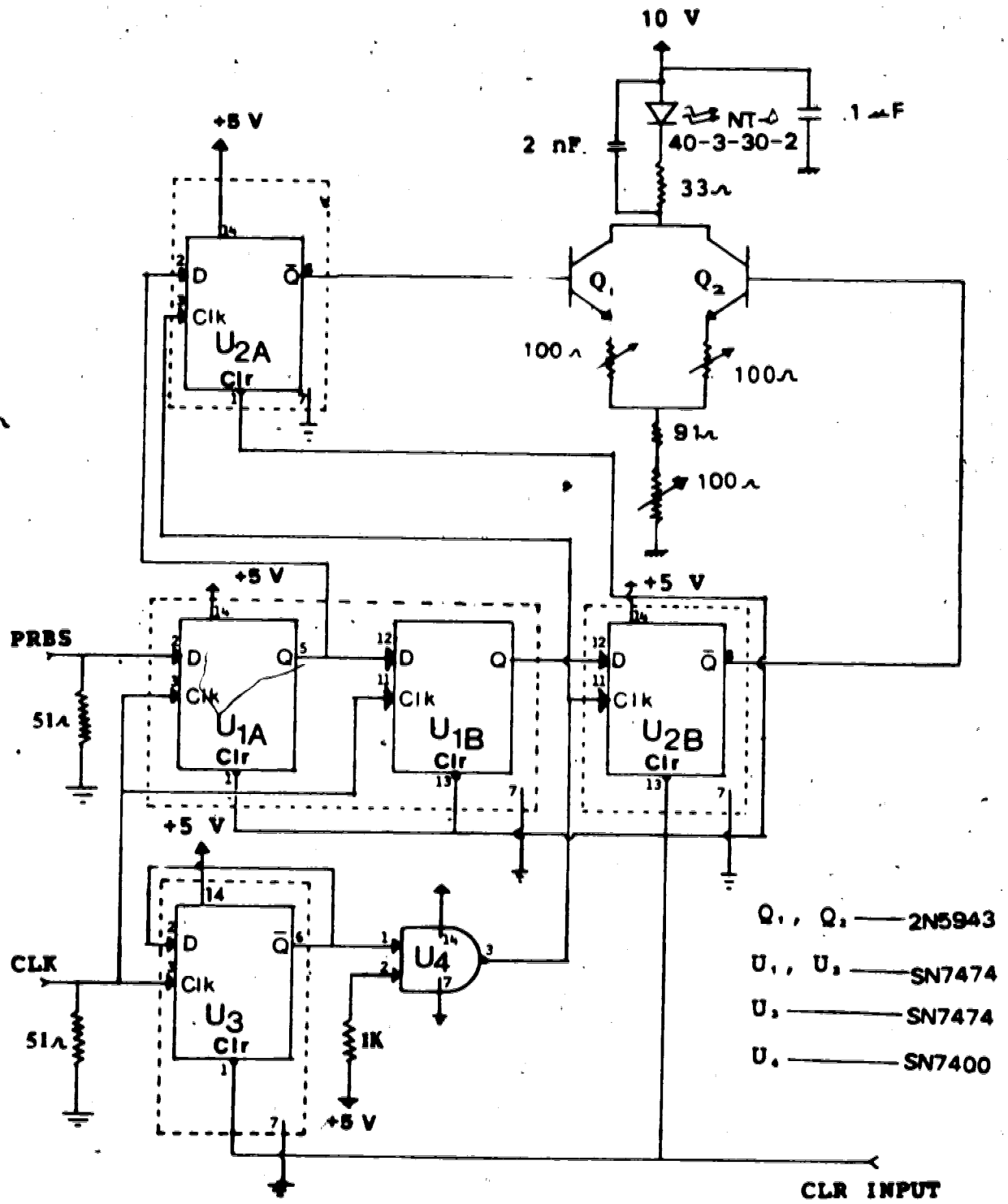


Figure 3.8 Circuit diagram of the 4-level modulator and LED driver.

3.1.4 The Choice of the Fiber

A typical fiber-optic system design requires the selection of the link length, the repeater spacing, the rise time budget and the loss budget. The aim of the present experiment was to observe the effect of the various noise sources on the BER. A major consideration in choosing the fiber type was that it should have a sufficiently narrow bandwidth that intersymbol interference will be observed. To observe intersymbol interference for a binary sequence transmitted at 4 Mb/sec., the bandwidth of the fiber should be lower than 8 Mhz. [33]. A GI Fiber (Siecor Super Fat Fiber Cable 155) with bandwidth of 5 Mhz.km was chosen. This fiber has a very large attenuation of 35 db/km. Keeping in mind the sensitivity of the receiver, the length of the fiber was chosen to be 600m. (these fibers are drawn to lengths of 100m, 400m and 600m). Other characteristics of this Siecor fiber are its comparatively high numerical aperture (i.e. its light gathering ability) of 0.4, its high strength and its flexibility.

3.1.5 Receiver Section

The front-end of an optical receiver consists of a photodetector (generally a PIN diode or an APD) along with some form of amplifying stage or stages. The overall combination of the detector, amplifier and subsequent filtering is designed to respond to the input light signal in such a way as to provide an output pulse shape (usually with raised cosine spectrum) appropriate for presentation to the digital decision circuit. The combination, referred to as a linear channel, must therefore have sufficient bandwidth to respond properly to the input pulse. It should also contribute as little noise as possible in order to give good optical sensitivity.

There are two approaches normally used for receiver design, i.e. the high input impedance method and the feedback method. In the high input impedance design, note is made of the fact that bit error probability is reduced by increasing the input resistance and decreasing the input capacitance. This, however, results in the integration of the detected signal. To compensate for this an equaliser stage is necessary at the end of the amplifier stage. Quite often the equaliser is just a differentiator. The equaliser does not introduce much noise because it follows the amplification stages. Most of the noise contribution occurs at the input. Thus a high-impedance equalised amplifier is capable of

extremely low noise while retaining the pulse shape. There are, however, a few problems with the high-impedance approach. The transfer function of the equaliser depends on the value of R_T and C_T (see Fig. 2.4, $R_T = R_a // R_b$ and $C_T = C_a + C_d$), which depend in turn on parasitic capacitances and on the β of the transistor. As a result, individual amplifiers may have to be individually equalised. In addition, temperature compensation schemes may be necessary. This complicates the equaliser design. Another problem is the reduction of the dynamic range due to the build-up of charge on the amplifier input capacitance. This problem can be eliminated by actively discharging the input capacitance, but this introduces more complexity into the receiver design.

Another preamplifier type, commonly employed for front end design is the transimpedance or current-to-voltage converter. The transimpedance amplifier has wider bandwidth (BW), greater dynamic range and a noise performance almost as good as the high-impedance amplifier [34]. The increased bandwidth is due to the feedback scheme being used. The wide dynamic range arises because the low-frequency signal has a closed loop amplification (which is controlled by external elements). It is the low frequency signal which is increased by front-end integration thereby causing the amplifier to saturate prior to the equaliser. Improvement in the dynamic range is proportional to the ratio of the open-loop gain to the closed loop gain. The major drawback of the transimpedance approach is the fact that it tends to oscillate for high gains.

The feature of the transimpedance amplifier that makes it desirable for the present use is that, compared to an unequalised amplifier not employing feedback, it is less noisy for a given BW (the resistor noise is reduced) or alternatively has more BW for a given noise level. It does this at the expense of extra optical power (typically 1 db.) to achieve a given error rate. Circuit simplicity, eliminating the need to employ equalisation and obtaining increased dynamic range were judged worth the 1 db loss in sensitivity.

Fig. 3.9 shows the circuit diagram of the FET preamplifier that was used for this experiment. The circuit used here is a modification of a GaAs FET amplifier designed by Ogawa and Chinook [35]. The design of the first stage requires particular attention since it normally contributes most of the amplifier noise. Since this particular feedback

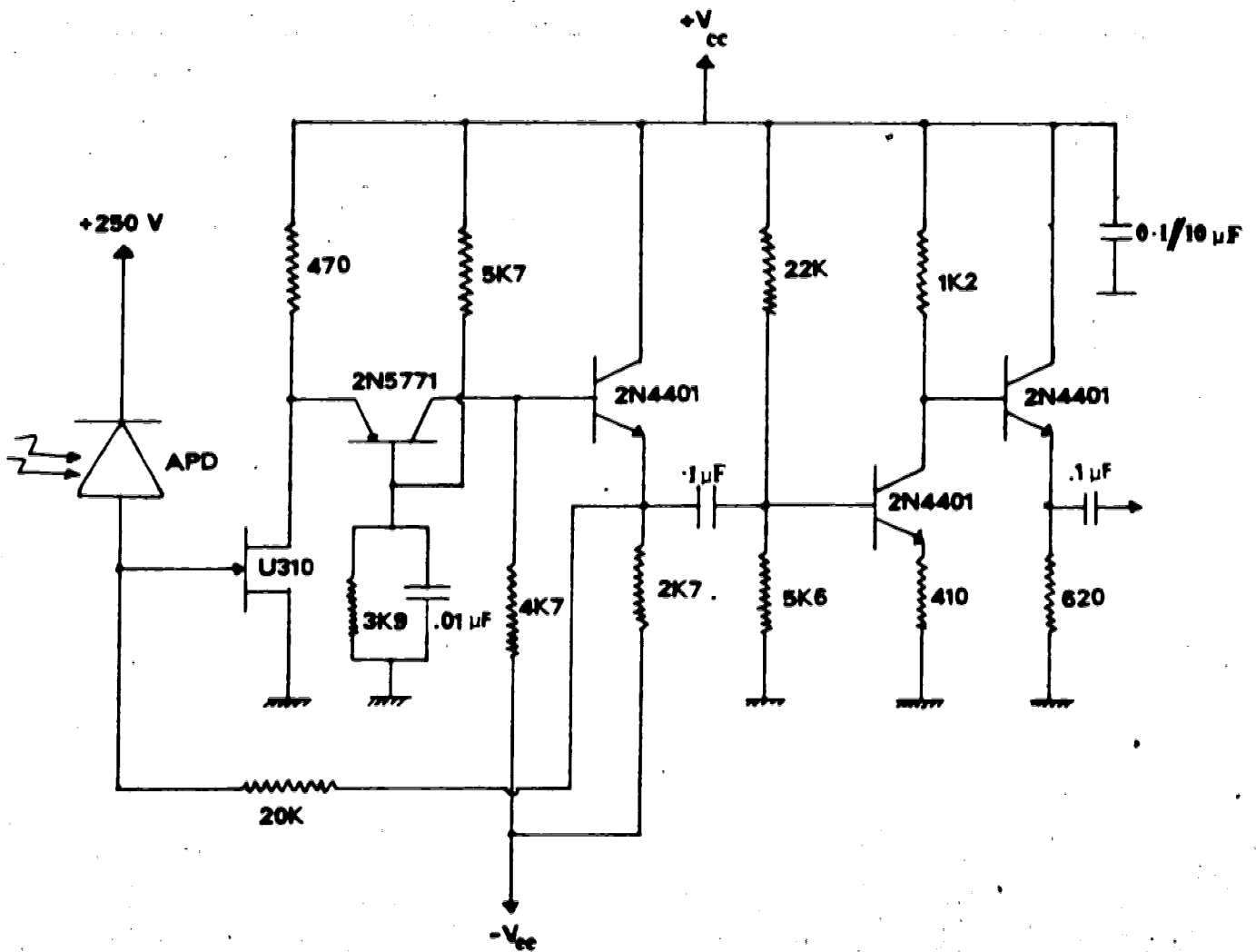


Figure 3.9 Circuit diagram of the FET preamplifier.

configuration is considered for application below 100 Mhz, a junction FET was chosen as the active device. At this frequency, commercially available FET's are generally less noisy than commercially available bipolar transistors.

The first stage FET is operated optimally in the common source mode. In this mode, the input impedance is high, as dictated by (2.31). A common-base stage follows the F.E.T. Such a configuration used with the a bipolar transistor minimises the Miller capacitances and produces a high open loop gain.

The emitter follower stage, using an $n-p-n$ transistor, is used after the common-base stage. The feedback resistance is connected from the emitter of this transistor to the base of the FET. The value of the feedback resistor was chosen to be equal to 20 k in order to avoid oscillation of the preamplifier. Further amplification is provided by the next stage. The final stage is an emitter follower which is used because of its low output impedance. A low output impedance is necessary for impedance matching with the main amplifier (Keithley 105 Pulse Amplifier) that was connected after the preamplifier. The voltage gain of the preamplifier was measured to be 30 and the gain of the main amplifier was set to 100.

3.1.6 Integrate-and-Dump Filter

The integrate and dump filter, at the output of the receiver main amplifier, helps to smooth out the noisy amplified voltage and thereby increase the signal to noise ratio. It is also needed in order to prevent oscillation of the comparator circuits used in the demodulator.

Fig. 3.10 is a circuit diagram of the integrate and dump filter that was used for the 4-level PAM communication system. The basic requirements of this filter are a slow integration time (between 100 to 200 ns.) and a very quick dump time (less than a few nanoseconds). To do this, an RC integrator has been used with a diode connected in series with R to avoid discharge of the capacitor. A VMOSFET switch (VN10KM) is connected across the capacitor. Whenever the gate signal is above the pinch-off voltage of the FET (in this case 2.0 V), the FET is turned on such that the drain-source resistance (r_{ds}) is very small (approx. 5 ohms).

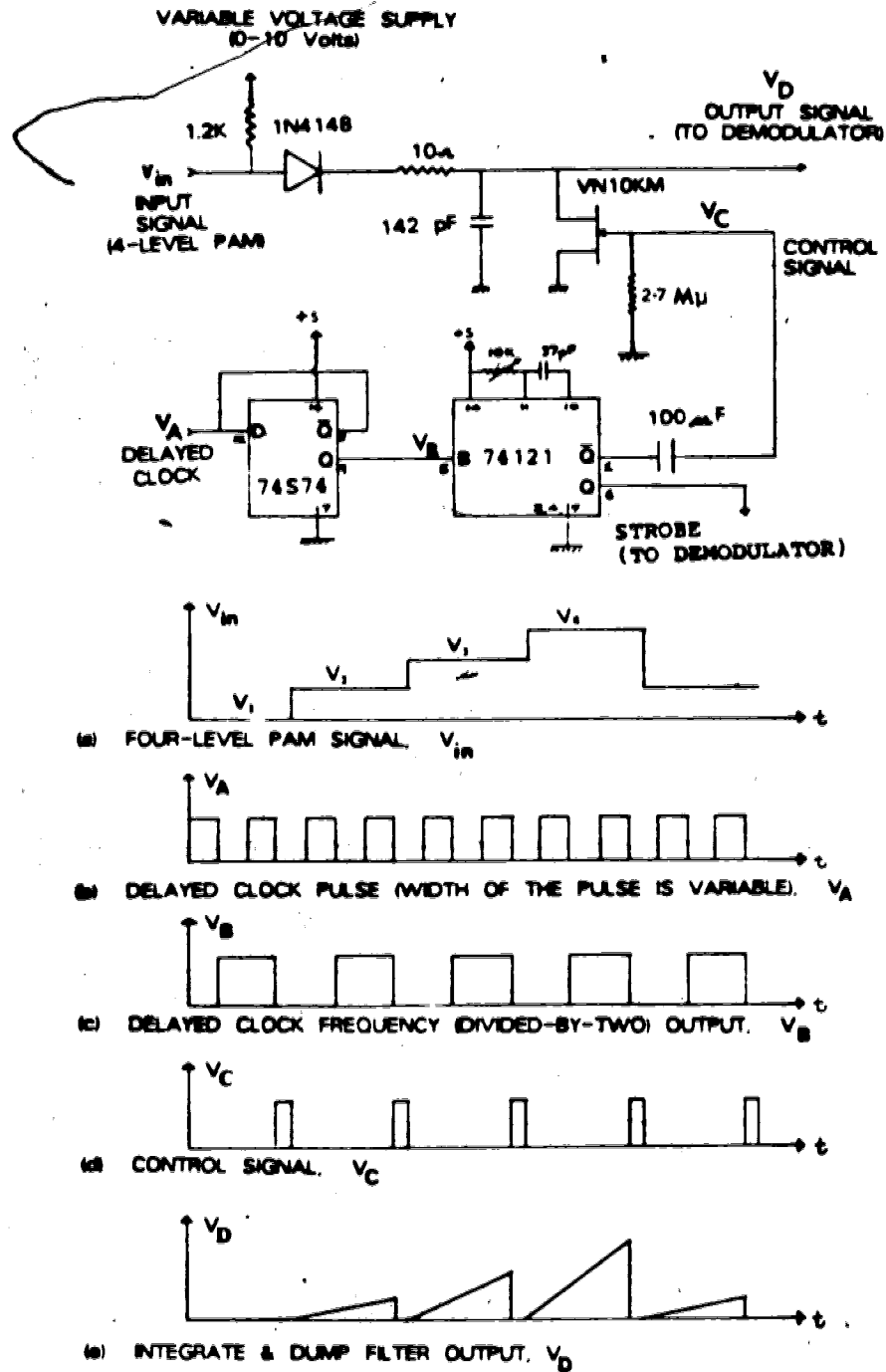


Figure 3.10 Circuit diagram of the integrate-and-dump filter used for the 4-level PAM system. Also shown are the input and output waveforms and the control signal.

3.1.7 Demodulator

The output of the integrate and dump filter is a sequence of 4-level signals which has to be converted back into a 2-level sequence before any error rate measurements can be made. This conversion is achieved by the demodulator circuit. The circuit diagram of the demodulator that was designed and built for this project, is given in Fig. 3.11. The clock signal to the demodulator is the same 4 Mb/sec. clock that was fed to the modulator, except that it is delayed by a certain time period. The delay of the clock should be set so as to match the delay in the transmission of the signal through the fiber. Since this delay is not known exactly it was adjusted so as to give the lowest value of BER.

The first stage consists essentially of three comparator circuits (LM361) which decide which of the 4 levels was transmitted. The rest of the circuit consists of NAND and OR gates which reconstruct the 2 level signal based on the output of the comparators. Fig 3.12 presents the timing diagram for this circuit.

3.1.8 Error Rate Measurements

The demodulator output is fed to the data input terminal of the Data Error Analyser. The Data Error Analyser correlates the received bit pattern with the transmitted data sequence and determines the number of errors occurring in a certain amount of data. It automatically computes the BER for that length of data.

Measurements were made of the BER as a function of the average avalanche gain of the APD and as a function of the average optical power reaching the detector. The results obtained have been plotted in Fig. 3.13 and in Fig. 3.14. The measured signal levels and error probabilities have been given in Table 3.3

3.2 DISCUSSION OF RESULTS

In order to compare the experimental results with theoretical calculations it is necessary to determine the following system parameters:

1. Thermal noise of the amplifier.
2. The value of the ionisation coefficient, K .
3. The value of the mean avalanche gain as a function of the reverse bias voltage.

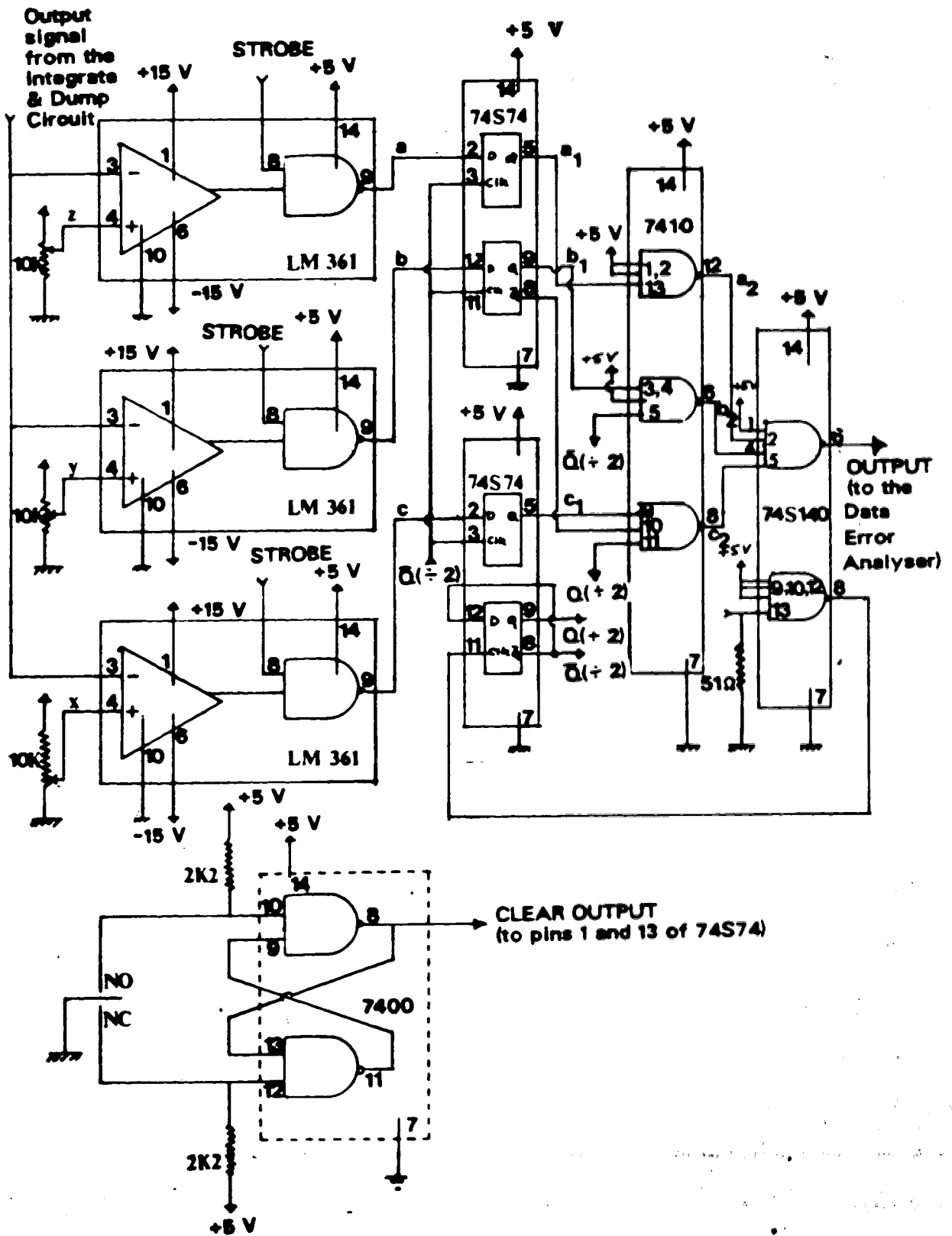


Figure 3.11 The 4-level demodulator circuit diagram.

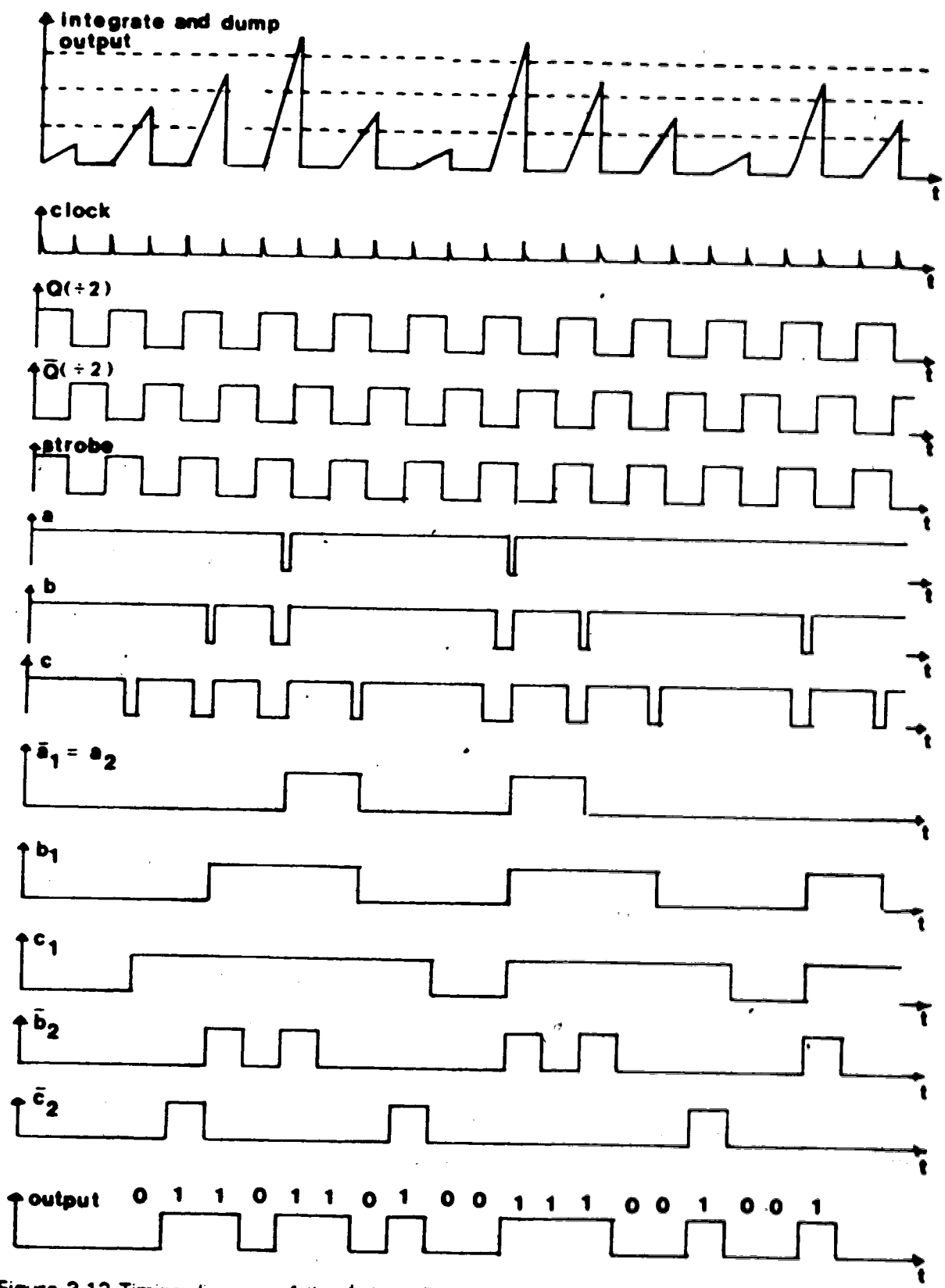


Figure 3.12 Timing diagram of the 4-level PAM demodulator.

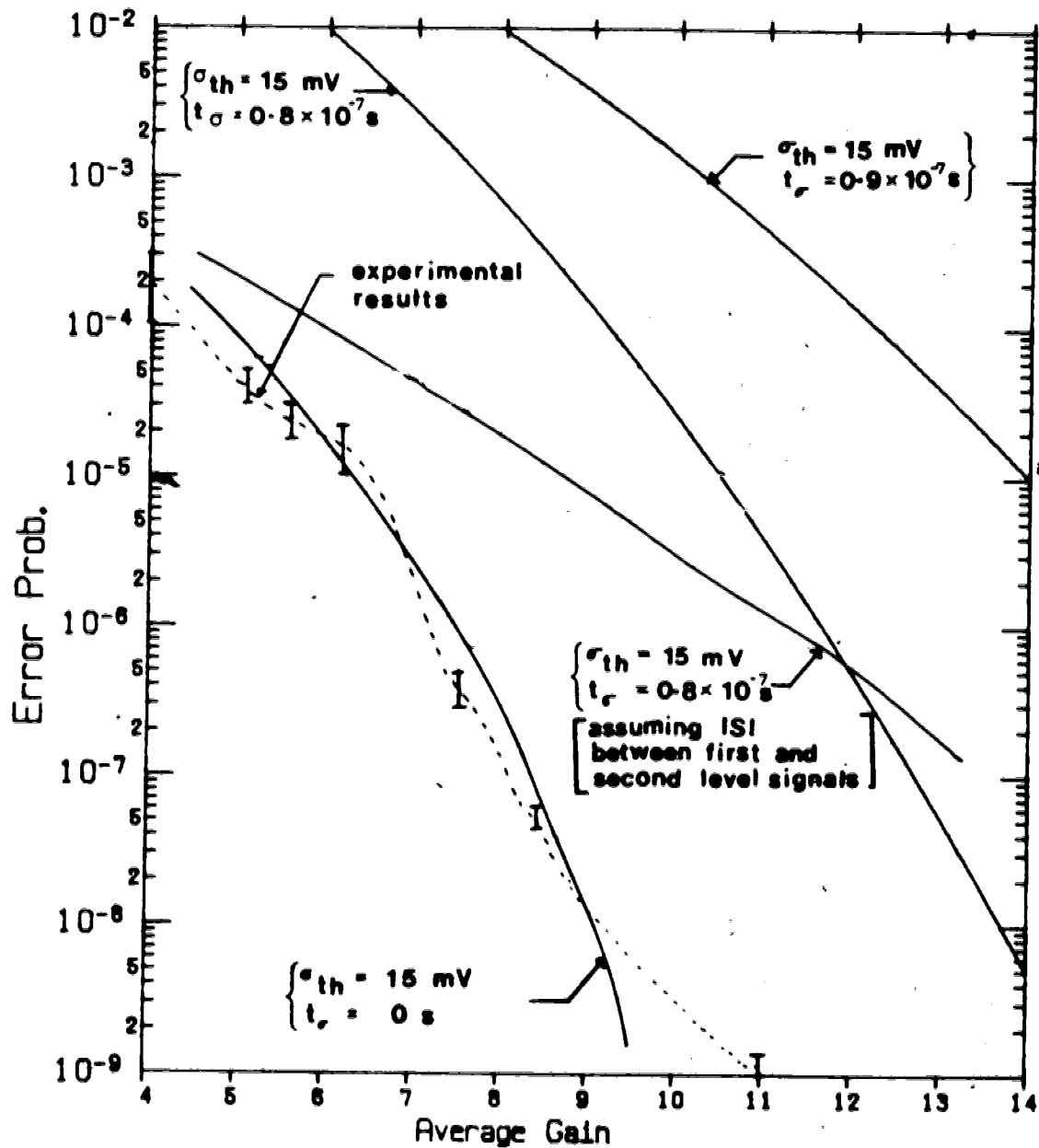


Figure 3.13 Error probability as a function of the mean avalanche gain of the APD for an experimental 4 level PAM system.

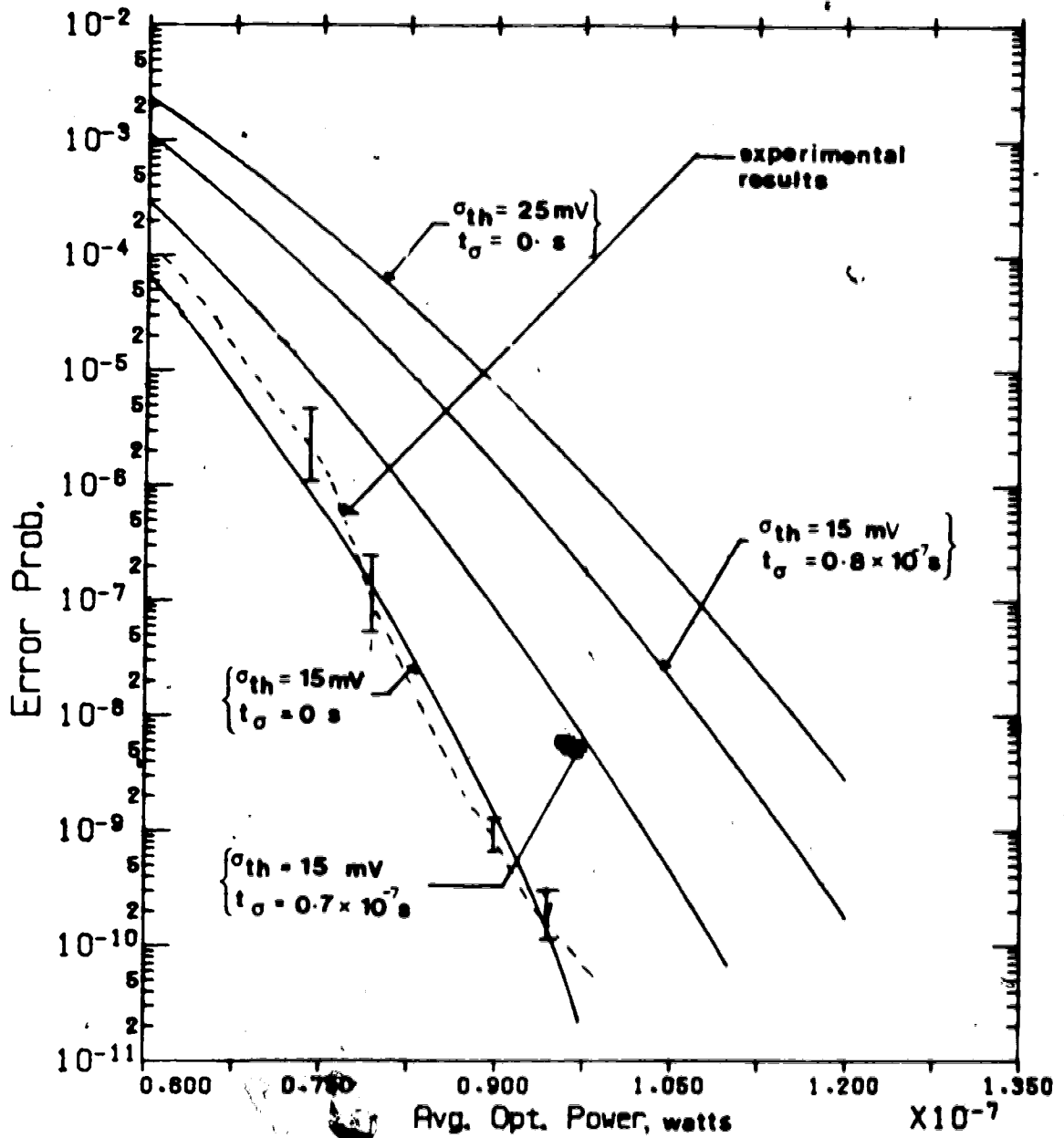


Figure 3.14 Error probability as a function of the average optical power at the input to the receiver for a 4 level PAM system.

TABLE 3.3

MEASURED VALUES OF SIGNAL LEVELS AND THRESHOLDS FOR THE
EXPERIMENTAL FOUR-LEVEL PAM SYSTEM

<G> v.s Error Probability

Pavg = 107nW

G	M(1) mV	X(1) mV	M(2) mV	X(2) mV	M(3) mV	X(3) mV	M(4) mV	Error Prob.
4	0	120	240	320	400	460	520	2.1×10^{-4}
5.13	0	200	400	530	660	730	800	4.2×10^{-5}
5.65	0	255	510	665	820	910	1000	1.8×10^{-5}
6.38	0	270	540	730	900	1000	1100	1.6×10^{-5}
7.5	0	280	560	750	965	1107	1250	4.3×10^{-7}
8.5	0	290	580	830	1080	1190	1300	5.3×10^{-8}
11.3	0	325	650	1025	1400	1550	1700	1.2×10^{-9}

Pavg vs. Error Probability

<G> = 5

Pavg (nW)	M(1) mV	X(1) mV	M(2) mV	X(2) mV	M(3) mV	X(3) mV	M(4) mV	Error Prob.
74.1	0	120	240	305	370	415	460	2.1×10^{-6}
79.4	0	140	280	360	440	480	520	$1. \times 10^{-7}$
89.1	0	170	340	440	540	580	620	8.3×10^{-10}
100	0	195	390	500	610	675	740	2×10^{-10}
110	0	200	400	520	640	710	780	0
120	0	225	450	580	710	785	865	0

4. The quantum efficiency of the APD.

The thermal noise was determined by measuring the output signal when there was no input signal to the amplifier. The value of thermal noise was estimated to be 15 mV, from measurements made with the Spectrum Analyser. The value of the ionisation coefficient is highly dependent on the individual device. For Silicon, its value is typically in the range 0.01 to 0.04. The calculated error probability did not vary much over this range of K , and a value of 0.02 was chosen in all the theoretical calculations.³

The value of the average avalanche gain as a function of the reverse bias voltage for an APD is determined industrially by fabricating a PIN diode and an APD on the same chip and taking the ratio of the output currents. This ratio directly gives the average avalanche gain of the APD. A simpler method, but not as accurate, is to determine the reverse bias voltage beyond which one actually observes increased output signal. This reverse bias voltage, or any smaller voltage, then can be assumed to correspond to a unity avalanche gain. For any other setting of reverse bias, the average avalanche gain can be assumed to be the ratio of the output signal for that setting to the output signal for an average gain equal to one. This method is accurate to within 10%.³ Fig. 3.15 is a plot of the average avalanche gain of the APD as a function of the reverse bias voltage.

The value of the quantum efficiency of the APD was not supplied by the manufacturer. The value of the quantum efficiency can vary typically from 0.6 to 0.9. The error rate was observed to be fairly insensitive to the value of the quantum efficiency over this range and was arbitrarily chosen as 0.85 for all the theoretical calculations.

Figs. 3.13 and 3.14 show the variation of the error probability as a function of the average avalanche gain of the APD and as a function of the average optical power reaching the detector. The experimental results are compared to the results obtained theoretically for a range of values of the thermal noise, σ_{th} . It is seen in this graph that the error probability is highly sensitive to the value chosen for σ_{th} .

The effect of intersymbol interference on error probability is also shown in Figs. 3.13 and 3.14 by considering different values of rise (or fall) times, t_{σ} , of the optical pulse reaching the detector. In actual practice, it is difficult to determine t_{σ} accurately.

³Private communication, R.J McIntyre, RCA labs, Montreal.

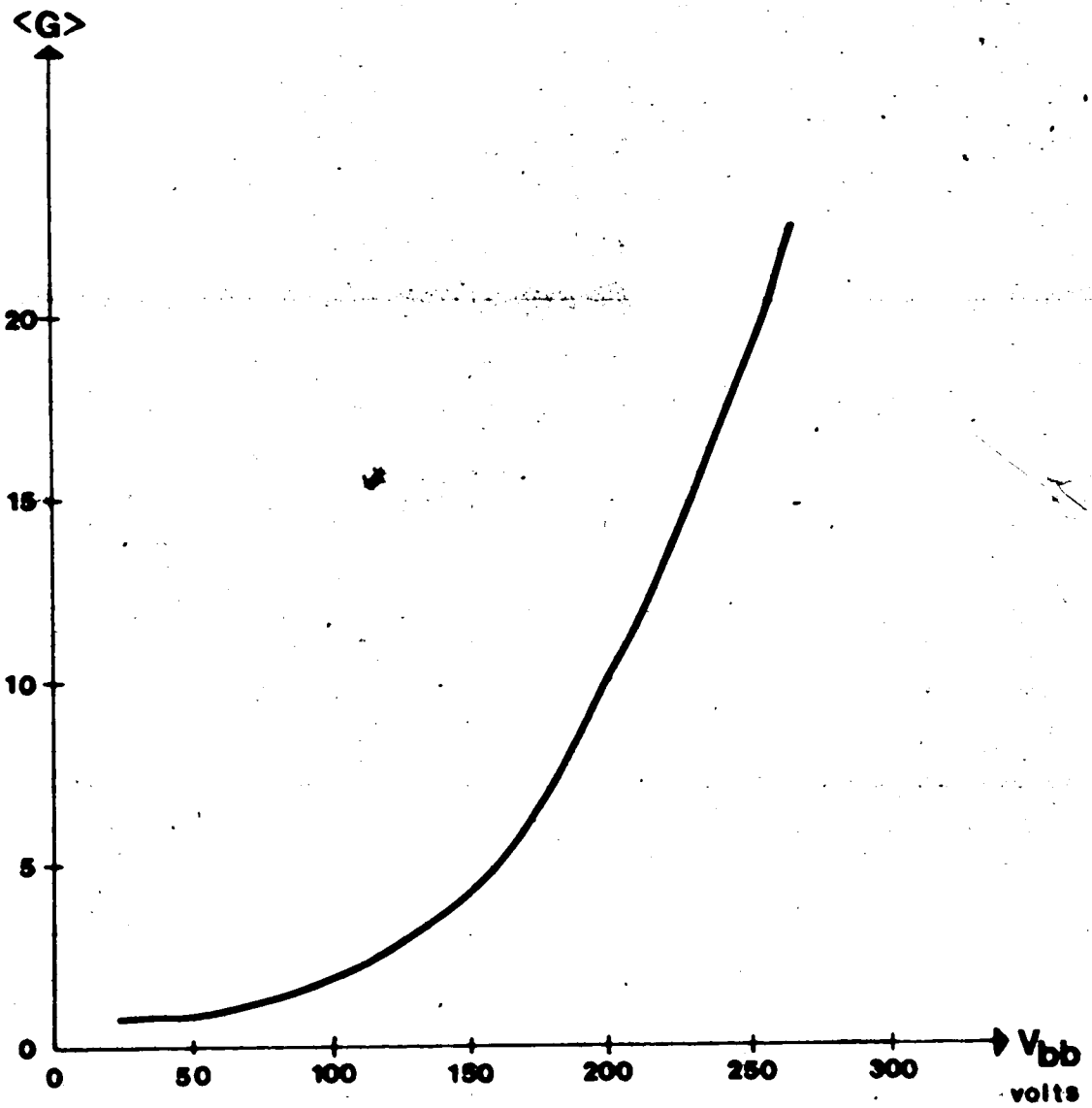


Figure 3.15 Mean avalanche gain of an APD as a function of the reverse bias voltage

Other factors which could affect the results are the inconstant delay of the clock pulse to the demodulator. The theoretical results were obtained assuming that the decision is made at the same position during each time slot. It was observed, however, that the delay of the clock pulse to the demodulator tended to vary with time. In addition, the readings of the optical power were accurate to ± 1 dB. It has already been shown that the error probability is highly sensitive to changes in the received optical power. From Fig. 3.5, even a 3 dB change in power can cause the error probability to change by a few orders of magnitude. Thus the errors in reading the optical power could result in a mismatch between experimental and theoretical results.

Despite the various inaccuracies that could result from all the above factors, the results shown in Figs. 3.13 and 3.14 match fairly well with the values obtained using the Gram-Charlier series. As seen in Fig. 3.13, there is a slight discrepancy between the theoretical and experimental values of error probability at higher values of avalanche gain (i.e., above 10). The discrepancy arises because the effect of saturation of the main amplifier, which occurs at high avalanche gains, was neglected in the theoretical calculations.

CHAPTER IV

MULTILEVEL PULSE WIDTH MODULATION

The advantages of multilevel signal transmission over regular binary signal transmission has been discussed in Chapter III. The analysis thus far has, however, been restricted to PAM systems. Multilevel PWM transmission is shown, in this chapter, to be an attractive alternative to multilevel PAM.

PWM and PPM transmission have been recognised to be more immune to noise than PAM transmission [37], provided the transmission channel has a sufficiently large bandwidth. PAM is likely to have fluctuations in the output amplitude due to the various noise sources in the system. Such fluctuations in the signal amplitude do not, however, affect the signal content of PWM or PPM systems. This is due to the fact that PWM and PPM techniques involve only the transmission of timing information and not amplitude information. PWM and PPM can, therefore, fully utilise the wideband characteristics of optical fibers in order to decrease the bit error rate.

In this chapter, the pulse widths and threshold levels required for a near-optimum 4-level PWM system are determined. This extends the work of Personick [12] for binary systems and Hullea and Muoi [31] for multilevel PAM systems. It is shown that, given a PDF for the noise amplitude, the PDF for pulse-width can be computed. Thus, the analysis of error probability for PWM can proceed in the same manner as that for PAM.

Two different PWM schemes, one employing a low pass filter (LPF) and the other an integrate and dump filter (IDF), are analysed. It is shown that the LPF scheme can achieve very low error probabilities, provided that a wideband fiber is used. The IDF scheme is shown to be advantageous in systems where such wideband fibers are not available. Examples comparing the two different schemes are given in this chapter. This analysis has been restricted to Gaussian shaped pulse edges at the fiber output. Also, for the sake of simplicity, a Gaussian PDF for the overall noise has been assumed. This analysis could be extended to a non-Gaussian case using the Gram-Charlier series [19].

4.1 MATHEMATICAL MODEL OF THE MULTILEVEL PWM SYSTEM

The fiber optical system model is shown schematically in Fig. 4.1. The message source generates a sequence of statistically independent random variables a_j with values $\{1, 2, 3, 4\}$:

$$x_s(t) = \sum_{j=1}^{\infty} a_j \delta(t-jT) \quad j \in (1, 2, 3, 4) \quad (4.1)$$

where T is the time slot available for each pulse.

The encoder converts the source signal into a symbol sequence suitable for transmission as PWM:

$$x_e(t) = \sum_{j=1}^{\infty} r(s_j, t-jT) \quad j \in (1, 2, 3, 4) \quad (4.2)$$

where $r(s, t)$ is an ideal rectangular pulse of duration s ,

and we assume that $s_1 < s_2 < s_3 < s_4 < T$.

The encoded pulses, $x_e(t)$, suitably amplified, drive the optical source. The optical pulses generated by the source will depend on the bias current, the modulating signal current and on the source response. We denote the output of the optical source as:

$$x_l(t) = \sum_{j=1}^{\infty} r_1(s_j, t-jT) \quad j \in (1, 2, 3, 4) \quad (4.3)$$

where $r_1(t)$ represents the pulse shape at the output of the optical source.

The optical signal suffers attenuation and distortion along the fiber channel. Assuming that the fiber has an impulse response $h_f(t)$, then the optical power, $P(t)$, at the output of the fiber is:

$$P(t) = h_f(t) * r_1(s_j, t) \quad j \in (1, 2, 3, 4) \quad (4.4)$$

The fiber response, $h_f(t)$, is assumed to be such that $P(t)$ has Gaussian leading and falling edges (as shown in Fig. 4.2). This assumption has been shown to be fairly accurate, under certain conditions [38]. For purposes of analysis, the pulse is assumed to start and end at the point where the amplitude of the Gaussian rising and falling edges is 10% of the maximum pulse height. Neglecting the tails of the Gaussian pulses (i.e., the areas below the 10% level) does not affect the calculated error rates for the LPF method of detection and causes only a slight error in the results for the IDF scheme. Thus the optical pulse shape

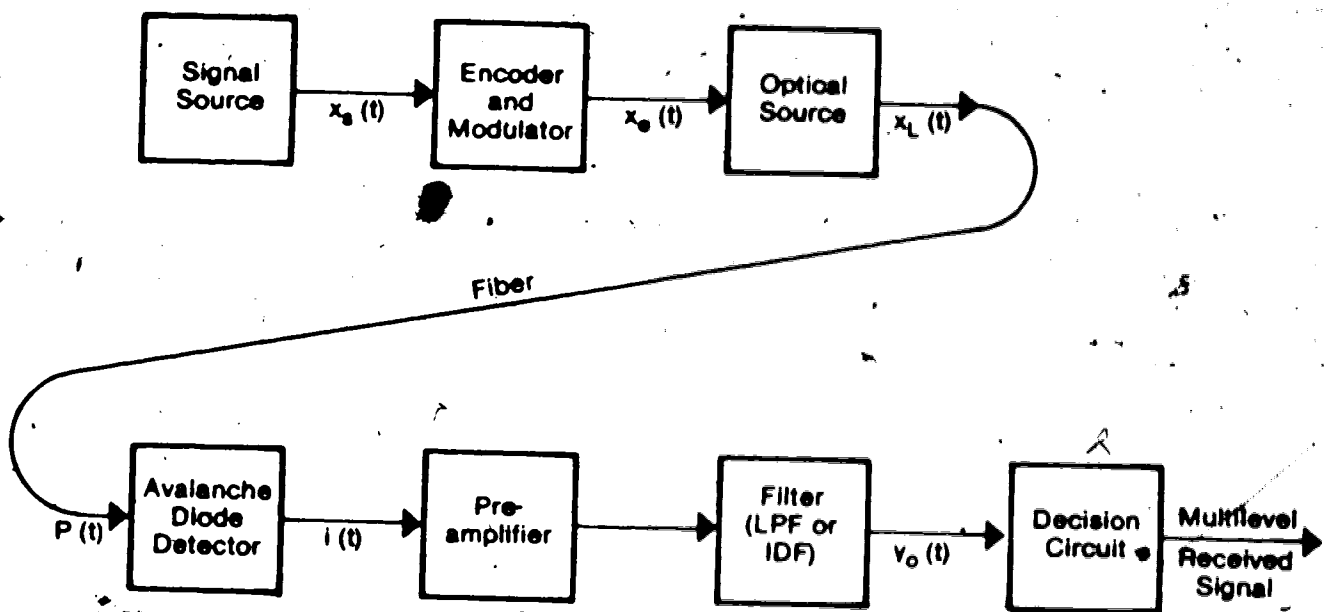


Figure 4.1 Block diagram of a multilevel PWM optical-fiber communication system.

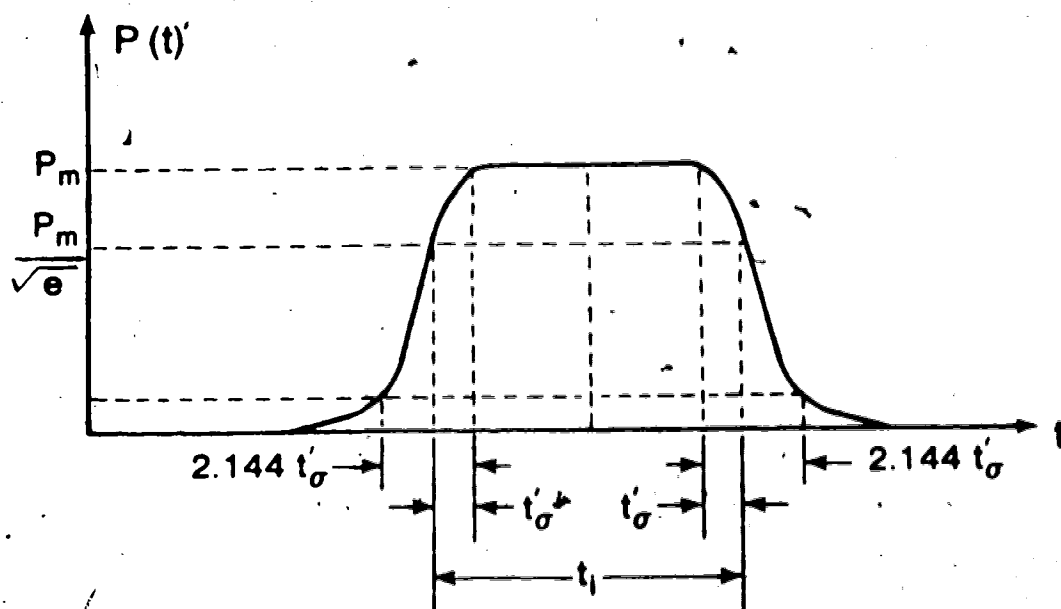


Figure 4.2 Assumed pulse-shape of the optical output power of the fiber.

at the output of the filter, within the i th time interval, can be represented as

$$P(t, iT) = \begin{cases} P_m \exp \left[-\frac{(t - iT - 2.144t'_0)^2}{2t'^2_0} \right] & \text{for } t \in (iT, iT + 2.144t'_0) \\ P_m & \text{for } t \in (iT + 2.144t'_0, iT + t_1 + 0.144t'_0) \\ P_m \exp \left[-\frac{(t - iT - t_1 - 0.144t'_0)^2}{2t'^2_0} \right] & \text{for } t \in (iT + t_1 + 0.144t'_0, iT + t_1 + 2.288t'_0) \end{cases} \quad (4.5)$$

where t'_0 is the time variance of the Gaussian edges and $2.144t'_0$ is the rise time of the optical pulses (from $1/10$ th of the max. value to the max. value).

The receiver section consists of an avalanche photodiode (APD), an amplifier, a filter and a decision circuit (Fig 4.1). The output current of the photodetector can be described as a filtered randomly-multiplied Poisson process. The current from the APD is

$$i(t) = \sum_{n=1}^{k(t_n)} g_n q h_n(t - t_n) \quad (4.6)$$

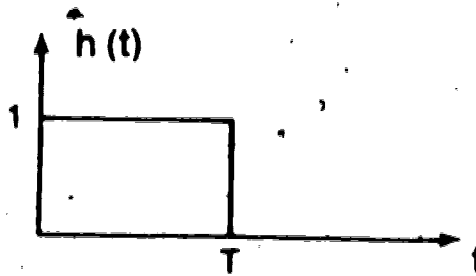
where q is the electronic charge, $h_n(t)$ is the response of the APD and where the number of primary electrons $k(t_n)$, the random time points t_n and the random avalanche gain g_n are statistically independent random variables. The amplifier section introduces Gaussian thermal noise

The average voltage at the filter output (Fig 4.1) at time t is given by (2.78)

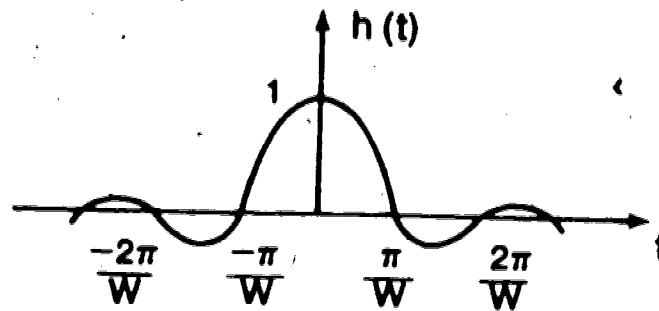
$$v_o(t) = \left(\frac{\eta}{h\nu}\right) (qRA) \langle G \rangle \int_0^t P(\tau) h(t - \tau) d\tau \quad (4.7)$$

where $h(t)$ is the ideal impulse response of the filter (Fig 4.3a & 4.3b)

The decision circuit for the LPF scheme can consist of a threshold detector (slicer), an integrator and a sampler. The output of the slicer is a "clean" pulse with sharp leading and trailing edges. The slicer preserves the width of the received pulses (as modified by noise). In other words, the slicer eliminates all the amplitude noise except



(a)



(b)

Figure 4.3 Impulse response of (a) an ideal IDF and (b) an ideal LPF.

that in the neighbourhood of the threshold, thus greatly reducing the final output noise of the system. One method of measuring the pulse width is to integrate and sample the sliced output every T seconds, yielding a PAM wave. The IDF also produces PAM signals. The original pulse samples can then be regenerated for both the LPF and the IDF schemes.

4.2 NOISE IN A 4-LEVEL PWM SYSTEM

The analysis of the noise properties of a 4-level PWM system are considered here. This analysis has been performed for both the LPF and the IDF schemes. These results are easily extendable to any multilevel PWM system.

4.2.1 LPF system:

Fig 4.4 shows the relationship between the noise amplitude and the timing error at the output of the LPF. The relationship between $\Delta\tau$ (i.e. the timing error due to noise amplitude n_t at time t) and n_t is:

$$\frac{n_t}{\Delta\tau} = \left| \frac{dv_o(t)}{dt} \right| \quad (4.8)$$

The threshold level A_{th} is chosen so as to minimise the effect of n_t on $\Delta\tau$ i.e.

$$\frac{n_t}{\Delta\tau} = \left| \frac{dv_o(t)}{dt} \right|_{\max} = \frac{V_{\max}}{t_\sigma \sqrt{e}} \quad (4.9)$$

where:

t_σ is the time variance of the Gaussian-shaped pulse edges at the output of the LPF.

V_{\max} is the maximum voltage at the output of the LPF given by:

$$V_{\max}' = \left(\frac{n}{h\nu} \right) (qRA) \langle G \rangle \int_{1T}^{t_1 + 0.144t_\sigma' + 1T} P(\tau) h(t_1 + 0.144t_\sigma' + 1T - \tau) dt \quad (4.10)$$

The normalised random output voltage, at time t , with mean m and variance σ_t is:

$$X = \frac{X' - m}{\sigma_t} = \frac{n_t}{\sigma_t} \quad (4.11)$$

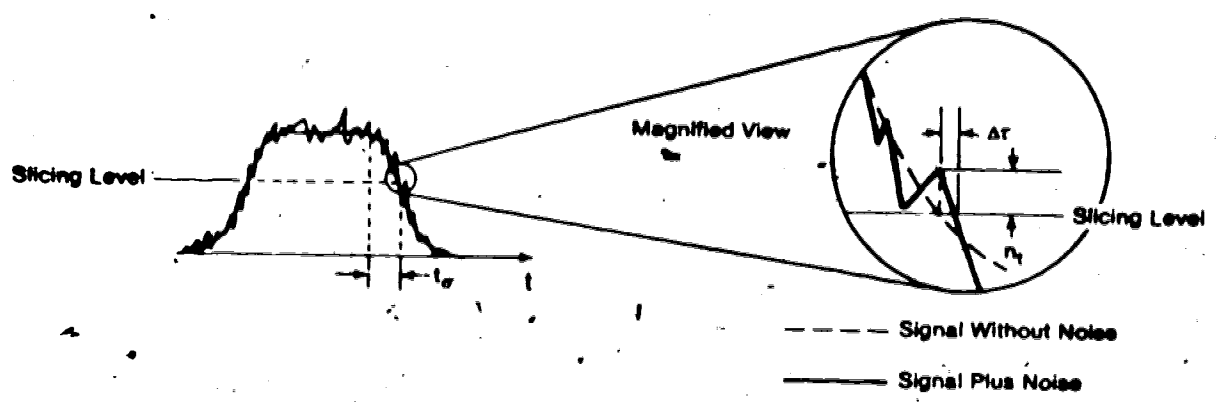


Figure 4.4 Relationship between the noise amplitude and the timing error at the output of the LPF.

or

$$n_t = \sigma_t X \quad (4.12)$$

where:

X' is the non-normalised random voltage and

X is the normalised random voltage.

The variance, σ_t , is given by (3.20):

$$\sigma_t = (\lambda_2 + \sigma_{th}^2)^{1/2} \quad (4.13)$$

where λ_2 is the second cumulant of the random voltage at the output of the filter and

σ_{th} is the thermal noise of the amplifier.

$$\lambda_2 = \left(\frac{n}{h\nu}\right) (qRA)^2 \langle G^2 \rangle \int_{1T}^{t_1 + 1.144t'_0 + 1T} P(\tau) h^2 (t_1 + 1.144t'_0 + 1T - \tau) d\tau \quad (4.14)$$

$\langle G^2 \rangle$ is the second moment of the gain of the APD given by [39]:

$$\langle G^2 \rangle = -(1-k) \langle G \rangle + 2(1-k) \langle G \rangle^2 + k \langle G \rangle^3 \quad (4.15)$$

where k is the ionisation coefficient of the APD.

Substituting (4.8) into (4.11) we get

$$\Delta\tau = \frac{\tau_\sigma \sqrt{e} \sigma_t X}{V_{max}} \quad (4.16)$$

or

$$X(\Delta\tau) = K \Delta\tau \quad (4.17)$$

where K is a constant for a particular pulse-width, given by

$$K = \frac{V_{max}}{\sigma_t \tau_\sigma \sqrt{e}} \quad (4.18)$$

From (4.16) the final relationship between the PDF of the normalised noise amplitude X and the PDF of the pulse width $\Delta\tau$, is derived as:

$$P(\Delta\tau) = P(X(\Delta\tau)) \frac{dX(\Delta\tau)}{d\Delta\tau} \quad (4.19)$$

Assuming that the PDF of X (the normalised random variable) is Gaussian, we have:

$$P(X) = \frac{1}{\sqrt{2\pi}} \exp\left(-\frac{X^2}{2}\right) \quad (4.20)$$

If τ represents the random pulse width, then:

$$\tau = t_1 + \Delta\tau \quad (4.21)$$

From (4.17) and (4.19) the PDF of τ is:

$$P(\tau) = \frac{K}{\sqrt{2\pi}} \exp\left[-\frac{\{K(\tau - t_1)\}^2}{2}\right] \quad (4.22)$$

where t_1 is the average pulse width. Fig. 4.5 shows the PDF for a 4-level PWM system using the LPF scheme. Here:

t_i ($i=1,2,3,4$) correspond to the mean pulse widths.

τ_j ($j=1,2,3$) correspond to the optimal thresholds.

The above theory can be used to compute the error probability as shown in Section 4.3.

4.2.2 IDF system:

An alternative to the LPF system of detecting pulse width is the IDF scheme. The pulses at the output of the preamplifier are integrated and a decision is made about the pulse width, depending on the amplitude of the integrated output.

The PDF of the random output voltage is assumed to be Gaussian, i.e.

$$P(X') = \frac{1}{\sqrt{2\pi} \sigma_{t_1}} \exp\left[-\frac{(X' - m_1)^2}{2\sigma_{t_1}^2}\right] \quad (4.23)$$

where σ_{t_1} is the noise variance term for the i 'th level.

The procedure for calculating σ_{t_1} is the same as for the LPF scheme, except that in (4.12) and (4.13) one must use the impulse response of the integrating filter, shown in Fig. 4.3b.

Fig. 4.6 shows the PDFs for a four-level PWM system using the IDF scheme.

Here:

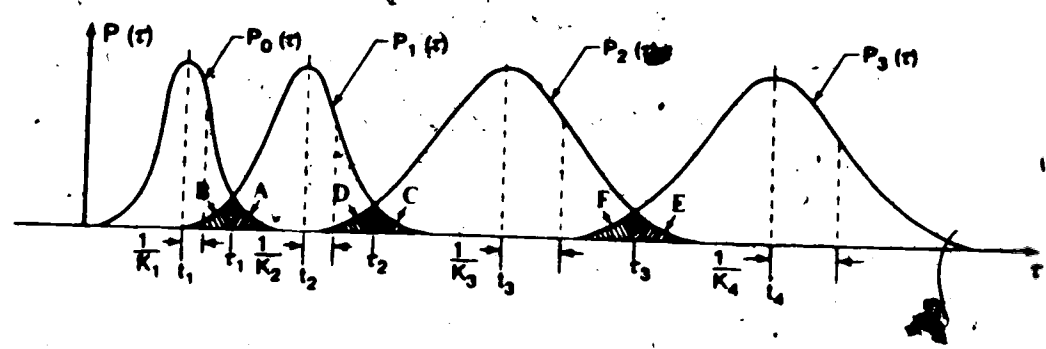


Figure 4.5 Probability density function of the random timing error at the output of a four-level PWM system using an LPF.

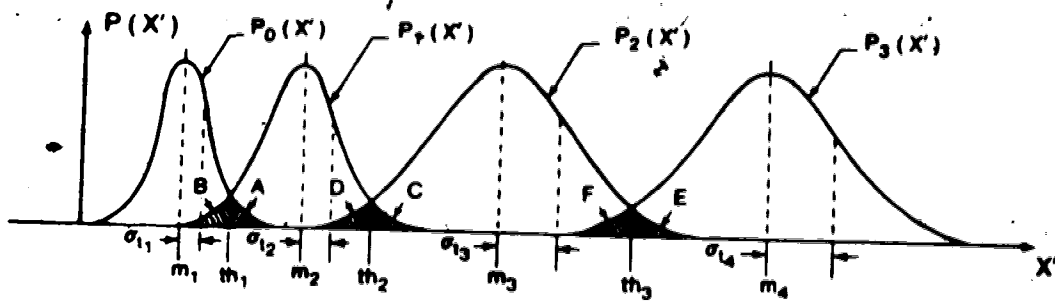


Figure 4.6 Probability density function of the random timing error at the output of a four-level PWM system using an IDF.

X is the random voltage at the output of the IDF.

m_{τ_i} is the mean voltage at the output of the IDF corresponding to a pulse of width

τ_i being transmitted. ($i=1,2,3,4$)

th_j is the amplitude threshold (chosen using the equal area criteria). These correspond to the time thresholds τ_j ($j=1,2,3$)

The error probability can then be computed as shown in the next section.

4.3 ERROR PROBABILITY FORMULATION FOR A 4-LEVEL PWM SYSTEM

The probability of error $P(\epsilon)$, for the 4-level system is

$$P(\epsilon) = p_1 P(2|1) + p_2 (P(1|2) + P(3|2)) + p_3 (P(2|3) + P(4|3)) + p_4 (P(3|4)) \quad (4.24)$$

where

$P(i|j)$ = probability of receiving level i when level j was transmitted ($i, j = 1, 2, 3, 4$)

and p_{τ_i} ($i = 1, 2, 3, 4$) is the probability of sending a pulse of width τ_i . Assuming that the signals have been efficiently randomised so that each of the four levels is equally probable, then p_{τ_i} will be equal to $1/4$. Secondary error terms such as $P(3|1)$ and $P(4|1)$ have been neglected in (4.23).

From Figs. 4.5 and 4.6 it is noted that the above conditional probabilities correspond to the areas A, B, C, D, E and F. Using the equal area criteria and (4.23), each of these areas must be equal to two-thirds of the overall error probability. The error probabilities can be found from (4.21) and (4.22) for the LPF and IDF schemes, respectively.

Thus, for a LPF:

$$A = \int_{\tau_1}^{\infty} \frac{K_1}{\sqrt{2\pi}} \exp \left[\frac{-(K_1(\tau_1 - \tau_1))^2}{2} \right] d\tau$$

$$= \frac{1}{2} \operatorname{Erfc} \left[\frac{K_1(\tau_1 - \tau_1)}{\sqrt{2}} \right] \quad (4.25)$$

and for an IDF:

$$\begin{aligned}
 A &= \int_{th_1}^{\infty} \frac{1}{\sqrt{2\pi} \sigma_{t_1}} \exp \left[\frac{-(x' - m_1)^2}{2 \sigma_{t_1}^2} \right] dx' \\
 &= \frac{1}{2} \operatorname{Erfc} \left[\frac{(th_1 - m_1)}{\sqrt{2} \sigma_{t_1}} \right]
 \end{aligned} \tag{25b}$$

The other areas B,C,D,E and F can be derived in a similar fashion. The following relation is used to compute the optimal pulse width levels t_1 once the m_1 's have been calculated.

$$m_1 = \left(\frac{n}{hV} \right) (qRA) \langle G \rangle \int_0^{t_1 + 2.288 t'_\sigma} P(\tau) h(t_1 + 2.288 t'_\sigma - \tau) d\tau \tag{4.26}$$

where $h(t)$ is the impulse response of the IDF as shown in Fig. 4.3b.

Thus, given the pulse levels and thresholds, the error probability can be computed using the above equations. Conversely, given the required error probability, the near-optimal pulse width levels and thresholds can also be computed.

4.4 NUMERICAL EXAMPLES

We proceed here with the calculations of pulse-width levels and thresholds needed to achieve an error probability lying in the range 10^{-4} to 10^{-10} . The system parameters chosen for this example are given in Table 4.1.

Unlike PAM, where pulses of unlimited amplitude can theoretically be used, in PWM the maximum pulse width is equal to the time slot. The pulse amplitude can, however, be set to achieve any particular error rate. For this example, the maximum pulse amplitude is assumed to be constant at 15 nW, with a minimum pulse width, t_1 , set to be 10 ns. Using equations (4.24a) to (4.24b) (and other equations derived similarly) one may obtain the thresholds and levels for the LPF and the IDF schemes for error probabilities varying from 10^{-4} to 10^{-10} . These are given in Table 4.2.

A graph of error probability vs. P_m is shown in Fig. 4.7 for both the LPF and IDF schemes. A mean avalanche gain of 100 has been used. The results for 3 different rise times have been shown. Fig. 4.8 is a plot of error probability vs. $\langle G \rangle$ for the LPF and IDF schemes. These plots have been made for different values of P_m (5nW, 15nW and

TABLE 4.1

PARAMETERS USED IN NUMERICAL CALCULATIONS

PARAMETER	DEFINITION	VALUE
η	Quantum efficiency of the APD	0.85
R	Amplifier input resistance	700 ohms
A	Amplifier gain	4000
$\langle G \rangle$	Average avalanche gain	100
ν	Optical carrier frequency	3.614×10^{14} Hz
K	APD Ionisation ratio	0.02
τ_0	Variance of Gaussian optical pulse edge	1 ns
σ_{th}	Thermal noise	3 mV
ω	Bandwidth of the LPF	$\pi \times 10^9$ rad/s

TABLE 4.2

REQUIRED PULSE WIDTH LEVELS, USING AN IDEAL LPF AND IDF FOR A RANGE OF ERROR PROBABILITIES (TIME IN nanoseconds)

P_{err} MAI	10^{-4}	10^{-3}	10^{-2}	10^{-1}	10^{-0}	10^{-0}	10^{-10}
τ_1	10.00	10.00	10.00	10.00	10.00	10.00	10.00
τ_1	12.19	12.90	12.78	13.03	13.26	13.48	13.69
τ_2	14.39	15.00	15.55	16.06	16.53	16.97	17.38
τ_2	16.58	17.50	18.33	19.09	19.79	20.65	21.07
τ_3	18.78	20.00	21.11	22.12	23.05	23.93	24.76
τ_3	20.97	22.51	23.89	25.15	26.32	27.41	28.45
τ_4	23.17	25.01	26.66	28.18	29.58	30.89	32.14
τ_1	10.00	10.00	10.00	10.00	10.00	10.00	10.00
τ_1	14.13	14.70	15.22	15.69	16.14	16.55	16.94
τ_2	19.94	21.07	22.45	23.75	24.98	26.16	27.29
τ_2	24.79	27.20	29.64	31.55	33.56	35.48	37.34
τ_3	31.29	34.95	38.38	41.64	44.77	47.78	50.71
τ_3	37.62	42.51	47.13	51.53	55.76	59.86	63.85
τ_4	45.18	51.65	57.78	63.66	69.34	74.87	80.25

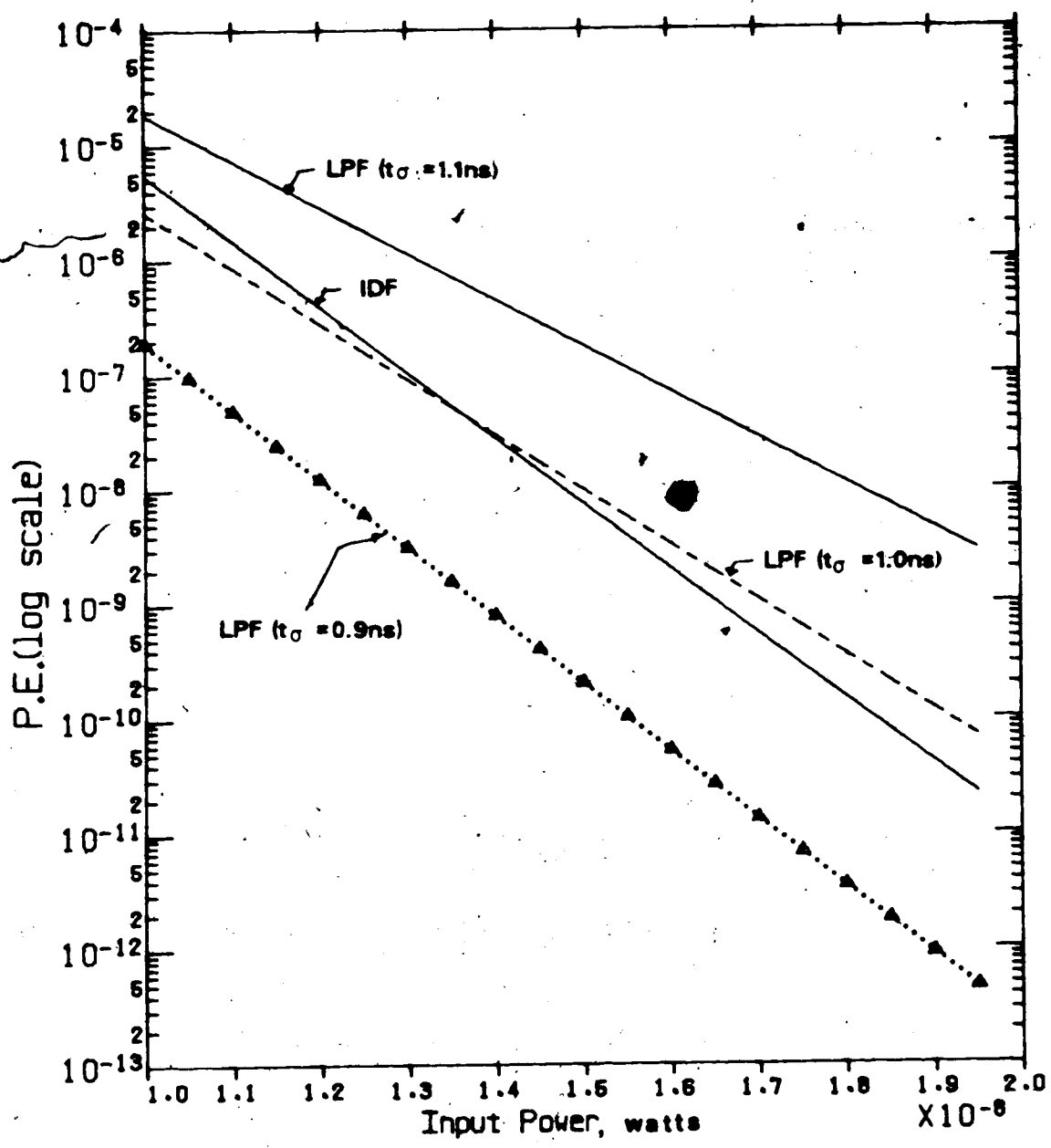


Figure 4.7 Error probability versus P_m for both the LPF and IDF schemes.

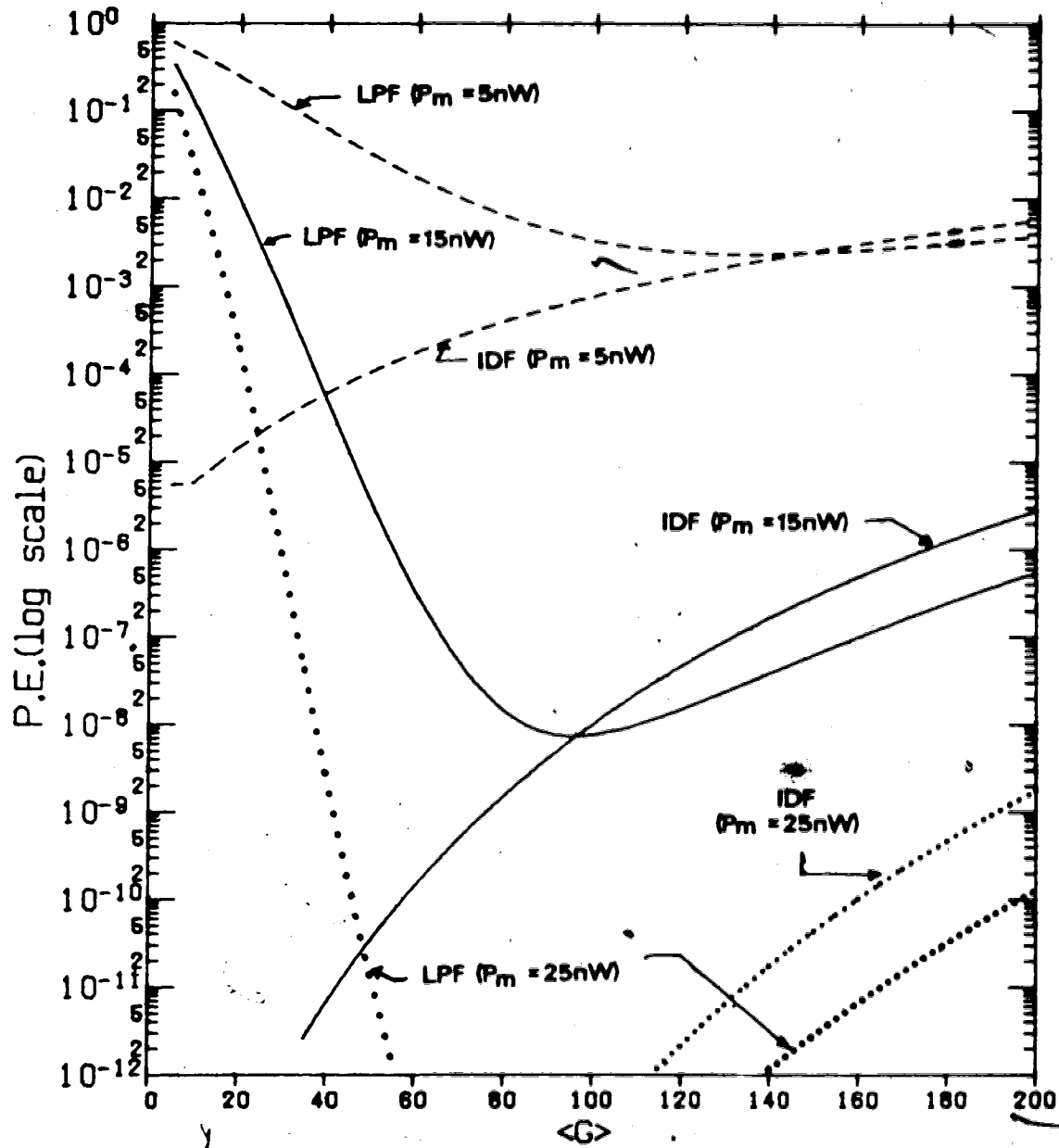


Figure 4.8 Error probability versus $\langle G \rangle$ for both LPF and IDF schemes.

$t_p = 1\text{ ns}$.

25nW). Finally, for the LPF scheme, error probability is plotted as a function of the rise time (t_r) of the optical pulse edges at the input of the receiver in Fig. 4.9, for different power levels. Figs. 7, 8 and 9 have been plotted using the same values of pulse widths as have been calculated for the LPF scheme above.

4.5 DISCUSSION OF RESULTS

From Table 4.2 it is seen that the error rate decreases rapidly with increased slot time. A relatively small change in t_s , from 28 ns. to 31 ns., reduces the $P(\epsilon)$ from 10^{-7} to 10^{-8} . From this table it appears that the LPF scheme gives lower $P(\epsilon)$, for a given slot time, than the IDF scheme. However, this is only true for the particular rise time chosen ($t_r = 1$ ns.). For higher values of rise time, the IDF scheme becomes better than the LPF scheme.

This effect is seen clearly in Fig. 4.7, where, although the value of t_r has very little effect on error rates in the IDF scheme, it is a crucial factor in the LPF method. Using an input power $P_m = 15$ nW., the $P(\epsilon)$ for $t_r = 1$ ns. is 10^{-8} , whereas for $t_r = .9$ ns. the $P(\epsilon)$ is 10^{-10} .

From Fig. 4.8 it is observed that, for $P_m = 15$ nW., the error probability for the IDF scheme initially decreases as gain is increased. For gains higher than about 90, the $P(\epsilon)$ starts to increase as gain is increased. Thus, there exists an optimal gain for the IDF scheme. For different values of P_m , one finds a similar behaviour except that the optimal gain decreases with increasing P_m .

A similar effect is observed theoretically for the LPF scheme, except that here the optimal gain is near 10. If the thermal noise term is increased, the optimal gain of the LPF shifts to higher values of $\langle G \rangle$.

From Fig. 4.9, which is a plot of error probability vs. t_r for a LPF scheme, it is clearly seen that $P(\epsilon)$ decreases greatly as t_r decreases, i.e. as the system bandwidth improves. Theoretically, one can reduce $P(\epsilon)$ to any desired level provided that the bandwidth of the system is large enough. The LPF scheme has two degrees of freedom in reducing $P(\epsilon)$ viz. either by increasing power levels or by increasing the system bandwidth. This is not possible for the integrate and dump scheme where the only way to reduce $P(\epsilon)$ is by increasing the power level.

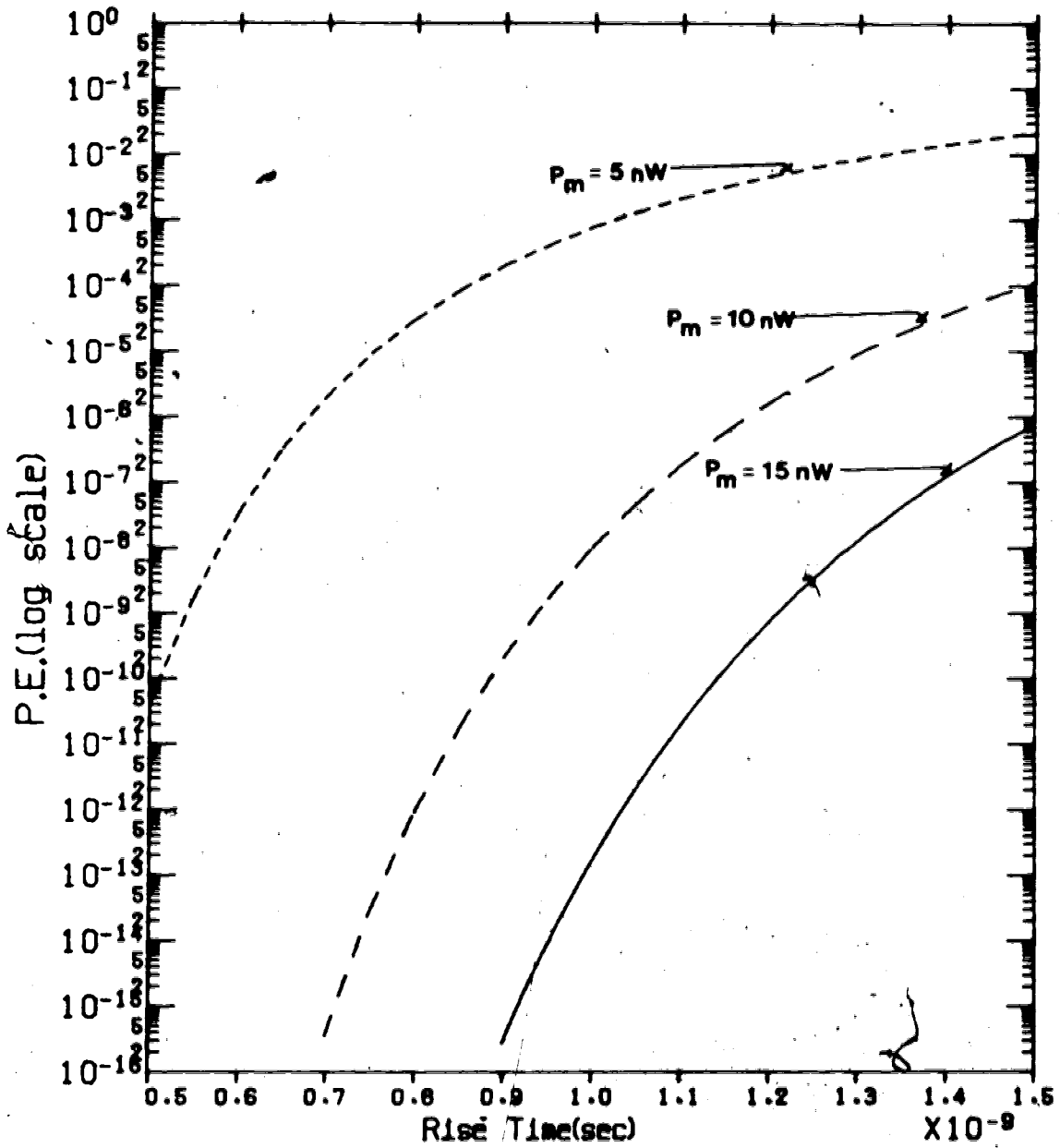


Figure 4.9 Error probability versus t_r for the LPF scheme.

The results for the IDF detection scheme show very similar characteristics to the results that are well known for PAM systems. This is to be expected, since a PAM detector usually employs an IDF, and it is the energy in each pulse that is measured. The LPF detection scheme does not measure the energy in each pulse, and therefore this method differs greatly from the IDF method. It is seen from the results that a LPF detector should be used to fully realise the advantages of PWM.

CHAPTER V

SUMMARY AND CONCLUSIONS

In this thesis, a mathematical model of the noise present in multilevel PAM and PWM systems has been used to predict the error rate in a 4-level PAM system. In order to verify the accuracy of the theory, a 4.023 Mb/s, pseudo-random, 4-level PAM sequence was transmitted over a .5 km. multimode fiber and measurements were made of the error probability of the system as a function of the avalanche gain and optical power incident on the photodiode.

The mathematical model makes use of the Gram-Charlier series to describe the PDF of the output voltage. The Gram-Charlier series takes into account the randomness of the avalanche gain, the amplifier's thermal noise and can include as well any generalised processing filter in the system. In addition to considering shot noise and thermal noise, the effect of intersymbol interference was also introduced into the Gram-Charlier series model.

Multilevel transmission is known to be advantageous compared to binary systems, since more information can be transmitted for a given channel bandwidth. The use of more than 4 levels, however, introduces a large amount of intersymbol interference. As a consequence, the analysis was restricted to 4-level PAM and PWM.

Numerical examples have been provided to assess the performance of 4-level PAM and PWM systems. The system parameters that were used in these examples (Tables 3.1 and 4.1) represent realistic values.

The optimal pulse amplitudes and thresholds were calculated for a range of error probabilities for a multilevel PAM system. The results obtained were given in Table 3.2. The pulse amplitudes and thresholds are seen, in this table, to be unequally spaced. To obtain the minimum error probability, the thresholds have to be chosen to lie closer to the lower level signals, rather than half-way between the signal levels. This results from the fact that the higher level optical signals have more shot noise than lower level signals.

Graphs of error probability as a function of the average avalanche gain, $\langle G \rangle$, of the APD and of the average optical power, P_{avg} , reaching the receiver, are given in Figs. 3.4 and 3.5, respectively. It is seen in Fig. 3.4, that, for $\langle G \rangle$ less than 100, the error probability decreases as $\langle G \rangle$ increases; while for $\langle G \rangle$ larger than 100 the error

probability increases. This behaviour can be explained as follows: At low values of $\langle G \rangle$, the thermal noise term dominates the overall noise. As $\langle G \rangle$ is increased, the output signal amplitude increases, but the thermal noise still dominates the shot noise. As a result of the thermal noise remaining constant while the signal increases, there is an overall increase in the SNR and, correspondingly, a decrease in the error probability. For $\langle G \rangle$ larger than 100, the shot noise starts dominating the overall noise. As $\langle G \rangle$ increases beyond 100, the shot-noise increases (the overall noise also increases) at a faster rate than the signal, thus resulting in an increase in the error probability.

Fig 3.5 shows that the error probability for a 4-level PAM system is highly dependent on the optical signal power reaching the detector. It is seen that a reduction of the optical power by only 3 db, causes the error probability to increase by four to five orders of magnitude.

To verify the above theoretical results, an experimental optical-fiber 4-level PAM system was designed, constructed and tested at a transmission rate of 4.023 Mb/s. Measurements were made of the error probability as a function of $\langle G \rangle$ and P_{avg} , and the results were plotted in Figs 3.13 and 3.14. The theoretical calculations, based on the measured system parameters, were also plotted in Figs. 3.13 and 3.14. The theoretical and experimental results were seen to match fairly well.

The experimental 4-level PAM system was seen to be thermal noise limited, as a consequence of which the probability density function of the output voltage was nearly Gaussian in shape. Only the first few terms of the Gram-Charlier series are necessary to determine the bit error rates of this system. Thus the Gram-Charlier series model and the analytical model using the Gaussian approximation give almost identical results. To really utilise the advantages of the Gram-Charlier series one should consider a system with much less thermal noise.

The analysis of the multilevel PWM system proceeds in the same manner as for multilevel PAM. In PWM systems, one is interested in preserving the timing content of the transmitted pulses. The pulse width is normally determined by threshold detecting the output pulse and measuring the width of the resulting regenerated pulse. Errors in determining the pulse width occur due to the noise present at the threshold levels. The timing error for the PWM system was expressed as a function of the noise amplitude.

Since the PDF of the noise amplitude can be characterised by means of a Gram-Charlier series, it is therefore also possible to characterise the timing error by means of a Gram-Charlier series.

Two different PWM schemes, one employing a LPF and the other an IDF, were analysed. The optimum pulse-widths and threshold levels required to achieve a range of error-probabilities, for both the LPF and IDF schemes, have been tabulated (Table 4.2). Graphs of error probability as a function of $\langle G \rangle$ and P_m were also plotted in Figs 4.7 and 4.8. From these figures one can observe the similarity in the characteristics of the PWM (IDF) system and the PAM system. This is to be expected, since the two schemes are basically the same. For both the PWM (IDF) scheme and the PAM scheme, the noise present during the whole pulse width is integrated and, depending on the value of the integrated noise, errors may or may not occur. The only difference between the PAM and PWM (IDF) scheme is that, whereas in the former, pulses of fixed width but different amplitudes are transmitted, in the latter, pulses of fixed amplitude but different widths are transmitted. The receiver section for both these systems is similar.

The PWM (LPF) system, on the other hand, represents a true pulse width modulation system. The receiver section for the LPF scheme is entirely different from that used for the PAM system, since the pulse width is measured directly and is not determined indirectly from the amplitude of the signal output (as was done for the PWM (IDF) scheme).

An intuitive understanding of the LPF scheme results from the analysis of equation (4.18). The value of K can be interpreted as the SNR of the LPF (PWM) system. It is seen that K is directly proportional to the signal amplitude, V_{max} , but is inversely proportional to the standard deviation of the noise, σ_n , and the rise time of the received pulse, t_r . Thus, for a LPF, as t_r is decreased, the SNR increases and correspondingly the error probability decreases (see Fig. 4.9). One can, therefore, use very high bandwidth fibers to achieve low error rates even for very noisy systems. This is not possible for the IDF scheme because there is no such dependence of error probability on the rise time, t_r .

In conclusion, the LPF scheme can achieve very low error probabilities, provided that a wideband fiber is used [39]. The IDF scheme is, however, advantageous in systems where such wideband fibers are not available.

It is felt that the above results and the corresponding plots prove the usefulness of employing multilevel PAM and PWM transmission for fiber-optic communications. Though these systems have been analysed fairly comprehensively, there is scope for further research. The following improvements in the experiment are suggested:

1. The pre-amplifier used in the experiment should be redesigned to provide much lower thermal noise. The Gram-Charlier series method could then be tested and compared to the other methods of calculating error rates.
2. The data error analyser available for this experiment (HP 1645A) could operate only up to a frequency of 5 Mb/s. It is suggested that the BER measurements be repeated at higher bit rates, using a faster data error analyser. The advantages of multilevel transmission over regular binary transmission should become more noticeable at higher bit rates.

Further research work could be undertaken in the following areas:

1. The analysis of the multilevel schemes was restricted to Gaussian shaped pulses. It would be interesting to note how the results would change if other pulse shapes, such as the raised-cosine were used. Impulse response measurements could be taken to determine the actual pulse-shape at the fiber output.
2. The analysis of the PAM and PWM systems has not taken into account the effect of jitter, i.e., the randomness of the timing signal. Jitter in the timing information, could strongly affect the error probability for commercial fiber-optic links. An analysis of jitter for PAM and PWM systems has been provided in [40]. The results obtained could be modified for multilevel systems.
3. A comparison between multilevel PAM and PWM could be an interesting area for further research. An experimental PWM system could be designed and the results compared with those of the experimental PAM system, using the same system parameters.

The author hopes that this thesis will provide a basis for further research work in the area of multilevel transmission for optical fiber communications.

APPENDIX I

DERIVATION OF THE MOMENTS OF THE AVALANCHE GAIN $\langle G \rangle$, FOR AN APD

Personick [41], McIntyre [42] and Dogliotti *et al* [26] have tackled the problem of deriving the moment generating function for the avalanche gain of an APD. An overall view of the various approaches is presented here. Special emphasis is given to finding moments of the gain in a form suitable for the Gram-Charlier series.

The avalanche detection process essentially obeys Poisson statistics. Optically generated electron-hole pairs generate new electron-hole pairs through collision ionisation. These new electron-hole pairs can, in turn, generate additional pairs by the same mechanism. The avalanche process is depicted in Fig. A1.1. Charge carriers are created in the high-field region principally due to light pulses or thermal effects. Carriers generated outside the high field region can also drift into this region. In the high-field region, let the probability of holes suffering ionisation collision be $\beta(x)$ and that for electrons be $\alpha(x)$, per unit length. We define $p_g(n,x)$ as the probability that n pairs ultimately result from the initially injected pair. The moment-generating function of the number of pairs, $M_g(s)$, is therefore

$$M_g(s, x) = \sum_{n=0}^{\infty} P_g(n, x) e^{sn} \quad (\text{A1.1})$$

The semi-invariant moment generating function (SIMGF), also called the cumulant, is defined as the natural logarithm of the moment-generating function and is given by:

$$\psi_g(s, x) = \ln[M_g(s, x)] = \ln\left[\sum_{n=0}^{\infty} P_g(n, x) e^{sn}\right] \quad (\text{A1.2})$$

To derive the moment generating function, $M(s, x)$, it is necessary to divide the high-field region into K intervals of width $dX = W/K$. These are labelled in the diagram (Fig. A1.1) as 1, 2, 3, ..., j , ..., K . Assume that the initial electron-hole pair is injected into interval j . The probability density of a total number of pairs, n , resulting from the avalanche process (including the initial pair) is $p_g(n, x)$ with x taken as the centre of the interval j .

The hole created in interval j moves to the left, towards $x=0$, the electron moves to the right, towards $x=W$. Both these holes and electrons can create new pairs in the other intervals in the high field region. The interval width, dX , is taken sufficiently small, such that either one or no new pairs are generated by the initial pair within this interval. If

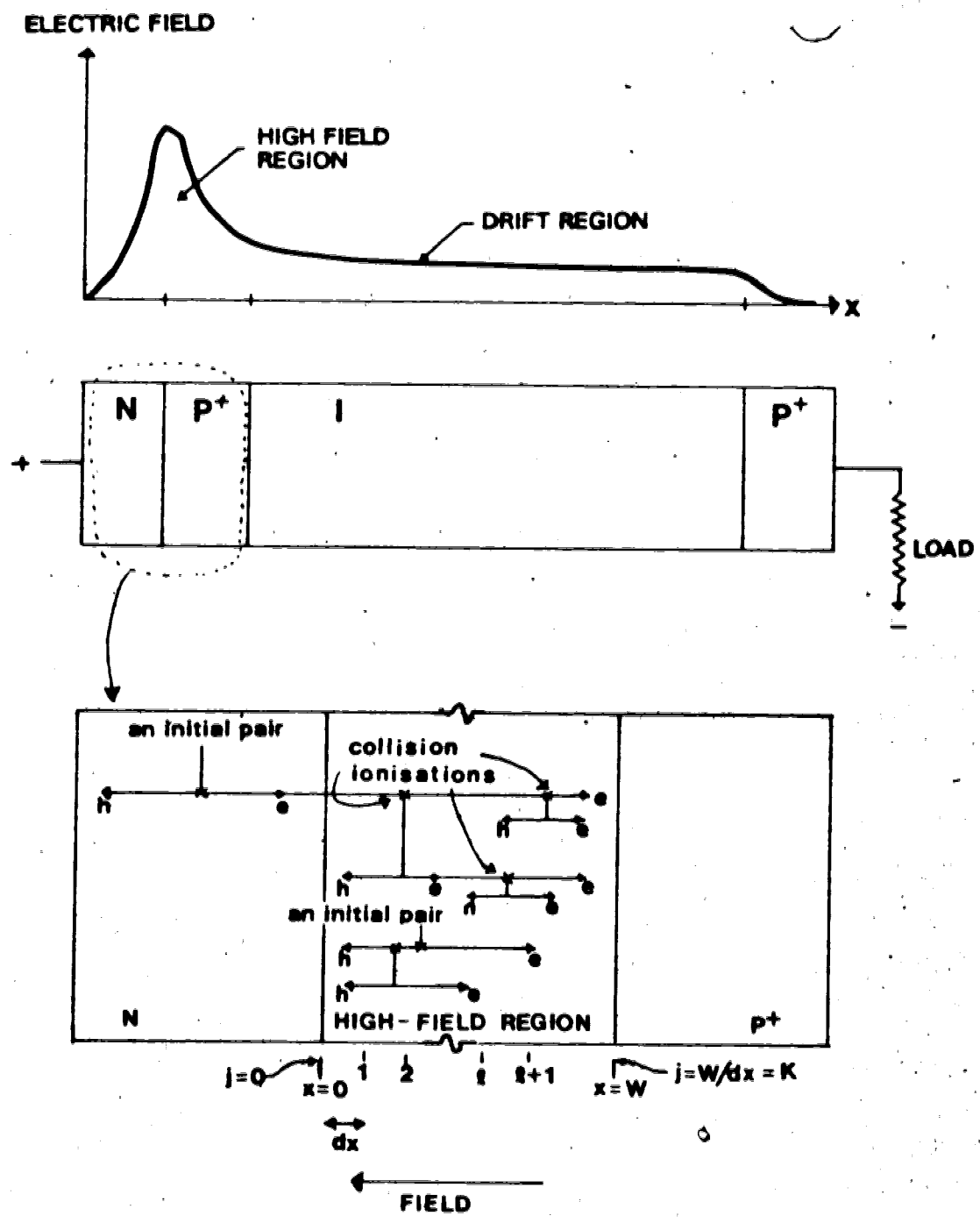


Figure 1.1 Schematic of the avalanche region in an APD

the initial electron-hole pair generates a new pair in some other interval k , then this new pair will ultimately generate N_k pairs, including itself due to the avalanche process. The total number of pairs generated is the sum of all the $\{N_k\}$ produced in the different intervals. In order to get the SIMGF of the total number of pairs, we make use of the fact that the collision ionisation events are all independent (and therefore the N_k are independent) and that the SIMGF of a sum of independent random variables is the sum of the individual SIMGF's. We denote the SIMGF of the total number of pairs by $\Psi_g(s, x)$, i.e.

$$\Psi_g(s, x) = S + \sum_{k=1}^{N/Ax} \Psi_{N_k}(s) \quad (\text{A1.3})$$

where:

S = SIMGF of the initial pair and

$\Psi_{N_k}(s)$ = SIMGF of N_k .

The SIMGF of N_k is obtained by noting that

$$\Psi_{N_k}(s) = \ln \left[\sum_{z=0}^{\infty} P_r[N_k=z] e^{sz} \right] \quad (\text{A1.4})$$

The probability that $N_k = z$ is given by

$$P_r(N_k=z) = \gamma dX P_g(zx) \text{ for } z > 0 \quad (\text{A1.5})$$

The probability that $N_k = 0$ is given by $1 - dX$

where:

$$\gamma = \begin{cases} \alpha(x) & \text{if } k > j \\ \beta(x) & \text{if } k < j \end{cases}$$

and X = centre of interval k

$P_g(Z, x)$ = the probability that the total number of electron-hole pairs ultimately resulting in the avalanche process is Z .

Equation (A1.4) is simplified to

$$\begin{aligned}
\psi_{n_2}(s) &= \ln \left[\sum_{z=0}^{\infty} P_z(N_2 - z) e^{sz} \right] \\
&= \ln \left[(1 - \gamma dX) e^{s^0} + \sum_{z=1}^{\infty} P_z(z, x) e^{sz} \gamma dx \right] \\
&= \ln \left[1 - \gamma dX + \gamma dX M_g(s, x) \right] \\
&= \ln(1) \left[\gamma dX (e^{\psi_g(s, x)} - 1) \right]
\end{aligned} \tag{A1.6}$$

Taking the limit as dX becomes infinitely small and using (A1.3) and (A1.6),

$$\begin{aligned}
\psi_g(s, x) &= S + \int_0^x \beta(x') [e^{\psi_g(s, x')} - 1] dx' \\
&\quad + \int_x^{\infty} \alpha(x') [e^{\psi_g(s, x')} - 1] dx'
\end{aligned} \tag{A1.7}$$

Using Leibnitz's rule for the differentiation of integrals, one obtains

$$\partial \psi_g(s, x) / \partial x = [\beta(x) - \alpha(x)] [e^{\psi_g(s, x)} - 1] \tag{A1.8}$$

Equation (A1.8) can be solved to get

$$\psi_g(s, x) = \ln \left\{ \left[1 / \left\{ 1 - C \exp \left\{ \int_0^x [\beta(x'') - \alpha(x'')] dx'' \right\} \right\} \right] - 1 \right\} dx' \tag{A1.9}$$

where

$$C = [e^{\psi_g(s, 0)} - 1] / e^{\psi_g(s, 0)}$$

Substituting (A1.9) into (A1.7) the value of $\psi_g(s, 0)$ is obtained:

$$\begin{aligned}
\psi_g(s, 0) &= S + \int_0^{\infty} \alpha(x') \cdot \\
&\quad \left\{ \left[1 / \left\{ 1 - C \exp \left\{ \int_0^{x'} [\beta(x'') - \alpha(x'')] dx'' \right\} \right\} \right] - 1 \right\} dx'
\end{aligned} \tag{A1.10}$$

We make the assumption that at each point in the high-field region

$$\beta(x) = k\alpha(x) \tag{A1.11}$$

where k is known as the ionisation coefficient, i.e., the ratio of the hole ionisation probability to the electron ionisation probability.

One can then solve (A1.10) to obtain

$$\begin{aligned} \Psi_g(s, 0) &= (s - \delta) + [1/(k-1)] \cdot \\ &\ln[e^{(k-1)\delta} / \{M_g(s, 0) - e^{(k-1)\delta} [M_g(s, 0) - 1]\}] \\ &= s + [1/(1-k)] \ln[M_g(s, 0) - e^{(k-1)\delta} [M_g(s, 0) - 1]] \end{aligned} \quad (A1.12)$$

where

$$\delta = \int_0^s \alpha(x) dx \quad (\text{the integrated ionisation coefficient for electrons})$$

$$\text{and } M_g(s, 0) = e^{\Psi_g(s, 0)}$$

Differentiating (A1.12) results in

$$\begin{aligned} \partial M_g(s, 0) / \partial s &= M_g(s, 0) [(k-1)/k] \cdot \\ &[1 - (1/k) \{M_g(s, 0) e^{-\Psi_g(s, 0)}\}^{k-1}]^{-1} \end{aligned} \quad (A1.13)$$

where $M_g(0, 0) = 1$

Equation (A1.13) can be solved numerically. We can rewrite (A1.13) into a more suitable form by making use of new variables.

$$\begin{aligned} M(s) &= (k-1)M(s)/k[1 - (1/k)M^{k-1}e^{-(s+\delta)(k-1)}] \\ &= \rho M(s) / \{1 - \beta[M(s)e^{-s}]^{\epsilon}\} \end{aligned} \quad (A1.14)$$

where

$$\begin{aligned} \rho &= (k-1)/k \\ \beta &= 1 - (\rho/\langle G \rangle) \\ \epsilon &= k - 1 \\ M(0) &= 1 \end{aligned}$$

Differentiating (A1.14) we obtain:

$$M^{(2)} = \frac{(M^{(1)})^3}{M^2} a_3 + \frac{(M^{(1)})^2}{M} a_2 + M^{(1)} a_1 \quad (A1.15)$$

where

$$\begin{aligned} a_1 &= \epsilon \\ a_2 &= 1 - \epsilon - (\epsilon/\rho) \\ a_3 &= \epsilon/\rho \end{aligned} \quad (A1.16)$$

Using (A1.15) one can derive the following relation.

$$\left[\frac{(M^{(1)})^{\ell}}{M^{\ell-1}} \right] = \ell a_3 \frac{(M^{(1)})}{M^{\ell+1}} + (\ell a_2 - \ell + 1) \frac{(M^{(1)})^{\ell+1}}{M^{\ell}} + \ell a_1 \frac{(M^{(1)})^{\ell}}{M^{\ell-1}} \quad (\text{A1.17})$$

Differentiating (A1.15) iteratively and applying (A1.17) gives the ℓ 'th derivative of $M(s)$ as

$$M^{(\ell)} = \sum_{k=1}^{2\ell-1} A_{k,\ell} \frac{(M^{(1)})^k}{M^{k-1}} \quad (\text{A1.18})$$

where $A_{k,\ell}$ are functions of a_1, a_2 , and a_3 ,

One can derive a relation between the coefficient $A_{k+1,\ell}$, $A_{k,\ell}$ and $A_{k,\ell-1}$ as:

$$\begin{aligned} A_{k+1,\ell} &= -\ell(1-k)A_{k,\ell} + [1+(\ell-1)(1-2k)]A_{k,\ell-1} + (\ell-2)kA_{k,\ell-2} \\ A_{k,\ell} &= 0 \quad \text{if } \ell < 0 \text{ or } \ell > 2k \\ A_{1,1} &= 0 \end{aligned} \quad (\text{A1.19})$$

Finally, the moments of G can be written as:

$$\langle g^{\ell} \rangle = \left[\frac{d^{\ell} M(s)}{ds^{\ell}} \right]_{s=0} = \sum_{k=1}^{2\ell-1} A_{k,\ell} \langle g \rangle^k \quad (\text{A1.20})$$

where the relations, $M(0) = 1$ and $M^{(1)}(0) = \langle g \rangle$, have been used

Note that, for $s=0$, (A1.15) gives an expression for $\langle g^2 \rangle$ which agrees with McIntyre's excess noise factor [42].

$$F = [\langle g^2 \rangle / \langle g \rangle^2] = k \langle g \rangle + (2 - (1/k))(1-k) \quad (\text{A1.21})$$

The moments of the gain $\langle g^n \rangle$, given in (A1.20), can be applied to (2.86) in order to obtain the cumulants of the received output voltage of a fiber-optic system.

APPENDIX II

DERIVATION OF THE CHARACTERISTIC FUNCTION OF THE VOLTAGE AT THE OUTPUT OF AN OPTICAL-FIBER RECEIVER

The aim of this appendix is to determine the characteristic function (CF) of the receiver output voltage. This is accomplished by first finding the CF of an electron-hole pair at the output of the detector. The effect of the avalanche gain on the CF is considered next. Finally the CF at the output of the filter is derived.

C.F. OF THE ELECTRON-HOLE PAIR AT THE OUTPUT OF THE DETECTOR

Let $g(t)$ be the shape of the optical pulse arriving at the input to the detector and let its width be τ . The probability of n_k electron-hole pairs being created in the sub-interval (t_k, t_{k+1}) , of length $\Delta\tau$, is given by the Poisson distribution:

$$p_k(n_k) = \frac{\mu_k^{n_k} \exp(-\mu_k)}{n_k!} \quad (\text{A2.1})$$

where: $\mu_k = \eta g(t_k) \Delta\tau / (h\nu)$

is the average number of charge carrier pairs in interval (t_k, t_{k+1}) .

The electron-hole pairs created by the optical pulse, $g(t)$, in different sub-intervals are independent of each other. The resulting output of the detector can be represented as a count vector, $\bar{n} = [n_1, n_2, \dots, n_k]$, whose joint PDF, $p_s(\bar{n}_s)$ is obtained as a product of the individual PDFs, i.e.,

$$p_s(\bar{n}_s) = \prod_{k=1}^K p_k(n_k) \quad (\text{A2.2})$$

The corresponding joint characteristic function, $\theta_s(j\nu)$, is given by:

$$\begin{aligned} \theta_s(j\nu) &= \prod_{k=1}^K \theta_k(j\nu) = \prod_{k=1}^K \sum_{n_k=0}^{\infty} \exp(j\nu n_k) p_k(n_k) \\ &= \prod_{k=1}^K \sum_{n_k=0}^{\infty} \exp(j\nu n_k) \frac{\mu_k^{n_k} \exp(-\mu_k)}{n_k!} \\ &= \prod_{k=1}^K (1 + e^{j\nu} \mu_k + (e^{2j\nu} \mu_k^2 / 2) + \dots) \exp(-\mu_k) \end{aligned} \quad (\text{A2.3})$$

But $\exp(x) = 1 + (x/1!) + (x^2/2!) + (x^3/3!) + \dots$

Therefore, (A2.3) reduces to:

$$\begin{aligned}
 \theta_s(j\nu) &= \prod_{k=1}^K \exp[e^{\nu} \mu_k] \exp(-\mu_k) \\
 &= \prod_{k=1}^K \exp[e^{\nu} \mu_k - \mu_k] \\
 &= \exp\left\{ (e^{\nu} - 1) \sum_{k=1}^K \mu_k \right\}
 \end{aligned} \tag{A2.4}$$

C.F. AT THE FILTER OUTPUT

The electron-hole pairs generated in the high field region of the p-n detector undergo avalanche gain multiplication. The CF of the final output electron-hole pairs after avalanche gain, in response to a single electron-hole pair, is given by (A1.12). This equation can be rewritten in the following form:

$$\ln \theta_s(j\nu) = j\nu + (1-k)^{-1} \ln[\theta_s(j\nu)(1-a) + a] \tag{A2.5}$$

where $a = \exp\{(k-1)\}$

$$\delta = \int_0^w \alpha(x) dx \quad (w \text{ is the high field region width})$$

where:

$\alpha(x)$ is the collision ionisation probability for an electron.

Assuming only electron ionisation events [i.e. the factor k given in (A1.11) is neglected], the above equation can be rewritten as:

$$\theta_s(j\nu) = \{1 - G[1 - \exp(j\nu)]\}^{-1} \tag{A2.6}$$

where $\bar{G} = \exp(\delta)$ is the mean multiplication.

For $\bar{G} > 10$, (A2.6) can be approximated as:

$$\theta_s(j\nu) = (1 - j\nu \bar{G})^{-1} \tag{A2.7}$$

Let $p_x(x)$ be the PDF of the number of charge carrier pairs after the random multiplication, in response to a single electron-hole pair. The PDF of the output in response to all the primaries in interval $\Delta\tau$, is given by:

$$P_A(x) = \sum_{n_k=0}^{\infty} P_x(n_k) P_s(x)^{n_k} \tag{A2.8}$$

where:

$$p_2(x) \otimes n_k = p(x) * p(x) * p(x) \dots * p(x)$$

Let the characteristic function corresponding to $p_2(x)$ be $\Theta_2(jv)$. Then

$$\begin{aligned} \theta_A(jv) &= \sum_{x=0}^{\infty} P_A(x_m) \exp(jvx_m) \\ &= \sum_{x=0}^{\infty} \sum_{n_k=0}^{\infty} P_k(n_k) P_s(x) \theta_k^{n_k} \exp(jvx_m) \\ &= \sum_{n_k=0}^{\infty} P_k(n_k) \sum_{x=0}^{\infty} P_s(x_m) \theta_k^{n_k} \exp(jvx_m) \\ &= \sum_{n_k=0}^{\infty} P_k(n_k) \theta_k^{n_k}(jv) = \sum_{n_k=0}^{\infty} P_k(n_k) \exp[n\psi_s(jv)] \\ &= \theta_k[\psi_s(jv)] \end{aligned} \tag{A2.9}$$

where:

$$\psi_s(jv) = \ln \theta_s(jv)$$

For the time interval $[0, \tau]$, the count vector, \bar{r} , representing the random multiplication output, will have the joint characteristic function $\Theta_r(jv)$:

$$\theta_r(jv) = \prod_{k=1}^K \theta_k[\psi_s(jv)] \tag{A2.10}$$

Since

$$\prod_{k=1}^K \theta_k(jv) = \exp \left\{ \left\{ \exp(jv) - 1 \right\} \sum_{k=1}^K \mu_k \right\}$$

(A2.10) can be reduced to:

$$\theta_r(jv) = \exp \left\{ \left\{ \exp(\psi_s(jv)) - 1 \right\} \sum_{k=1}^K \mu_k \right\}$$

But

$$\psi_s(jv) = \ln \theta_s(jv)$$

$$\text{or } \theta_s(jv) = \exp \psi_s(jv)$$

$$\begin{aligned} \theta_r(jv) &= \exp \left\{ \left\{ \theta_s(jv) - 1 \right\} \sum_{k=1}^K \mu_k \right\} \\ &= \exp \left\{ \left\{ \theta_s(jv) - 1 \right\} \mu_r \right\} \end{aligned}$$

(A2.11)

The characteristic function of the intersymbol interference and dark current electrons is

the same as (A2.11). Therefore, the APD output characteristic function [if we consider $(p+q)$ interference components plus dark current], is just a multiplication of terms like (A2.11), i.e.,

$$\theta(j\nu) = \exp \left[\left\{ (\mu_0 |d_{10}) + \mu_d \sum_{i=1}^q (u_i |d_i) \right\} \cdot \{ \theta_s(j\nu) - 1 \} \right] \quad (\text{A2.12})$$

where $u_i |d_{10}$ = average number of primary electron-hole pairs due to the bit under detection.

u_d = average number of primary electron-hole pairs due to the dark current

$\sum_{i=1}^q (u_i |d_i)$ = the conditional intersymbol interference.

Equation (A2.13) is used in Chapter II to derive the cumulant of the voltage at the output of the receiver. The characteristic function of the Gaussian distributed thermal noise is derived separately in Chapter II. Since all the noise sources are independent, the overall characteristic function is the multiplication of the characteristic functions of the shot noise, intersymbol interference and the thermal noise.

APPENDIX III
COMPUTER PROGRAMS

```

C *****
C THIS PROGRAM COMPUTES THE MINIMUM ERROR PROBABILITY
C AND THE OPTIMUM THRESHOLD FOR A TWO-LEVEL PAM SYSTEM
C A MEAN AVALANCHE GAIN, GA, OF 100 HAS BEEN ASSUMED
C *****
REAL C(100,200), K, E, B, D, GI(100), LAM(100), GA, X1, X2, X3
REAL LA(100), MU(100), BC(100,200), INDI(100), B0
REAL A(100), PO, ETA, H, NU, T, SIGMA2, A0, LA2S
REAL X, PX, PHI(100), PI, LA2, LAMDA(100), FACT(100)
INTEGER L, Z
C *****
GA = 100
K = 0.02
PO = 15E-9
ETA = 0.85
H = 6.62E-34
NU = 3.5E14
T = 1E-8
SIGMA2 = 1E4
PI = 3.1415927
NOTRM = 84
NOTRM1 = NOTRM - 1
NOTRM2 = NOTRM - 1
C *****
C THIS PROGRAM READS THE VALUES OF THE FACTORIAL FROM
C ANOTHER FILE
DO 20 I = 1, 100
  READ (5,10) FACT(I)
10  FORMAT (4X, E13.7)
20  CONTINUE
C *****
DO 30 N = 1, NOTRM
  DO 30 M = 1, NOTRM
    C(N,M) = 0
30  CONTINUE
C(1,1) = 1
C(2,1) = -(1 - K)
C(2,2) = 2 * (1 - K)
C(2,3) = K
G(2) = C(2,1) * GA + C(2,2) * GA * GA + C(2,3) * GA * GA * GA

```

```

LA2 = ((ETA)/(H*NU))*PO*T*(G(2)) + SIGMA2
MU(1) = 0.
MU(2) = 0.
PX = 0.
DO 120 N = 3, NOTRM
  LAM = ((ETA)/(H*NU)) * PO * T
  LAMM = 0.
  DO 60 M = 1, NO1
    IF (M GE (2*N)) GO TO 60
    E = -M * (1 - K)
    B = 1 + (M - 1) * (1 - 2*K)
    D = (M - 2) * K
    IF ((M - 1) LE 0) THEN DO
      C(N,M) = E * C((N - 1),M)
    ELSE DO
      IF ((M - 2) LE 0) THEN DO
        C(N,M) = E * C((N - 1),M) + B * C((N - 1), (M - 1))
      ELSE DO
        X1 = E * C((N - 1),M)
        X2 = B * C((N - 1), (M - 1))
        X3 = D * C((N - 1), (M - 2))
        C(N,M) = X1 + X2 + X3
      END DO
    END IF
  END IF
C PRINT, LA2, LA2
LA2S = SORT(LA2)
C PRINT, LA2S, LA2
IF (ABS(C(N,M)) LE 1.E10) GO TO 40
C(N,M) = C(N,M) * 1.E-70
A0 = LAM * C(N,M)
B0 = ABS(A0)
LAMDA(N) = ALOG(B0) + FLOAT(M) * ALOG(G) + ALOG(1.E70) -
1  FLOAT(N) * ALOG(LA2S)
GO TO 50
40  A0 = LAM * C(N,M)
    B0 = ABS(A0)
    LAMDA(N) = ALOG(B0) + FLOAT(M) * ALOG(G) + ALOG(G) - FLOAT(N) * ALOG(
1  LA2S)
50  IF (LAMDA(N) LE - 50) GO TO 60
    LAMM = LAM * SIGN(XP(LAMDA(N)), A0)
C PRINT, LAMM, LAMM
60  CONTINUE

```

```

70  MU(N) = 0
DO 100 M = 2, NOTRM1
IF (M.GT. (N - 1)) GO TO 110
I = N - 1
L = (I - M)
IF (L.GE. 1) GO TO 80
BC(I,M) = EXPFACT(I) - FACT(M)
GO TO 90
80  BC(I,M) = EXPFACT(I) - FACT(M) - FACT(L)
90  IF ((N - M - 1).EQ. 0) THEN DO
      MU(N) = MU(N) + BC(I,M) * LAMMM + 1)
    ELSE DO
      MU(N) = MU(N) + BC(I,M) * LAMMM + 1) * MU(N - M - 1)
    END IF
100 CONTINUE
110  IND(N) = (-1)** (N)
      A(N) = EXP(ALOG(MU(N)) - FACT(N))
      A(N) = A(N) * IND(N)
C.  PRINT,N,A(N)
120 CONTINUE
      X = -7.5
DO 150 Z = 1, 61
PH0 = (EXP(-(X*X)/2)) * (1/SQRT(2*PI))
PH1(1) = -(EXP(-(X*X)/2)) * (X/SQRT(2*PI))
PH1(2) = -(X*PH1(1) + PH0)
PX = PH0
DO 130 N = 3, NOTRM
PH(N) = -(X*PH(N - 1) + (N - 1)*PH(N - 2))
PX = PX + A(N) * PH(N)
130 CONTINUE
X1 = 9.01355E-16 * X + 8.805E-15
Y1 = 6.285785E-16 * X + 2.201E-15
WRITE (6,140) X1, PX
140 FORMAT (3X, E14.7, 4X, E13.6)
      X = X + 0.25
150 CONTINUE
160 STOP
      END

```

C THIS PROGRAM COMPUTES THE OPTIMUM SIGNAL LEVELS AND THRESHOLDS
 C FOR A 4-LEVEL PAM SYSTEM FOR ERROR PROBABILITIES VARYING FROM
 C 1E-4 TO 1E-10

1 DOUBLE PRECISION A,A1,B,BETA,G,G2,H,K,K1,LAM2,M,N,U,P,PE,
 S,PI,Q,R,SIG,SIGT,T,T,S,V,X,X1,X2,X3

2 DIMENSION PI(5),M(5),X(5),LAM2(5),SIG(5),V(7),PE(7)

C V(I) IS THE INVERSE ERROR FUNCTION OF $(1-(4/3)*PI(E))$, WHERE
 C PI(E) IS THE ERROR PROBABILITY VARYING FROM 1E-4 TO 1E-10

C *****

3 V(1)=2.7013

4 V(2)=3.07914

5 V(3)=3.41866

6 V(4)=3.72943

7 V(5)=4.01759

8 V(6)=4.28742

9 V(7)=4.54197

10 PE(1)=1E-4

11 PE(2)=1E-5

12 PE(3)=1E-6

13 PE(4)=1E-7

14 PE(5)=1E-8

15 PE(6)=1E-9

16 PE(7)=1E-10

C *****

17 WRITE(6,100)

18 100 FORMAT(1,' THE OPTIMUM SIGNAL LEVELS AND THRESHOLDS ARE,

S' GIVEN BELOW FOR A / 4-LEVEL PAM SYSTEM,

S' FOR DIFFERENT ERROR PROBABILITIES)

C *****

19 PI=3.141593

20 K1=0.02

21 G=100.

22 G2=(K1-1)*G+2*(1-K1)*G*G+K1*G*G*G

23 P(1)=0

24 TS=1E-9

25 T=50E-8

26 NU=3614E14

27 Q=1603E-19

28 R=700.

29 A1=4000.

30 SIGT=3E-3

31 H=6625E-34

```

32 ETA=85
33 A=(ETA/(H*NJ))*(O*R*A1)*G*DSQRT(2.*PI)
    S*(TS/T)*DERF(T/(2.*1.4142*TS))
34 B=(ETA/(H*NJ))*(O*R*A1)**2*G2*DSORT(2.*PI)
    S*(TS/(T*TI))*DERF(T/(2.*1.4142*TS))
35 DO 10 I=1,7
36 WRITE(6,200) PE(I)
37 200 FORMAT(/,
    S-----/,10X,
    S' ERROR PROBABILITY = ',1PE7.1)
38 DO 20 J=1,3
39 MJ=A*P(J)
40 LAM2(J)=B*P(J)
41 SIG(J)=DSORT(LAM2(J)+(SIGT**2))
42 X(J)=(V(I))*1.4142*(SIG(J)+M(J)
43 X1=(X(J)/A)+(V(I)*V(I))*B/(A*A)
44 X2=X1**2
45 X3=(X(J)*X(J)/(A*A))-(2.*V(I)*V(I))*(SIGT**2)/(A*A)
46 P(J+1)=X1+DSQRT(X2-X3)
47 20 CONTINUE
48 M(4)=A*P(4)
49 WRITE(6,300) M(1),X(1),M(2),X(2),M(3),X(3),M(4)
50 300 FORMAT(/,10X,M(1)='2PE11.4/,10X,X(1)='2PE11.4,
    S/,10X,M(2)='2PE11.4/,10X,X(2)='2PE11.4/,
    S10X,M(3)='2PE11.4/,10X,X(3)='2PE11.4/,
    S10X,M(4)='2PE11.4)
51 40 CONTINUE
52 STOP
53 END

```


C*****
 C THIS PROGRAM COMPUTES THE ERROR PROBABILITY AS A FUNCTION
 C OF THE AVG. OPTICAL SIGNAL REACHING THE DETECTOR, PAVG.
 C FOR A FOUR-LEVEL PAM SYSTEM

1 DOUBLE PRECISION A,B,AREA,AREA1,AREA2,ERROR,ETA,
 SG,G2,H,K,LAM2,M,NU,P,P1,PAVG,PI,Q,SIG,SIGT,T,TS,X
 2 DIMENSION AREA(15),AREA2(15),LAM2(15),M(5),PI(5),
 SP(15),SIG(5),X(5)

C*****
 C THE PARAMETERS SELECTED BELOW WERE BASED ON THE VALUES
 C OBTAINED EXPERIMENTALLY. THE SYSTEM IS ASSUMED TO OPERATE
 C AT A BIT RATE OF 4 MB/SEC. SIGT REPRESENTS THE THERMAL
 C NOISE OF THE SYSTEM AND TS IS ASSUMED TO BE THE STANDARD
 C DEVIATION OF THE OPTICAL POWER PULSE SHAPE (ASSUMED TO
 C BE GAUSSIAN). K IS THE IONISATION COEFF. AND G IS THE
 C MEAN AVALANCHE GAIN OF THE APD. G2 REPRESENTS THE
 C SECOND MOMENT OF THE AVALANCHE GAIN. NU IS THE FREQUENCY
 C OF OPERATION OF THE LED (CORRESPONDS TO 830 NM). H IS
 C HEISENBERG'S CONSTANT. A1 IS THE OVERALL GAIN OF THE AMP.
 C AND THE PREAMPLIFIER. Q IS THE CHARGE OF AN ELECTRON.
 C AND ETA IS THE QUANTUM EFFICIENCY OF THE PHOTODETECTOR.
 C*****

3 PI=3.141593
 4 K=0.02
 5 G=10
 6 G2=(-1-K)*G+2*(1-K)*G*G+K*K*G*G*G
 7 TS=2.5E-7
 8 T=5E-7
 9 NU=3614E14
 10 Q=1.603E-19
 11 R=700
 12 A1=1500
 13 SIGT=35E-3
 14 H=6.625E-34
 15 ETA=85



C*****
 C A AND B REPRESENT THE CONSTANT PORTION OF THE AVG. OUTPUT
 C VOLTAGE AND ITS SECOND CUMULANT RESP.

C*****
 16 A=ETA/(H*NU)*(Q*R*A1)*G*DSORT(2*PI)
 S*TS*DERF(T/2*1.4142*TS)/T
 C*****

```

17 B=(ETA/(M*NUJ))*(Q*R*A 1)**2*(G2*DSQRT(2 *PI)
   S*TS*DERF(T/(2.*1.4142*TS)))/(T*T)
C*****
C THE SIGNAL LEVELS AND THRESHOLDS WHICH ARE GIVEN BELOW ARE
C ASSUMED EQUALLY SPACED WITH AN AVG POWER OF PAVG.
C*****
18 WRITE(6,10)
19 10 FORMAT('1',ERROR PROB, AS A FUNCTION OF THE AVERAGE,
   S' OPTICAL POWER,/,15X,'PAVG',10X,'ERROR PROB')
C*****
20 DO 20 I=60,120
21 PAVG=I*1E-9
22 P(1)=0
23 P 1(1)=(1./3)*PAVG
24 P 2(1)=(1./1.5)*PAVG
25 P 1(2)=PAVG
26 P 3(1)=(2./1.5)*PAVG
27 P 1(3)=(5./3)*PAVG
28 P 4(1)=2 *PAVG
29 P 1(4)=0
C*****
C THE MEAN OUTPUT VOLTAGE LEVELS, MUJ AND THE THRESHOLDS,
C X I(J), ARE CALCULATED FOR THE FIXED POWER LEVELS
C CHOSEN EARLIER
C*****
30 DO 30 J=1,4
31 MUJ=A*P(J)
32 X I(J)=A*P 1(J)
33 LAM2(J)=P I(J)*B
34 SIGJ=DSQRT(LAM2(J)*(SIGT**2))
35 30 CONTINUE
C*****
36 AREA=0
C*****
37 DO 40 J1=1,3
38 AREA 1(J1)=5*(1- DERF((X I(J1)-MUJ1)))/(1.4142*SIGJ 1)))
39 AREA2(J1)=5*(1- DERF((MUJ 1+ 1)- X I(J1)))/(1.4142*SIGJ 1+ 1)))
40 AREA=AREA +AREA 1(J1)+AREA2(J1)
41 40 CONTINUE
C*****
42 ERROR=AREA/4
43 WRITE(6,100) PAVG,ERROR

```

44 100 FORMAT(10X,E14.7,4X,E136)
45 20 CONTINUE
46 STOP
47 END

C *****
 C THIS PROGRAM COMPUTES THE ERROR PROBABILITY AS A FUNCTION
 C OF THE AVALANCHE GAIN, G, WHICH VARIES FROM 6 TO 12, FOR
 C A FOUR-LEVEL PAM SYSTEM
 C *****

1 DOUBLE PRECISION A, AREA, B, ETA, G, G2, H, K, LAM2, M, NU, PE,
 S, P, Q, SIG, SIGT, TS, X
 2 DIMENSION AREA(13), AREA2(3), LAM2(4), M(4), SIG(4), X(4)

C *****
 C THE PARAMETERS SELECTED BELOW WERE BASED ON THE VALUES
 C OBTAINED EXPERIMENTALLY. THE SYSTEM IS ASSUMED TO OPERATE
 C AT A BIT RATE OF 4 MB/SEC. SIGT REPRESENTS THE THERMAL
 C NOISE OF THE SYSTEM AND TS IS ASSUMED TO BE THE STANDARD
 C DEVIATION OF THE OPTICAL POWER PULSE SHAPE (ASSUMED TO
 C BE GAUSSIAN). K IS THE IONISATION COEFF. AND G IS THE
 C MEAN AVALANCHE GAIN OF THE APD. G2 REPRESENTS THE
 C SECOND MOMENT OF THE AVALANCHE GAIN. NU IS THE FREQUENCY
 C OF OPERATION OF THE LED (CORRESPONDS TO 830 NM). H IS
 C HEISENBERG'S CONSTANT. A IS THE OVERALL GAIN OF THE AMP.
 C AND THE PREAMPLIFIER. Q IS THE CHARGE OF AN ELECTRON.
 C AND ETA IS THE QUANTUM EFFICIENCY OF THE PHOTODETECTOR.
 C *****

3 K=0.02
 4 PI=3.141593
 5 TS=2.5E-7
 6 T=5E-7
 7 NU=3.614E14
 8 Q=1.603E-19
 9 R=700
 10 A=1500
 11 SIGT=35E-3
 12 H=6.625E-34
 13 ETA=85

C *****
 14 WRITE(6, 10)
 15 10 FORMAT(11X, G, 6X, 'ERROR PROB')
 C *****

C THE INPUT POWER LEVELS AND THRESHOLDS WHICH ARE GIVEN BELOW ARE
 C OBTAINED FOR ERROR PROB OF 1E-6 AT AN AVALANCHE GAIN OF 10.
 C THESE LEVELS HAVE TO BE RECALCULATED FOR THE ACTUAL AVALANCHE
 C GAIN

```

C*****
16 DO 20 I=1,13
17 M1)=0.
18 X(1)=16.9213E-2
19 M2)=33.8699E-2
20 X(2)=50.8183E-2
21 M3)=67.7939E-2
22 X(3)=84.7693E-2
23 M4)=10.1772E-1
24 G=(I*5)+5.5
25 G2=((K-1)*G)+I2*(1-K)*G+K*G*G)
C*****
26 DO 30 J=1,3
27 LAM2(J)=(M(J)*Q*R*A*G2)/(10.*T)
28 SIG(J)=DSORT(LAM2(J)+(SIGT**2))
29 M(J)=M(J)*G/10
30 X(J)=X(J)*G/10
31 30 CONTINUE
C*****
32 LAM2(4)=(M(4)*Q*G2)/(10.*T)
33 SIG(4)=DSORT(LAM2(4)+(SIGT**2))
34 M(4)=M(4)*G/10.
C*****
35 1 AREA=0.
C*****
36 DO 40 J=1,3
37 AREA1(J)=5*(1-DEF(X(J)-M(J)/(1.4142*SIG(J))))
38 AREA2(J)=5*(1-DEF((M(J)+1)-X(J)/(1.4142*SIG(J)+1)))
39 AREA=AREA+AREA1(J)+AREA2(J)
40 40 CONTINUE
C*****
41 AREA=AREA/4
42 WRITE(6,100) G,AREA
43 100 FORMAT(10X,F4.1,4X,E13.7)
44 20 CONTINUE
45 STOP
46 END

```

C THIS PROGRAM COMPUTES THE ERROR PROBABILITIES
 C WITH INTERSYMBOL INTERFERENCE FOR A 4-LEVEL PAM
 C SYSTEM THE POWER LEVELS CHOSEN CORRESPOND TO AN
 C ERROR PROB OF 1E-6 WHEN ISI IS NOT CONSIDERED
 DOUBLE PRECISION A,A1,A2,AREA1,B,B1,ERROR,ETA,G,G2,
 SH,K,LAM21,M,NU,P,P1,P4,PE,PI,Q,R,SIG1,SIGT,T,TS,X
 DIMENSION M(4),P(4),X(4)
 PI=3.141593
 K=0.02
 G=100.
 G2=(K-1)*G+(2*(1-K)*G+G)+(K*G*G*G)
 TS=1E-7
 T=50E-8
 NU=3.614E14
 Q=1.603E-19
 R=700
 A1=4000.
 SIGT=3E-3
 H=6.625E-34
 ETA=85
 A2=(ETA/(H*NU))*(Q*R*A1)*G*DSQRT(2.*PI)*TS/T
 A=A2*DERF(T/(2.*1.4142*TS))
 B1=(ETA/(H*NU))*(Q*R*A1)**2)*G2*DSQRT(2.*PI)
 S*(TS/(T*T))
 B=B1*DERF(T/(2.*1.4142*TS))

1
2
3
4
5
6
7
8
9
10
11
12
13
14
15
16
17
18
19

C THE SIGNAL LEVELS AND THRESHOLDS WHICH ARE GIVEN BELOW ARE
 C THE OPTIMAL LEVELS FOR ERROR PROB OF 1E-6

M(1)=0
 X(1)=14.5040E-3
 M(2)=37.2967E-3
 X(2)=60.0693E-3
 M(3)=91.1706E-3
 X(3)=12.2252E-2
 M(4)=16.1622E-2

C*****

P1=M(1)/A
 P4=M(4)/A
 M(1)=A*P1
 M(1)=M(1)+A2*P4*DERF(3*T/(2.*1.4142*TS))
 M(1)=M(1)-A*P4
 LAM21=B*P1
 LAM21=LAM21+B1*P4*DERF(3*T/(2.*1.4142*TS))

27
29
31
33
35
37
39

```
41 LAM21=LAM21-B*P4
43 SIG1=DSQRT(LAM21*(SIGT**2))
45 AREA1=5*(1-DEFI(X11-M11))/(1.4142*SIG1))
46 PRINT,AREA1 =,AREA1
47 ERROR=(AREA1*(10/3)**1.E-6)**25
48 WRITE(6,100)ERROR
49 100 FORMAT(1,' THE ERROR CONSIDERING INTERSYMBOL INTERFERENCE :
      S'is = ,E13.7)
50 WRITE(6,101)T,TS
51 101 FORMAT(//,10X,' T = ,E10.3//,10X,' TS = ,E10.3)
52 STOP
53 END
THE ERROR CONSIDERING INTERSYMBOL INTERFERENCE is = 0.8744881D-05
T = 0.500D-06
TS = 0.100D-06
THE ERROR CONSIDERING INTERSYMBOL INTERFERENCE is = 0.1712148D-02
T = 0.500D-06
TS = 0.120D-06
```

C THIS PROGRAM COMPUTES THE OPTIMUM PULSE WIDTHS AND THRESHOLDS FOR
 C A 4-LEVEL PWM SYSTEM (EMPLOYING AN IDF) FOR ERROR PROBABILITIES
 C VARYING FROM 1E-4 TO 1E-10. THE VALUES USED HERE ARE FOR A
 C 4 MB/SEC SYSTEM. T(1) IS ASSUMED TO BE 5 NS AND THE RISE TIME,
 C TS, IS ASSUMED TO BE 5 NS.

REAL V, V1, T, LAM2, K, KC, TS, TAU, ETA, H, NU, Q, R, A, K1, K2, PM, B, C
 S C1, C2, G, G2, SIGT, SIG2

DIMENSION T(4), LAM2(4), TAU(4), K(4), V(7), V1(7), PE(7)

C*****

- V(1)=2.7013
- V(2)=3.07914
- V(3)=3.41866
- V(4)=3.72943
- V(5)=4.01759
- V(6)=4.28742
- V(7)=4.54197
- PE(1)=1E-4
- PE(2)=1E-5
- PE(3)=1E-6
- PE(4)=1E-7
- PE(5)=1E-8
- PE(6)=1E-9
- PE(7)=1E-10

C*****

- PM=15E-9
- KC=0.02
- ETA=.85
- H=6.625E-34
- NU=3.5E14
- Q=1.603E-19
- R=700
- A=3000
- G=100
- G2=(KC-1)*G+12*(1-KC)*G*G+(KC*G*G*G)
- TSLOT=50E-8
- T(1)=1E-8
- TS=1E-9
- K1=(ETA/(H*NU))*(O*R*A)*G*PM*(1/TSLOT)
- K2=(ETA/(H*NU))*(O*R*A)**2)*G2*PM/(TSLOT*TSLOT)
- SIGT=(3E-3)**2

C*****

WRITE(6, 100)


```

100 FORMAT(1,' THE OPTIMUM PULSE WIDTH LEVELS AND THRESHOLDS',
$ ARE GIVEN BELOW',/, FOR A 4-LEVEL PWM SYSTEM',
$ USING AN IDF)

```

```

C*****

```

```

DO 10 I=1,7
V1(I)=V(I)*SORT(2)
WRITE(6,200) PE(I)
200 FORMAT(0,

```

```

$-----
$

```

```

S/, ERROR PROBABILITY = ,1PE7 1)

```

```

C*****

```

```

DO 20 J=1,3
LAM2(I,J)=K2*(42633*TS)+T(I,J)
SIG2(I,J)=SORT(LAM2(I,J)+SIGT)
K(I,J)=K1/SIG2(I,J)
TAU(I,J)=(V1(I)/(K(I,J))+T(I,J)
B=-f2*TAU(I,J)-(V1(I)*K2)/(K1*K1)
C1=(TAU(I,J))**2
C2=(f2 42633*TS*K2)+SIGT)
C=C1-(V1(I)/K1)**2*C2
T(I,J+1)=(-B+SQRT((B*B)-(4*C1)))/2

```

```

20 CONTINUE

```

```

C*****

```

```

WRITE(6,300) T(1),TAU(1),T(2),TAU(2),T(3),TAU(3),T(4)
300 FORMAT(0,' T(1) = ,2PE114/, TAU(1) = ,2PE114,
$/, T(2) = ,2PE114/, TAU(2) = ,2PE114,
$/, T(3) = ,2PE114/, TAU(3) = ,2PE114,
$/, T(4) = ,2PE114)

```

```

C*****

```

```

10 CONTINUE
STOP
END

```

C THIS PROGRAM COMPUTES THE OPTIMUM PULSE WIDTHS AND THRESHOLDS FOR
 C A 4-LEVEL PWM SYSTEM (EMPLOYING A LPI) FOR ERROR PROBABILITIES
 C VARYING FROM 1E-4 TO 1E-10 THE VALUES USED HERE ARE BASED
 C ON T3 RATES. T(1) IS ASSUMED AS 10 NS AND RISE TIME. TS, IS
 C TAKEN AS 1 NS.

1 REAL V,V1,T,LAM2,TS,TH,A,PM,PE,H,NU,SIGT,Q,ETA,
 SK,G,G2,SIG,CONST,A1
 2 DIMENSION T(4),TH(4),V(7),V1(7),PE(7)
 C V(I) IS THE INVERSE ERROR FUNCTION OF (1-(4/3)*PIE(I)), WHERE
 C PIE(I) IS THE ERROR PROBABILITY VARYING FROM 1E-4 TO 1E-10

3 V(1)=2.7013
 4 V(2)=3.07914
 5 V(3)=3.41866
 6 V(4)=3.72943
 7 V(5)=4.01759
 8 V(6)=4.28742
 9 V(7)=4.54197
 10 PE(1)=1E-4
 11 PE(2)=1E-5
 12 PE(3)=1E-6
 13 PE(4)=1E-7
 14 PE(5)=1E-8
 15 PE(6)=1E-9
 16 PE(7)=1E-10

C*****

17 PM=15.0E-9
 18 T(1)=1.0E-8
 19 TS=1.0E-9
 20 K=0.02
 21 H=6.625E-34
 22 ETA=85
 23 NU=3.5E14
 24 Q=1.603E-19
 25 SIGT=(3E-3)**2
 26 R=700
 27 A=4000
 28 G=100
 29 G2=(-(1-K)*G)+(2*(1-K)*G*G)+(K*G*G*G)
 30 A1=ETA/(H*(NU)**Q*(R*A))*G*(PM**0.51123E-9)
 31 LAM2=(ETA/(H*(NU)**Q*(R*A)**2))*G2*(PM**0.412368E-9)
 32 SIG=SQRT(LAM2+SIGT)
 33 CONST=A1/(SIG*TS*SQRT(2.718282))

```

C*****
34 WRITE(6,100)
35 100 FORMAT(1,'THE OPTIMUM PULSE WIDTH LEVELS AND THRESHOLDS',
    $ ' ARE GIVEN BELOW FOR A 4-LEVEL PWM SYSTEM FOR DIFF. ERROR',
    $ ' PROBABILITIES')
C*****
36 DO 10 I=1,7
37 V1(I)=V(I)*SQRT(2)
C*****
38 WRITE(6,200) PE(I)
39 200 FORMAT(0,
    $ -----
    $ '
    $ ' ERROR PROBABILITY = ',PE7(1))
C*****
40 DO 20 J=1,3
41 TH(J)=(V1(I)/CONST)+T(I,J)
42 T(J+1)=(V1(I)/CONST)+TH(J)
43 20 CONTINUE
C*****
44 WRITE(6,300) T(1),TH(1),T(2),TH(2),T(3),TH(3),T(4)
45 300 FORMAT(0,' T(1) = ',2PE11.4,' TH(1) = ',2PE11.4,
    $ ' T(2) = ',2PE11.4,' TH(2) = ',2PE11.4,
    $ ' T(3) = ',2PE11.4,' TH(3) = ',2PE11.4,
    $ ' T(4) = ',2PE11.4)
46 10 CONTINUE
C*****
47 STOP
48 END

```

REFERENCES

- [1] W.S. Boyle, "Light Wave Communications", *Scientific American*, Vol. 237, No. 2, pp 40-48, Aug 1977.
- [2] T.G. Giannelis, "Optical Communications Research and Technology", *Fiber Optics*, *Proc. IEEE*, Vol 66, No. 7, pp 744-780, July 1978.
- [3] K.C. Kao, T.W. Davies, "Spectrophotometric Studies of Ultra-Low-Loss Optical Glasses", *J. Sci. Instrum., Series 2*, Vol. 1, p. 1063, 1968.
- [4] Ira Jacobs, "Atlanta Fiber System Experiment Overview", *Bell Syst. Tech. J.*, Vol 57, No 6, pp 1717-1721, July-Aug 1978.
- [5] T.L. Maione, D.D. Sell, "The Chicago Lightwave Project Experimental Fiber-Optic Transmission System for Interoffice Trunks", *IEEE Trans. Commun.*, Vol COM-25, No 5, pp 517-523, May 1977.
- [6] S.M. Abbott, W.M. Muska, T.P. Lee, A.G. Dental, C.A. Burrus, "1.1 Gbit/s Pseudorandom Pulse-Code Modulation of 1.27 μ m Wavelength CW InGaAsP/InP DH Lasers", *Electronics Letters*, Vol. 14, No. 14, p 349, 1978.
- [7] R. Petrovic, "Multilevel Signals in Digital Optical-Fiber Communications", *Electronics Letters*, Vol 14, No 25, pp 806-808, Dec 1978.
- [8] G. Mogensen, "Review Wide-band Optical Fibre Local Distribution Systems", *Opt. Quant. Elect.*, Vol. 12, pp 353-381, 1980.
- [9] -----, Course Notes 440, "Fiber Optic Communication Systems", *Integrated Computer Systems Inc.*, pp 7-17, 1979.
- [10] H. Kressel, Editor, "Semiconductor Devices for Optical Communication", *Topics in Applied Physics*, Vol 39, Springer-Verlag, N.Y., p 9, 1980.
- [11] M.K. Barnoski, "Semiconductor Devices for Optical Communication", *Topics in Applied Physics*, Vol. 39, Chap 6, Springer-Verlag, N.Y., 1980.
- [12] S.D. Personick, "Receiver Design for Digital Fiber Optic Communication Systems, Part 1", *Bell Syst. Tech. J.*, Vol. 52, No. 6, pp. 843-874, July-Aug 1973.
- [13] S.D. Personick, "Receiver Design for Digital Fiber Optic Communication Systems, Part 2", *Bell Syst. Tech. J.*, Vol. 52, No 6, pp 875-896, July-Aug 1973.

- [14] D.R. Smith and I. Garret, "A Simplified Approach to Digital Optical Receiver Design", *Opt. Quant. Elect.*, Vol. 10, pp. 211-221, 1978.
- [15] S.D. Personick, P. Balaban, J.H. Bobsin and P.R. Kumar, "A Detailed Comparison of Four Approaches to the Calculations of the Sensitivity of Optical Fiber System Receivers", *IEEE Trans. Commun.*, Vol. COM-25, No. 5, pp. 541-548, May 1977.
- [16] Raymond A.M. Rugemalira, "Calculation of Error Probability in an Optical Communication Channel in the Presence of Intersymbol Interference, Using a Characteristic Function Method", *Opt. Quant. Elect.*, Vol. 12, pp. 119-129, 1980.
- [17] Raymond A.M. Rugemalira, "The Calculation of Average Error Probability in a Digital Fibre Optical Communication System", *Opt. Quant. Elect.*, Vol. 12, pp. 130-141, 1980.
- [18] P. Balaban, "Statistical Evaluation of the Error Rate of the Fiberguide Repeater Using Importance Sampling", *Bell Syst. Tech. J.*, Vol. 55, No. 6, pp. 745-766, July-Aug 1976.
- [19] M. Mansuripur, J.W. Goodman, E.G. Rawson and R.E. Norton, "Fiber Optics Receiver Error Rate Prediction Using the Gram-Charlier Series", *IEEE Trans. Commun.*, Vol. COM-28, No. 3, pp. 402-407, March 1980.
- [20] R.J. McIntyre, "Multiplication Noise in Uniform Avalanche Diodes", *IEEE Trans. Electron Devices*, Vol. ED-13, No. 1, pp. 164-168, Jan. 1966.
- [21] P.P. Webb, R.J. McIntyre and J. Conradi, "Properties of Avalanche Photodiodes", *RCA Rev.*, Vol. 35, pp. 234-276, June 1974.
- [22] M. Abramowitz and I.A. Stegun, *Handbook of Mathematical Functions*, Dover, 1965.
- [23] G.H. Golub and J.H. Welsch, "Calculation of Gauss Quadrature Rules", *Math. Comput.*, Vol. 23, pp. 221-230, Apr. 1969.
- [24] W. Hauk, F. Bross and M. Ottka, "The Calculation of Error Rates for Optical Fiber Systems", *IEEE Trans. Commun.*, Vol. COM-26, No. 7, pp. 1119-1126, Jul. 1978.
- [25] S.O. Rice, "Mathematical Analysis of random noise", *Bell Syst. Tech. J.*, Vol. 23, No.1, p. 284, 1944.

- [26] R. Dogliotti, A. Luvison and G. Pirani, "Error Probability in Optical Fiber Transmission Systems", *IEEE Trans. Inform. Theory*, Vol. IT-25, No. 2, pp. 170-178, Mar 1979
- [27] H. Cramer, *Mathematical Methods of Statistics*, Princeton University Press, 1946.
- [28] M. Rocks, "Measurements Performed on L.E.D. 4-Level Digital Optical-Fibre System for 68 Mbit/s", *Electronics Letters*, Vol. 15, No. 21, pp 676-677, 11 Oct 1979.
- [29] S.D. Personick, "Comparison of Equalising and Nonequalising Repeaters for Optical Fiber Systems", *Bell Syst. Tech. J.*, Vol. 55, No. 7, pp 957-972, Sept 1976.
- [30] R. Dogliotti et. al., "Baseband Equalisation in Fiber-Optic Digital Transmission", *Opt. Quart. Elect.*, Vol. 8, pp 343-353, 1976.
- [31] T.V. Muoi and J.L. Hullett, "Receiver Design for Multilevel Digital Optical Fiber Systems", *IEEE Trans. Commun.*, Vol. COM-23, No. 9, pp 987-994, Sept 1975.
- [32] Hewlett Packard Company, *Operating and Service Manual, Model 1645A Data Error Analyzer*, Printed Oct 1978.
- [33] A. Bruce Carlson, *Communication Systems, An Introduction to Signals and Noise in Electrical Communication*, McGraw-Hill, N.Y., pp. 99-102, 1968
- [34] J.L. Hullett and T.V. Muoi, "A Feedback Receiver Amplifier for Optical Transmission Systems", *IEEE Trans. Commun.*, Vol. COM-24, No. 10, pp. 1180-1185, Oct 1976.
- [35] K. Ogawa and E.L. Chinook, "GaAs F.E.T. Transimpedance Front-End Design for a Wideband Optical Receiver", *Electronics Letters*, Vol. 15, No. 20, pp. 650-652, 27 Sept 1979.
- [36] S.D. Personick, *Optical Fiber Transmission Systems*, Applications of Communication Theory series, Plenum Press, N.Y. and London, p. 38, 1980.
- [37] H.E. Rowe, "Signals and Noise in Communication Systems", D. Van Nostrand Company, Inc., Princeton, N.J., pp. 257-321, 1965.
- [38] L.G. Cohen and S.D. Personick, "Length Dependence of Pulse Dispersion in a Long Multimode Optical Fiber", *Applied Optics*, Vol. 14, No. 6, pp. 1357-1360, Jun 1975.

- [39] D. Xianda, C.G. Englefield, P.A. Goud and R. Razdan, "Four-Level Pulse Width Modulation for Fiber Optic Communications", In press, *IEEE Trans. Commun.*
- [40] A. Luvison, G. Pirani and U. Mengali, "A Simple Timing Circuit for Optical PCM Repeaters", *Opt. Quant. Elect.*, No. 13, pp. 309-322, 1981.
- [41] S.D. Personick, "Statistics of a General Class of Avalanche Detectors with Applications to Optical Communication", *Bell Syst. Tech. J.*, Vol. 50, No. 10, pp. 3075-3095, Dec 1971.
- [42] R.J. McIntyre, "The Distribution of Gains in Uniformly Multiplying Avalanche Photodiodes: Theory", *IEEE Trans. Elect. Devices*, Vol. ED-19, No. 6, pp. 703-712, June 1972.